2019-08-22

The Development and Validation of a Novel Non-Invasive Assay Based on Cell Free-DNA to Detect Acute Allograft Rejection After Heart Transplantation

Pattar, Sabrina Kaur

UNIVERSITY OF CALGARY

The Development and Validation of a Novel Non-Invasive Assay Based on Cell Free-DNA to Detect Acute Allograft Rejection After Heart Transplantation

by

Sabrina Kaur Pattar

A THESIS

SUBMITTED TO THE FACULTY OF GRADUATE STUDIES

IN PARTIAL FULFILMENT OF THE REQUIREMENTS FOR THE

DEGREE OF MASTER OF SCIENCE

GRADUATE PROGRAM IN BIOCHEMISTRY AND MOLECULAR BIOLOGY

CALGARY, ALBERTA

AUGUST, 2019

Abstract

Immune-mediated injury (rejection) of a transplanted organ is a serious problem that can lead to allograft dysfunction and patient death. The gold standard for diagnosing acute cellular rejection (ACR) after heart transplantation (HT) is the endomyocardial biopsy (EMB), an invasive procedure with significant limitations. Dying cells release fragments of DNA into the circulation and increased levels of donor-derived cell-free DNA (dd-cfDNA) have been associated with ACR. Current methods to measure dd-cfDNA employ single nucleotide polymorphisms (SNPs) but an epigenetics-based assay could also accurately quantify dd-cfDNA in recipient blood.

This thesis aimed to validate the use of ventricle-specific methylation patterns in human cfDNA as an alternative and novel biomarker for ACR following HT. We hypothesized that dd-cfDNA released due to ACR-mediated injury could be quantified in recipient plasma based on epigenetic differences and would correlate better with tissue apoptosis than EMB-based rejection.

We identified increased cellular apoptosis within the myocardium as the severity of ACR increased, which provided a biological rationale for the use of cfDNA as a biomarker for rejection. We also initiated validation of an alternative sequencing platform and panel of highly polymorphic SNPs, which may improve a previously-established SNP-based assay. Finally, we established a bioinformatic pipeline for the identification of ventricle-specific differentially methylated regions (DMRs). These DMRs underwent retrospective validation using cfDNA samples from adult HT patients, which were associated with a known biopsy-proven rejection grade, to demonstrate the ability of these novel blood biomarkers to non-invasively detect acute rejection following HT.

In conclusion, we successfully demonstrated the efficacy of cfDNA as a biomarker for immune-mediated tissue injury and introduced the potential use of two ventricle-specific DMRs for the identification and quantification of cfDNA released from a donated heart due to ACR.

Keywords: Heart transplantation, endomyocardial biopsy, acute cellular rejection, non-invasive, cell-free DNA, dd-cfDNA, differentially methylated regions, DMRs, ventricle-specific

Preface

This thesis is original, unpublished, independent work by the author Sabrina K. Pattar. Sections of Chapter One and Appendix II have been recently published as a review paper and copyright permission has been obtained from the co-author Steven C. Greenway.

The methods contained within this thesis were performed solely by the author, Sabrina K. Pattar with assistance from the following individuals: Ms. Rasha Sabouny provided guidance on confocal microscopy and imaging of the TUNEL and DAPI stained ventricular tissues; Ms. Fatima Iqbal, under my supervision, helped analyze the images taken of TUNEL and DAPI stained ventricular tissues using ImageJ; Mr. Samuel Blaise and Dr. Frédéric Dallaire (Université de Sherbrooke) who performed the statistical analysis of the degree of tissue apoptosis at each rejection grade; Ms. Dimple Prasher who generated preliminary data for the confirmation of the similarity of left and right ventricular methylomes; the team at Illumina Canada who helped recreate our previously implemented SNP panel and produced our newly curated custom SNP panel for the Illumina MiSeq sequencing platform; Ms. Jene Weatherhead and Dr. Richard Pon who helped with the sequencing protocols for both the SNP-based and DMR-based assays.

The experiments using patient materials were approved by the Conjoint Health Research Ethics Board (CHREB) at the University of Calgary (ethics certificate number REB14-1244) for the project “Cell-Free DNA as a Non-Invasive Biomarker for Injury in Transplantation”.

Acknowledgements

I would like to thank my supervisor, Dr. Steven C. Greenway, for not only giving me this amazing research opportunity, but also for his immense amount of support and guidance over the last two years. He fostered a productive and welcoming work environment that encouraged critical and independent thinking, which ultimately allowed me to become more confident in my own abilities as a researcher. In addition to this, Dr. Greenway gave me the unforgettable opportunity to both share my research at an international level and learn from the leading researchers in the field of molecular diagnostics following heart transplantation. Thank you for everything.

To my committee members, Dr. Nowell Fine and Dr. Karl Riabowol, thank you for providing a unique perspective on my research and suggestions that improved the quality of my assay design. You were both incredibly supportive of my progress throughout the last two years.

To my friends and fellow members of the Greenway laboratory, Ashna Maredia and Dimple Prasher, who began their journey through graduate school alongside me; we shared our findings, successes, and mistakes so as to improve all of our work collectively. I could not have gotten through these last two years without your support and encouragement during those long hours in the laboratory troubleshooting our bioinformatics, PCR, and tissue staining protocols, I cannot thank you enough. This also extends to all of the members of the Greenway laboratory, as well as all of the other great people I met during this time, as I am truly grateful for all of the advice and inspiration that each of you gave me to complete my research to the best of my ability.

Finally, to my family, who have supported everything I have done in my academic career thus far. You all provided the reassurance I needed to get past any obstacles I came across and more importantly, were the first to celebrate my achievements over these last two years. I can confidently say that I would not be here without the constant love, support, and encouragement each of you give me every day and I cannot say thank you enough for that.

Table of Contents

List of Tables

List of Figures and Illustrations

List of Symbols, Abbreviations, and Nomenclature

Symbol	Definition	Symbol	Definition
°C	Degrees Celsius	**HT**	Heart transplantation
μL	Microliter	***INS***	Insulin gene
mL	Milliliter	***IRX4***	Iroquois homobox protein 4 gene
μM	Micromolar	**FasR**	Fas receptor
mM	Milimolar	**FMC**	Foothills Medical Centre
nm	Nanometer	**GTD**	Genome transplant dynamics
Q	Quality score	**gDNA**	Genomic DNA
ACR	Acute cellular rejection	**HT**	Heart transplantation
cfDNA	Cell-free DNA	**ISHLT**	International Society for Heart and Lung Transplantation
Chr	Chromosome	**MMF**	Mycophenolate mofetil
Chr 9-1	Chromosome 9:130,622,579-130,622,629	**NGS**	Next-generation sequencing
Chr 9-2	Chromosome 9:101,595,534-101,595,574	**PCR**	Polymerase chain reaction
Chr 12	Chromosome 12:106,132,052-106,132,096	**rTdT**	Recombinant terminal deoxynucleotidyl transferase
CHREB	Conjoint Health Research Ethics Board	**RRBS**	Reduced-representation bisulfite sequencing
dd-cfDNA	Donor-derived cell-free DNA	***SNC5A***	Sodium voltage-gated channel alpha subunit 5 gene
DAPI	4′,6-diamidino-2-phenylindole	**SNP**	Single nucleotide polymorphism
DMR	Differentially-methylated region	**Tm**	Melting temperature
DNMT	DNA methyltransferase	**TUNEL**	Terminal deoxynucleotidyl transferase dUTP nick end labeling
H&E	Hematoxylin and eosin	**WGBS**	Whole-genome bisulfite sequencing
EMB	Endomyocardial biopsy		

CHAPTER ONE: GENERAL INTRODUCTION

1.1 Heart Transplantation and Associated Complications

The first successful heart transplantation (HT) was carried out in 1967 in Cape Town, South Africa at the Groote Schuur Hospital (*1*). In this case, the heart from a cadaver was transplanted into a 54-year-old man to replace his own, which had been severely damaged by recurrent myocardial infarction (*1*). Since then, based on data submitted to the International Society for Heart and Lung Transplantation (ISHLT) Registry, over 118,788 heart transplants in recipients of all ages, including 113,472 adult heart transplants, have been performed (*2*, *3*). Cardiac transplantation is typically employed to treat patients who either have severe end-stage heart failure despite undergoing intense medical therapy and/or complex congenital heart disease that cannot be surgically corrected (*2*, *3*). When looking at the number of transplants performed on a global scale, North America, which comprises 7.5% of the world population, accounted for 55.8% of transplants recorded in the 2012 ISHLT Registry (*4*).

The trajectory of survival following the first year after HT has remained essentially unchanged for the past >30 years (*2*, *3*). Immunosuppressant therapies such as cyclosporin A, which was first introduced in 1984, have played a critical role in improving the success of cardiac transplantations by reducing the number and severity of toxic rejection episodes and virulent infections (*5*). Despite the use of immunosuppressant drugs, complications still arise that lead to rejection (organ damage mediated either by T-cells or antibodies) of the allograft. Acute cellular rejection (ACR) can occur at any point post-transplantation, however, it most often occurs with the first three to six months post-transplant (*6*). This form of rejection involves the accumulation of mononuclear cells, specifically CD4+ and CD8+ T-cells, in the interstitial space of the allograft due to the antigens on the donated tissue being identified as foreign to the recipient (*6*). This ultimately leads to one

of two pathways, the first being the release of cytotoxic granules, such as perforin and granzyme A and B, thereby causing apoptosis of the targeted tissue cells and inflammation of the associated vasculature is also observed (*6*). The second pathway involves the expression of the cytotoxic effector ligand, FasL, on the surface of the T cell, which binds to the Fas receptor (FasR) that is expressed on the surface of the "target" cell (*6*). This binding triggers apoptosis of the target cell through the classical caspase cascade (*6*). Thus, methods to accurately detect rejection in a timely manner are critical for ensuring maximal patient survival.

1.2 Endomyocardial Biopsy

Monitoring for rejection after HT currently requires an endomyocardial biopsy (EMB), which was first introduced in 1962 by Sakakibara and Konno (*7*). This technique employs a bioptome, which is inserted percutaneously and enters the right heart most commonly via the right internal jugular vein and superior vena cava under fluoroscopic or echocardiographic guidance (*7*). Once inside the heart, the pincers of the bioptome are used to obtain a small piece of myocardium, approximately 1 mm^3, from the interventricular septum that includes both the endocardium and myocardium (*7*). This technique was improved in 1972, by the Stanford group, when the Sakakibara-Konno bioptome was combined with flexible biopsy forceps, which allowed for serial right ventricular endomyocardial biopsies after transplantation (*8*). In general, routine EMB in adults are performed weekly for the first month, then every 2 weeks during the second month, as acute rejection is most likely to occur during the first few months post-HT (*9*). The number of biopsies is then reduced to once a month once the patient is 8-12 months post-HT and, after 1 year, biopsies are done every 4 to 6 months or when rejection is suspected (*9*). Furthermore, should a patient be treated for an episode of rejection, an EMB is generally repeated within 14 days to

ensure the treatment was effective (*9*). Upon sampling the ventricular tissue, it undergoes histological analysis in order to assign the transplant recipient a rejection grade of either 0R, 1R, 2R, or 3R, according to the revised guidelines recently created by the ISHLT (*10*). A grade of 0R would be assigned to those displaying no signs of rejection (*10*). In other cases, a grade of 1R would be assigned to a patient who shows interstitial infiltration by lymphocytes and macrophages and has a single region of myocyte damage (*10*). In more severe cases, a rejection grade of 2R is assigned if the patient displays two or more regions of infiltration with accompanying myocyte damage of the donor cardiac tissue (*10*). It should be noted that with modern immunosuppressant therapy, a rejection grade of 3R, indicating severe rejection with multifocal injury and edema, vasculitis or hemorrhage, is almost never observed (*10*).

EMB is often criticized since the biopsy site is confined to a usually discrete focus on the right side of the interventricular septum and therefore, provides limited information on the status of the allograft as a whole, particularly since ACR does not damage the myocardium in a uniform fashion (*11*, *12*). Moreover, the invasive nature of the procedure leads to several potential complications, such as puncturing of the adjacent carotid artery during catheter insertion, cardiac perforation with tamponade, pneumothorax, damage to the tricuspid valve, air embolism, atrial arrhythmias, and prolonged bleeding (*12–14*). There is also the logistical difficulty of organizing an EMB on short notice and the need for a general anesthetic in children. Finally, the interpretation of the EMB can be subjective and poorly reproducible. Conversely, non-invasive tests are safer and allow for more frequent monitoring. However, currently used non-invasive tests, such as echocardiography, are too non-specific and insensitive for reliable rejection monitoring (*12*). It should be noted that cardiac MRI has shown promise in identifying tissue changes associated with allograft injury but these findings are not universal (*15*, *16*). Thus, despite the fact that the incidence of complications

associated with EMB remains low, a non-invasive procedure would eliminate any procedure-related risks associated with monitoring for rejection in the transplanted heart. This could ultimately allow for even more frequent monitoring of the allograft which could potentially lead to improved long-term outcomes for the transplanted organ and the patient.

1.3 Current Non-Invasive Methods for the Detection of Rejection Following HT

Substantial effort has been made to develop non-invasive assays that could replace or reduce the use of EMB, especially for patients who are asymptomatic or who are more that 1-year post-transplant and in whom the likelihood of finding significant rejection is very low. In these patients, the probability of biopsy-related complications, although low, is greater than the detection of subclinical allograft rejection requiring treatment. Perhaps logically, initial efforts focused on monitoring the recipient's immune response and gene-expression profiling of peripheral blood mononuclear cells (PBMCs) was used to detect the presence of rejection (*17*). More specifically, an assay that utilized 11 informative genes was developed to discriminate between the absence of rejection (ISHLT grade 0R) and moderate to severe rejection (ISHLT grade ≥2R) non-invasively (*17*). By combining information from the literature regarding pathways involved in immune activation, recruitment and mobilization during rejection, bioinformatics, and publicly available cDNA libraries of stimulated and resting leukocytes, a total of 7,370 genes were represented on a custom microarray. Analysis of this microarray was conducted using patient PBMC samples, whereby 252 candidate genes were identified and subjected to real-time PCR (RT-PCR) using samples from patients with and without a confirmed episode of rejection. Overall, four individual genes (*ARHU*, *PDCD1*, *ITGA4*, and *SEMA7A*) and three aggregates of gene expression (*ITGAM*, *FLT3*, and *IL1R2*; *G6B* and *PF4*; *WDR40A* and *MIR*) provided a total of 11 gene classifiers that

could be used to effectively distinguish between rejection and quiescent samples. The majority of these genes were associated with T-cell production, activation, and mobilization, which is consistent with their role in driving allograft rejection. However, it should be noted that SNP within *PDCD1* has been associated with a susceptibility to systemic lupus erythematosus (*18*). Therefore, should a heart transplant recipient also suffer from this auto-immune disorder the efficacy of this assay may be compromised, as the expression of this gene could alter the patient's score and overestimate the severity of rejection (*18*). As such, through the use of a linear discriminant equation, a score between 0 and 40 was assigned to each sample based on gene expression, where a score ≥20 indicated the presence of rejection. This work resulted in the AlloMap test, the first FDA-approved, non-invasive method for the detection of rejection following cardiac transplantation that showed sufficient correlation with results obtained from an EMB. Follow-up clinical studies have been conducted to systematically confirm the effectiveness of this assay in comparison to the EMB.

The Invasive Monitoring Attenuation through Gene Expression (IMAGE) trial conducted by Stanford University gathered 602 heart transplant recipients from 13 U.S. centers between January 2005 through October 2009 (*19*). It should be noted that participants had received a heart transplant between 6 months and 5 years prior to the study and were randomized to either undergo routine EMB or be monitored using the AlloMap assay in a 1:1 ratio (*19*). On average, the participants were 54 years of age, and the majority of the study group were Caucasian males (*19*). The IMAGE trial defined the primary outcome as the first occurrence of rejection with hemodynamic compromise and/or graft dysfunction due to other causes, death, or retransplantation. Secondary outcomes included death from any cause, the number of biopsies performed, and biopsy-related complications (*19*). In addition to this, information regarding the participants' quality of life and

satisfaction with their assigned monitoring method was also collected. It was found that patients in the gene-profiling group were more satisfied with the non-invasive protocol than those in the EMB group and the level of satisfaction increased in the second year, while the scores in the biopsy group remained lower and consistent over the same two-year period (*19*). Notably, a total of 34 episodes of rejection were detected in the gene-profiling group out of 1190 (2.9%) serum samples obtained and analyzed throughout the trial (*19*). In comparison, 47 episodes of rejection were observed out of the 1249 EMBs (3.8%) performed in the biopsy group over the course of the study (*19*). In the gene-profiling group, 6 of the 34 rejection events (18%) were treated as a result of a gene-expression score >30, which warranted EMB confirmation. In the biopsy group, 22 treated episodes of rejection were asymptomatic and were detected on routine biopsy alone (*19*). Overall, the use of the AlloMap test, in conjunction with clinical observation and echocardiograms, safely reduced the number of biopsies performed without increasing risk of serious cardiovascular events (*19*). However, more recently there has been a shift from monitoring the recipient's immune response to approaches that directly interrogate the health of the donated organ, including the use of organ-derived circulating nucleic acids.

1.4 Cell-free DNA as a Biomarker

All cells undergoing apoptosis release fragments of double-stranded genomic DNA, roughly 140-160 bp in size and referred to as cell-free DNA (cfDNA), into the circulation (*20*). CfDNA was first formally described by Mandel and Metais in 1948 (*21*) but recently has come under intense study as a biomarker for many different diseases. Since the presence of cfDNA in the plasma is due to the natural process of apoptosis, all individuals have some detectable levels of cfDNA in their blood and, in the case of healthy individuals, the majority of the cfDNA detected

in the plasma is derived from hematopoietic cells (*9*). However, the concentration of cfDNA can increase under certain circumstances, including physical trauma, surgery, stroke, cardiovascular disease, sepsis, or even exhaustive exercise (*22*, *23*). It should be noted that these elevated levels of cfDNA are usually temporary, especially if the cause of cfDNA release is short-lived, as it is rapidly cleared from the body (*24*). More specifically, the half-life of cfDNA ranges from 4-30 minutes, although the exact mechanism of how it is cleared has not yet been elucidated (*23*, *24*).

Since its discovery, cfDNA has been used as a clinical indicator of disease. Some notable examples include the detection of fragments of fetal DNA in the circulation of the mother, which can then undergo next-generation sequencing (NGS) to detect aneuploidies or other genetic aberrations in the fetus, thereby replacing the invasive procedure of amniocentesis (*25*, *26*). Another major use of cfDNA has been seen in cancer biology, wherein it is known that tumors release fragments of the DNA into the circulation from the cells that comprise the cancer (*20*, *27*, *28*). As such, "liquid biopsies" can be employed where cfDNA is isolated from serum or plasma, followed by NGS to better understand the underlying genetic causes of the given cancer (*20*, *27*, *29*, *30*). In the case of transplantation, the cfDNA in the plasma of the patient would be derived from both the donated heart under conditions of rejection, as well as the recipient's tissues and hematopoietic cells from routine apoptosis (*31*, *32*). It should be noted that because ACR involves apoptosis of the myocardial cells, the challenge of a short half-life would likely be negated by the fact that cell death would be constantly occurring to maintain an elevated level of cfDNA in the plasma. Moreover, despite the fragmentation of the genomic DNA prior to release into the circulation, all other characteristics remain intact, including genetic and epigenetic features (i.e. SNPs that are unique to the donor and organ specific DNA methylation patterns). These features can then be leveraged to identify and quantify cfDNA derived from the donated organ during

immune-mediated tissue injury. Thus, since this molecule can be obtained from a simple blood draw and is increased in concentration with an increase in cellular apoptosis in the allograft, this potentially makes cfDNA an excellent candidate for a non-invasive biomarker for monitoring rejection after transplantation.

By definition, a biomarker is an objective, quantifiable, and reproducible characteristic of a biological process, or more specifically, of a medical state (*33*). The key to developing a successful biomarker is to determine its relationship to a clinical endpoint, which is the point when the patient has begun to present the symptoms of interest (*33*). In the case of using cfDNA as a biomarker, the goal would be to create a "surrogate endpoint," wherein these molecules are a part of the pathophysiological pathway associated with allograft rejection, and would be used to consistently and accurately predict a clinical outcome (*33*). Also, in order to be considered a surrogate endpoint, a biomarker must provide clinically relevant information and effectively indicate the medical state of the patient (*33*). Thus, the cfDNA must objectively, accurately, and reproducibly measure a quantifiable characteristic, which in this case is a grade of rejection as outlined by the ISHLT or the degree of apoptosis within the transplanted organ. Finally, another feature of a surrogate biomarker would be its capacity to be applied to similar studies, such as monitoring the rejection of other types of transplants (e.g. kidney, liver). Overall, the use of cfDNA appears to be promising method to non-invasively monitor for heart transplant rejection.

Levels of cfDNA can vary for several reasons apart from rejection, such as surgery, trauma, infection, or even exhaustive exercise (*22*, *23*). Therefore, understanding the kinetics of the release of dd-cfDNA into the recipient's plasma is imperative for determining the likelihood of organ survival, as different solid organ transplants result in distinguishing levels of dd-cfDNA. For example, at one day post-heart transplant, the fraction of dd-cfDNA from the total pool of cfDNA

has been observed to reach 3.8 ± 2.3% (*34*). However, the fraction of dd-cfDNA rapidly declined within the first week and remained low (<1%) in the absence of rejection, thereby displaying single-decay kinetics (*34*). Patients who received a kidney transplant displayed very similar kinetics for the level of dd-cfDNA (*35*). In contrast to this, on the first postoperative day for bilateral lung transplants, the level of dd-cfDNA was observed to be 26 ± 14% (*36*). In addition to this, the decline in dd-cfDNA displayed two-step decay kinetics, whereby the level of dd-cfDNA declined rapidly within the first week but then slowed and generally remained elevated throughout the posttransplant course, in comparison to levels observed in stable heart and kidney transplant recipients (*34–36*). During episodes of acute rejection in lung transplant patients, the level of dd-cfDNA spiked to 14-15% from the baseline levels of 1-3% just prior to the event (*36*). Similar to this, when an episode of acute rejection was experienced by a heart transplant recipient, the plasma dd-cfDNA levels jumped to 4-5%, from the baseline level of ~0.06% observed during quiescence (*34*)**.**

The characteristic levels of dd-cfDNA observed following each of these solid organ transplants can be attributed to the variation in tissue mass and the corresponding cell turnover rate. For example, when comparing bilateral and single-lung transplants, the rate of turnover has been observed to be, on average, 107 and 58 cells per second, respectively (*36*). Conversely, more than 14 days post-heart transplant, where no rejection event had been experienced, an average turnover rate of 8 cells per second tended to be observed (*36*, *37*). The vast differences in cell mass and cell turnover alone contribute to the discrepancies in dd-cfDNA levels observed, even in stable solid organ transplant recipients. Thus, an understanding of the expected levels of dd-cfDNA over time associated with a given solid organ transplant not only allows for the identification of any perturbations, which may be a sign of acute rejection, but also to determine the best form of

rejection monitoring. As mentioned above, current non-invasive assays require dd-cfDNA levels to not exceed 14%, which tends to be the case for lung transplant recipients for at least the first 10 days post-transplant (*36*, *38*). Therefore, designing assays that account for these elevated levels would be a point of interest for the future of non-invasive rejection monitoring.

1.5 Research Hypothesis and Objectives

Due to the significant limitations associated with the current gold standard for the detection of rejection following HT, the development of a specific and sensitive blood biomarker would allow for safer and potentially more frequent monitoring of the donated heart. In addition to this, a non-invasive assay based on cfDNA could allow for individualized immunosuppressive drug dosing, thereby preventing rejection and over-immunosuppression.

> We hypothesized that cfDNA released from the donated heart due to rejection can be quantified in recipient plasma based on genetic or epigenetic differences, whereby a better correlation will be observed with the degree of tissue apoptosis than the pathology-assigned rejection grade.

To address our hypothesis, we utilized both tissue samples (paraffin-embedded ventricular tissue) and plasma samples collected from adult heart transplant recipients undergoing scheduled endomyocardial biopsies at the Foothills Medical Centre (FMC) between 2014 and 2017. The tissue samples were used to determine the incidence of apoptosis during rejection (Chapter 2). The blood samples, which contained a mixture of cfDNA derived from both the donated heart and the recipient cells and tissues were used to validate the use of either SNPs (Chapter 3) or ventricle-

specific differentially-methylated regions (Chapter 4) for the quantification of dd-cfDNA at various levels of rejection.

Objectives:

1) To demonstrate the mechanism of the release of cfDNA from myocardial cells undergoing apoptosis due to ACR following HT.
2) To implement potential improvements to the previously established SNP-based assay
3) To identify and validate the use of sensitive and ventricle-specific differentially-methylated regions in cfDNA as a non-invasive blood biomarker for tissue injury caused by ACR following HT.

CHAPTER TWO: DEMONSTRATION OF cfDNA RELEASE DURING ACR

2.1 Introduction

In this chapter, we utilized serial right ventricular tissue samples prospectively obtained from consented adult heart transplant recipients undergoing routine EMBs at the FMC between 2014 and 2017. Slides created from these paraffin-embedded tissues were stained using terminal deoxynucleotidyl transferase dUTP nick end labeling (TUNEL) and 4′,6-diamidino-2-phenylindole (DAPI) in order to determine the degree of tissue apoptosis as the severity of rejection increased. Therefore, quantifying the amount of apoptosis observed at the various rejection grades allowed for the demonstration of the increased release of cfDNA from the donated heart due to ACR.

Cells that undergo apoptosis show characteristic morphological and biochemical features, which including chromatin condensation, cell and nuclear shrinkage, formation of membrane-bound cell fragments called apoptotic bodies, and rapid phagocytosis by neighboring cells or macrophages without associated inflammation (*39*). It has been noted that chromatin cleavage is the biochemical hallmark of the late stages of programmed cell death, or apoptosis, but is also observed in necrotic cells as well (*39*, *40*). DNA degradation is carried out by endonucleases, which produce blunt-end double-stranded DNA fragments that are eventually released into the circulation (*39*, *40*). In general, it is difficult to distinguish *in situ* cells undergoing apoptosis by light microscopy as the morphological features associated with apoptosis are only visible for a few minutes (*40*). Furthermore, extracting DNA from a culture of cells to detect the presence of fragmented DNA prevents the identification of which individual cells had undergone apoptosis. Thus, an alternative method for visualizing apoptosis at the individual cell level *in situ* was required. Terminal deoxynucleotidyl transferase-mediated dUTP nick end labeling (TUNEL)

provides the ability to label cells that have undergone apoptosis, based on the presence of fragmented genomic DNA (gDNA) *in situ*. As such, a terminal deoxynucleotidyl transferase enzyme catalyzes the attachment of a labelled dUTP to the free 3'-OH ends of the fragmented DNA. In some cases, the dUTP will be biotinylated, which can be visualized using a streptavidin-Cyanine 3 conjugate (*39*). In other cases, such as the protocol outlined below, the dUTP is labelled with a fluorescent marker that can be visualized by fluorescence microscopy. Overall, TUNEL allows for the visualization and quantification of apoptosis within a tissue or cell culture without having to disrupt the sample. Individual cells are identified with the nuclear stain DAPI and cells undergoing apoptosis co-localize fluorescence for both TUNEL and DAPI.

2.2 Hypothesis and Specific Aim for Chapter Two

Our **objective** was to demonstrate that presence of increased apoptosis with rejection and, therefore, demonstrate a mechanism for the release of cfDNA from myocardial cells due to cell-mediated rejection. We **hypothesize** that biopsy samples from patients assigned a pathology rejection grade of 2R (moderate rejection with two separate foci of lymphocyte infiltration) would display the highest levels of apoptosis which would be reflected by the greatest proportion of cells positively stained for both TUNEL and DAPI. Conversely, samples from patients in which the biopsy was graded as 0R (no rejection), very little apoptosis was expected with only a small proportion of cells within the tissue expected to be TUNEL and DAPI positive. Finally, samples from patients with a biopsy-proven rejection grade of 1R were expected to display an intermediate level of apoptosis, as reflected by the proportion of cells stained with TUNEL and DAPI.

Specific Aim:

1) Quantify the proportion of cells undergoing apoptosis corresponding to a rejection grade of 0R, 1R, or 2R.

2.3 Materials and Methods

2.3.1 Patient Data

Adult heart transplant recipients undergoing routine endomyocardial biopsies at the Foothills Medical Centre were recruited to allow ventricular tissue obtained from the serial biopsies to be stained for the quantification of immune-mediated apoptosis. All patients provided informed written consent for participation in this study which was approved by the CHREB (REB14-1244). Of the 47 patients recruited, six patients were selected for analysis. These patients had no signs of antibody-mediated rejection, had at least three serial samples, and diplayed either stable quiescence (patient 1017) or a fluctuation in the severity of rejection over time (patients 1002, 1007, 1011, 1021, and 1025).

Table 1. The demographics of six heart transplant recipients selected for the analysis of myocardial apoptosis due to acute cellular rejection.

Parameter	Patient Fraction
Sex (Male:Female)	1:1
Mean Age	53.33
Race (%)	
Caucasian	83.33
South Asian	16.67
Mean Days Post-HT at Recruitment	51.33

2.3.2 Apoptosis Assay – TUNEL staining

The DeadEnd™ Fluorometric TUNEL System kit (Promega) was used to visualize apoptotic and necrotic myocardial cells within right ventricular tissue sections obtained from routine EMBs (Appendix I). A crucial characteristic of apoptosis is the presence of fragmented gDNA. As such, this kit utilized a recombinant terminal deoxynucleotidyl transferase enzyme (rTdT) which catalyzed the attachment of a dUTP nucleotide, labelled with a 19-fluorescein-12 fluorescent marker, to the free 3'-OH group on the end of the fragmented DNA. Therefore, all cells that contained fragmented DNA, and were therefore, apoptotic or necrotic, stained positively for TUNEL. In order for the tissue to be stained, slides created from the paraffin embedded biopsy samples were initially de-paraffinized using xylene substitute, and then fixed using 4% paraformaldehyde in PBS. The samples were then rehydrated by immersing the slides in increasingly more dilute ethanol solutions, followed by a dilute NaCl solution. The slides were then permeabilized using a 20 µg/ml Proteinase K solution and fixed once more using 4% paraformaldehyde in PBS. The slides were then allowed to equilibrate prior to the addition of the rTdT enzyme and the mixture of dUTP nucleotides, labelled with a 19 fluorescein-12 fluorescent marker. During the addition of the enzyme and nucleotides, the slides were kept in a humidified chamber covered in aluminum foil to protect the slides from direct light to prevent photobleaching of the fluorescent label. The reaction was then terminated using a 20X SSC (sodium chloride and sodium citrate) solution and the slides were washed several times using PBS to remove any unincorporated fluorescein-12-dUTP. Finally, in addition to the TUNEL staining, the tissues were then stained with DAPI (NucBlue Fixed Cell Stain DAPI (Invitrogen)) to visualize the total number of nucleated myocardial cells within the sample. This ultimately allowed for the determination of the proportion of apoptotic and necrotic cells within the tissue samples. The slides

were then covered using plastic coverslips provided by the Promega TUNEL kit and Calbiochem's Fluorsave as an adhesive agent (Appendix I).

2.3.3 Confocal Microscopy

The stained ventricular tissue slides were then imaged using a spinning disk confocal super resolution microscope (SpinSR10 (Olympus)) from Dr. Timothy Shutt's laboratory. A green fluorescent signal was observed at 488 nm in regions that contained apoptotic or necrotic myocardial cells, while DAPI-stained nuclei emitted a blue signal at 405nm. The images were taken at 10X magnification to allow for the visualization of each of the 3-5 individual tissue sections taken during the EMB within 1-3 images, depending on the size of each tissue section. Images were saved in a .TIFF format.

2.3.4 Analysis of Images of TUNEL stained Tissue Sections Using ImageJ

The images taken at 488 and 405nm for each tissue section were opened on ImageJ plugin, Fiji. The brightness and contract were adjusted to a minimum of 122 and a maximum of 145 for each image taken at 488nm, while all images taken at 405nm were adjusted to a minimum of 105 and maximum of 145. This allowed for the clearest visualization of all TUNEL and DAPI signals within each set of images, as these settings removed any background staining within the images. Then, using the selection tool the image of the tissue section taken at 488nm was traced whereby the edges and any areas of thin or torn tissue were omitted. This ensured that any cells that stained positively for TUNEL and DAPI due to physical damage, rather than immune-mediated damage, did not skew the results. This traced outline was then pasted and aligned on the image taken at 405nm, which contained all of the nucleated, DAPI-stained, cells. The traced outlined was applied,

which removed all areas of the image outside of the outline, leaving behind only the tissue section of interest. Next, both images taken at 488 and 405 nm were further enhanced by removing any residual noise using the "despeckle" option in Fiji. Following this, the cropped image taken at 405nm was then used to create a mask, which functioned as a control for the expected number and location of all nucleated cells within the tissue sections when determining the colocalization of TUNEL and DAPI. Finally, the "coloc 2" test in Fiji was employed, whereby channel 1 was assigned as the image taken at 488 nm and displayed all TUNEL positive cells, channel 2 was assigned as the image taken at 405 nm and displayed all DAPI positive cells, and the mask created from the image taken at 405 nm was also plugged in. The test was allowed to run and resulted in the creation of a PDF, which listed the proportion of cells that displayed a colocalization of TUNEL and DAPI, and therefore, represented apoptotic or necrotic cells within the tissue.

2.3.5 Statistics

Statistical analysis was completed in collaboration with Samuel Blais and Dr. Frédéric Dallaire of the Université de Sherbrooke. The percentage of cellular apoptosis showed a log-normal distribution. Therefore, we presented the mean percentage of apoptosis as geometric means. As such, we used multilevel linear regression to evaluate the association between rejection grade and percentage of cellular apoptosis while adjusting for the potential cluster effect of comparing multiple samples per biopsy and repeated biopsies for each patient. We used an iterative approach to test several models and the necessity of including random effects for each level (*41*). The final model consisted of a three-level hierarchical linear regression of log-transformed apoptosis percentage according to rejection grade. Also, the attributable variance was too small to be calculated in the covariance matrix and was removed, but we could not exclude with certainty that

this might have been caused by a lack of statistical power. All analyses were performed using SAS software version 9.4 (SAS Institute Inc., Cary, NC, USA).

2.4 Results

2.4.1 Images

The use of DAPI and TUNEL staining allowed for the visualization of the total number of cells within the biopsied tissues (Figure 1A) and the number of those cells that had fragmented DNA (Figure 1B), respectively. Myocardial cells that displayed colocalization of DAPI and TUNEL (Figure 1C) were considered to have undergone apoptosis or necrosis. It should be noted that no cells displayed only TUNEL staining. If fragmented DNA was detected, which indicated the occurrence of cell death, a green (TUNEL) and blue (DAPI) signal was present at that cell. This indicated that there was no unwanted or off-target TUNEL staining within the tissues.

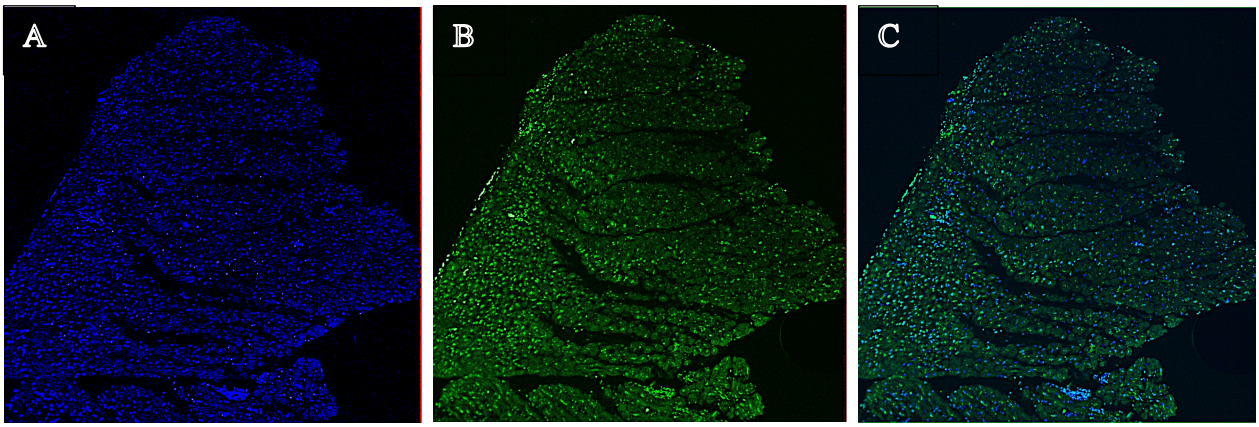

Figure 1. **Examples of tissue staining for DAPI and TUNEL.** Right ventricular tissue obtained from a routine EMB for patient 1007 in which a rejection of 2R was assigned and was stained with DAPI (A) and TUNEL (B), whereby colocalization indicated an apoptotic or necrotic cell (C). Images taken at 10X magnification using a spinning disc confocal microscope.

2.4.2 Individual Patient Data

Of the consented heart transplant recipients, six patients were selected for further testing (Table 1), in which tissue samples taken from the EMB were stained with TUNEL and DAPI in order to determine the degree of tissue apoptosis occurring within the donated heart during rejection. A noticeable trend emerged in which the biopsy-proved ISHLT rejection grades corresponded well with the number of areas within the biopsied tissues that displayed elevated levels of apoptosis, as indicated by the percentage of cells that stained positively for both TUNEL and DAPI. Based on the ISHLT guidelines, a rejection grade on 0R is associated with an absence of lymphocyte infiltration and damage. This was reiterated in the TUNEL and DAPI stained tissue samples taken from biopsies in which a rejection grade of 0R was assigned. In these cases, the percentage of cells in any given area that displayed colocalization of TUNEL and DAPI did not exceed 12%, with majority of the regions displaying a colocalization percentage of 1-5% (Figures 2, 3, 6, and 7). Samples that were assigned a rejection grade of 1R displayed the most interesting results due to the variability in the TUNEL results despite all of the samples meeting ISHLT's criteria for a 1R rejection grade, which includes a single area of lymphocyte infiltration and accompanied damage. As such, the TUNEL results indicated a single area of elevated apoptosis, in which 20-35% of the cells within the area displayed colocalization of TUNEL and DAPI (Figures 2, 4-6). Notably, while patient 1021 had several biopsies that were assigned a rejection grade of 1R, and a single area of elevated apoptosis was displayed, the proportion of cells that stained positively for TUNEL and DAPI in these areas ranged from only 11.8-17.6% (Figure 7). However, the more striking results were the differences in the degree of apoptosis occurring in all other regions of these 1R tissue samples, which will be referred to as "baseline" levels of the given sample. 1R samples that preceded a 2R rejection event displayed a typical single area of elevated

apoptosis (>20%), with all other areas displaying very little colocalization of TUNEL and DAPI (<5%) (Figures 2, 4, and 5). Conversely, 1R samples taken during a routine EMB directly following a 2R rejection event displayed elevated "baseline" levels of apoptosis relative to those displayed in 1R samples taken prior to a 2R rejection event (Figures 4-6). In some cases, such as the 1R sample taken from patient 1025 following the 2R rejection event, the "baseline" level of apoptosis was greater that the "baseline" level of apoptosis displayed in the 2R tissue sample (Figure 6). Finally, based on the ISHLT criteria, samples assigned a rejection grade of 2R must display at least two areas of lymphocyte infiltration and associated damage. This was consistent with the number of areas with elevated levels of apoptosis, as all 2R samples displayed two areas in which 20-34.3% of the myocardial cells stained positively for both TUNEL and DAPI (Figures 2, 4-6).

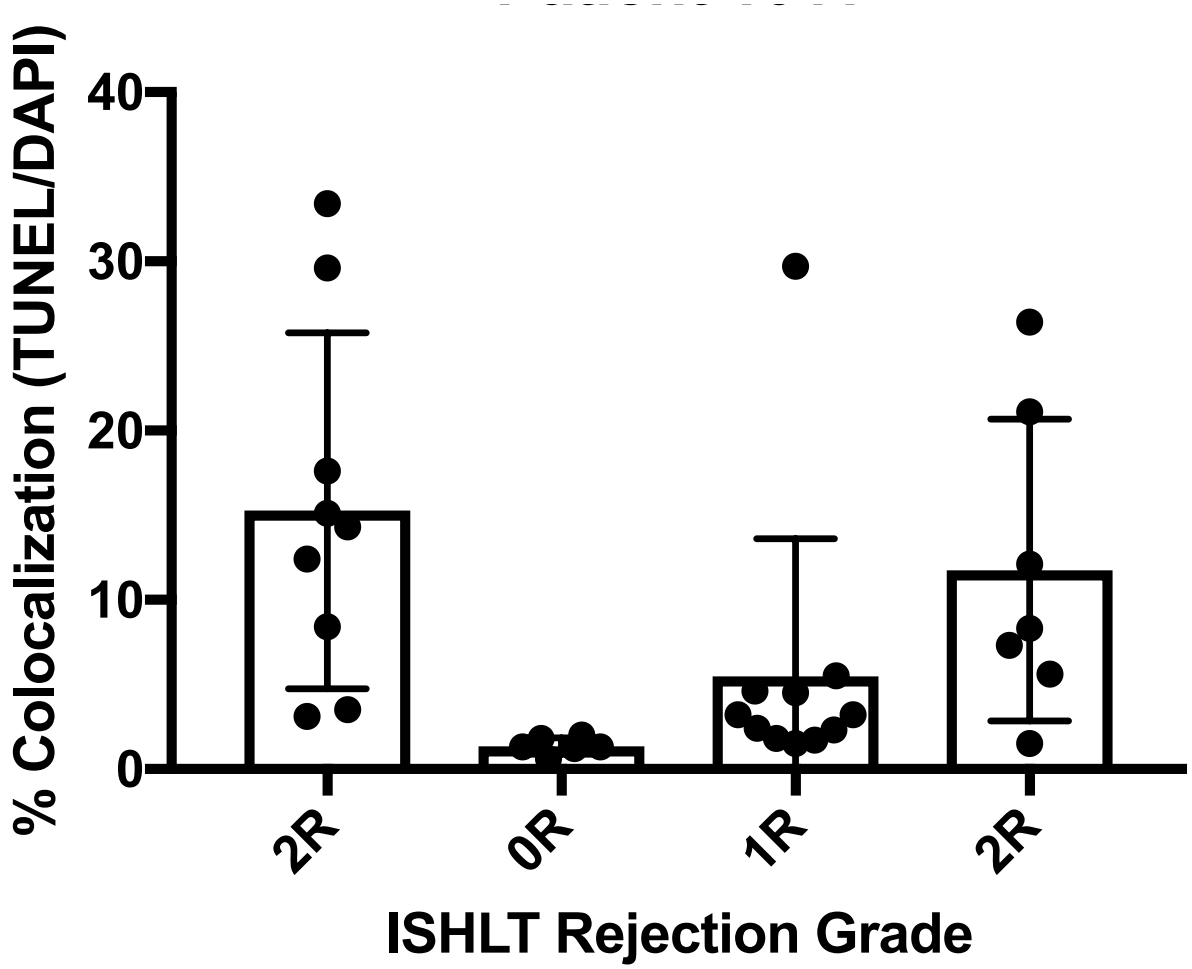

Figure 2. TUNEL/DAPI ratio for samples from patient 1011. The proportion of myocardial cells within a given area of the ventricular tissue slides that had stained positively for both TUNEL and DAPI, represented by each individual data point. Associated ISHLT rejection grades are listed for each routine biopsy in which the tissues were obtained from patient 1011. Bars represent standard deviation of the mean.

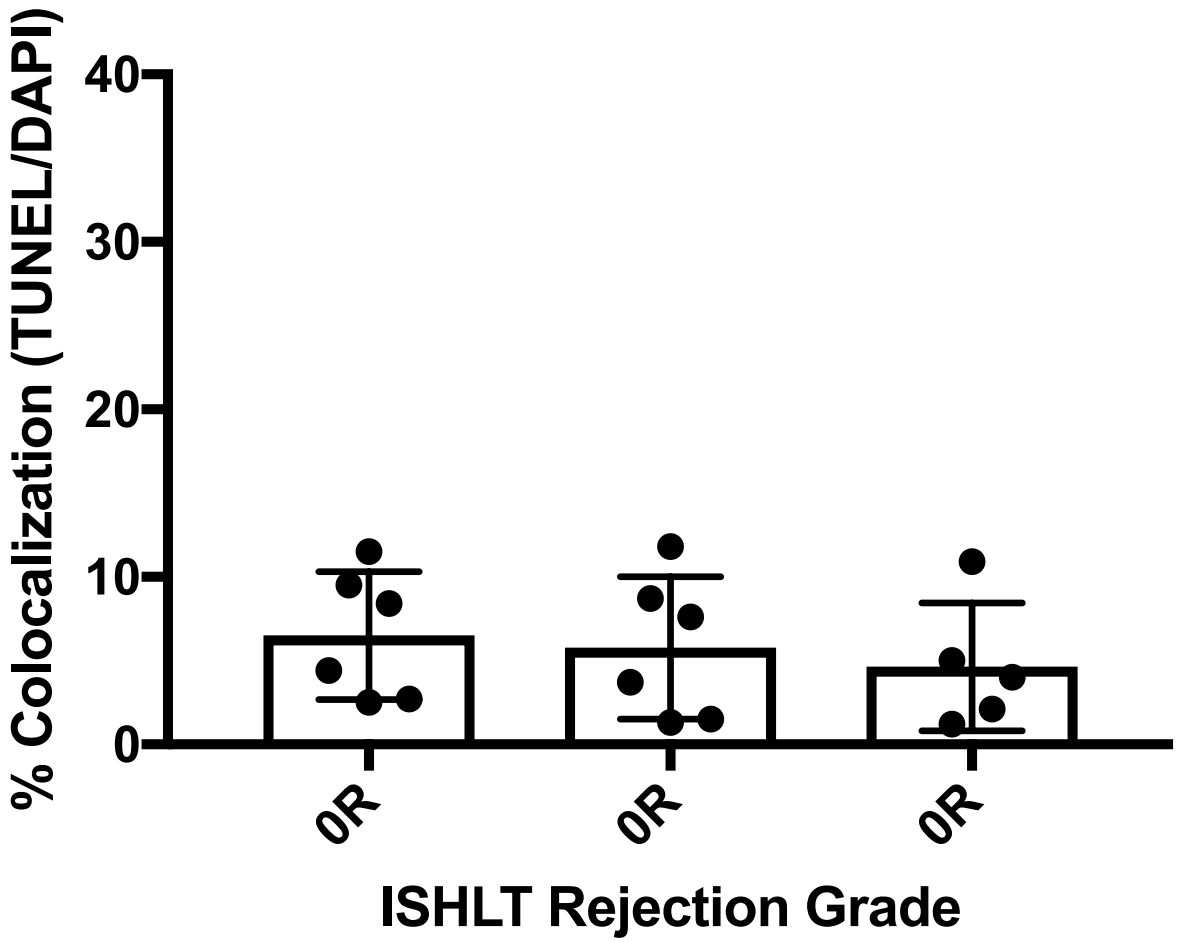

Figure 3. TUNEL/DAPI ratio for samples from patient 1017. The proportion of myocardial cells within a given area of the ventricular tissue slides that had stained positively for both TUNEL and DAPI, represented by each individual data point. Associated ISHLT rejection grades are listed for each routine biopsy in which the tissues were obtained from patient 1017. Bars represent standard deviation of the mean.

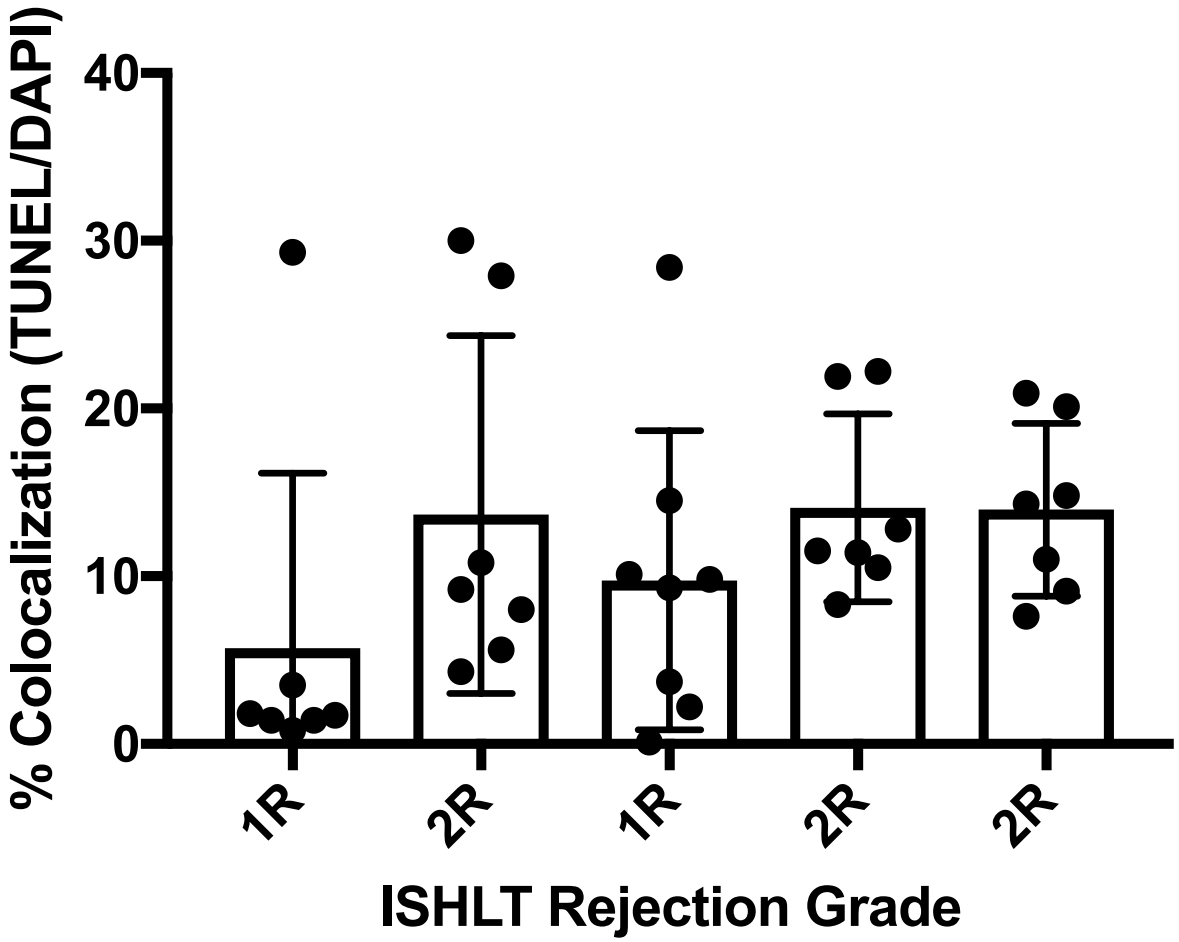

Figure 4. TUNEL/DAPI ratio for samples from patient 1007. The proportion of myocardial cells within a given area of the ventricular tissue slides that had stained positively for both TUNEL and DAPI, represented by each individual data point. Associated ISHLT rejection grades are listed for each routine biopsy in which the tissues were obtained from patient 1007. Bars represent standard deviation of the mean.

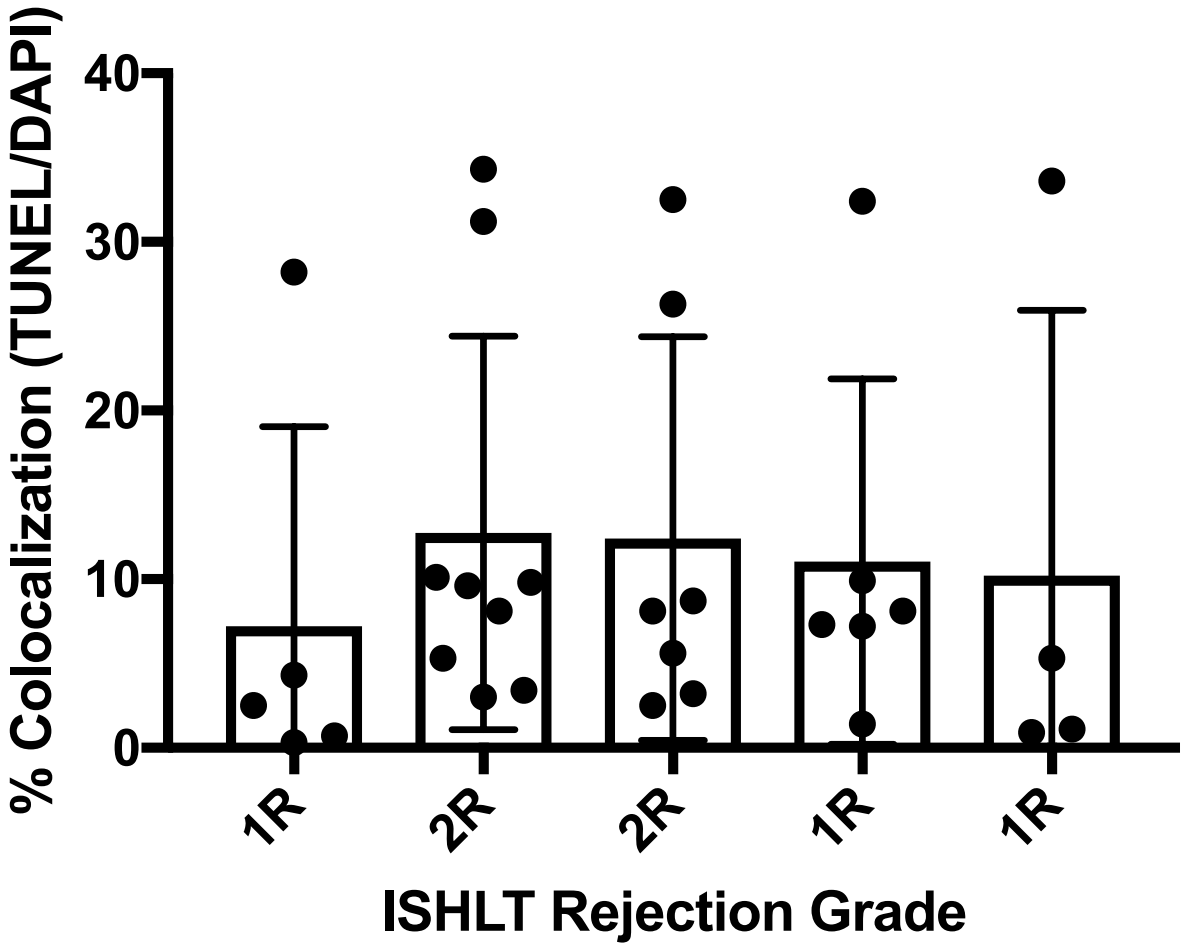

Figure 5. TUNEL/DAPI ratio for samples from patient 1002. The proportion of myocardial cells within a given area of the ventricular tissue slides that had stained positively for both TUNEL and DAPI, represented by each individual data point. Associated ISHLT rejection grades are listed for each routine biopsy in which the tissues were obtained from patient 1002. Bars represent standard deviation of the mean.

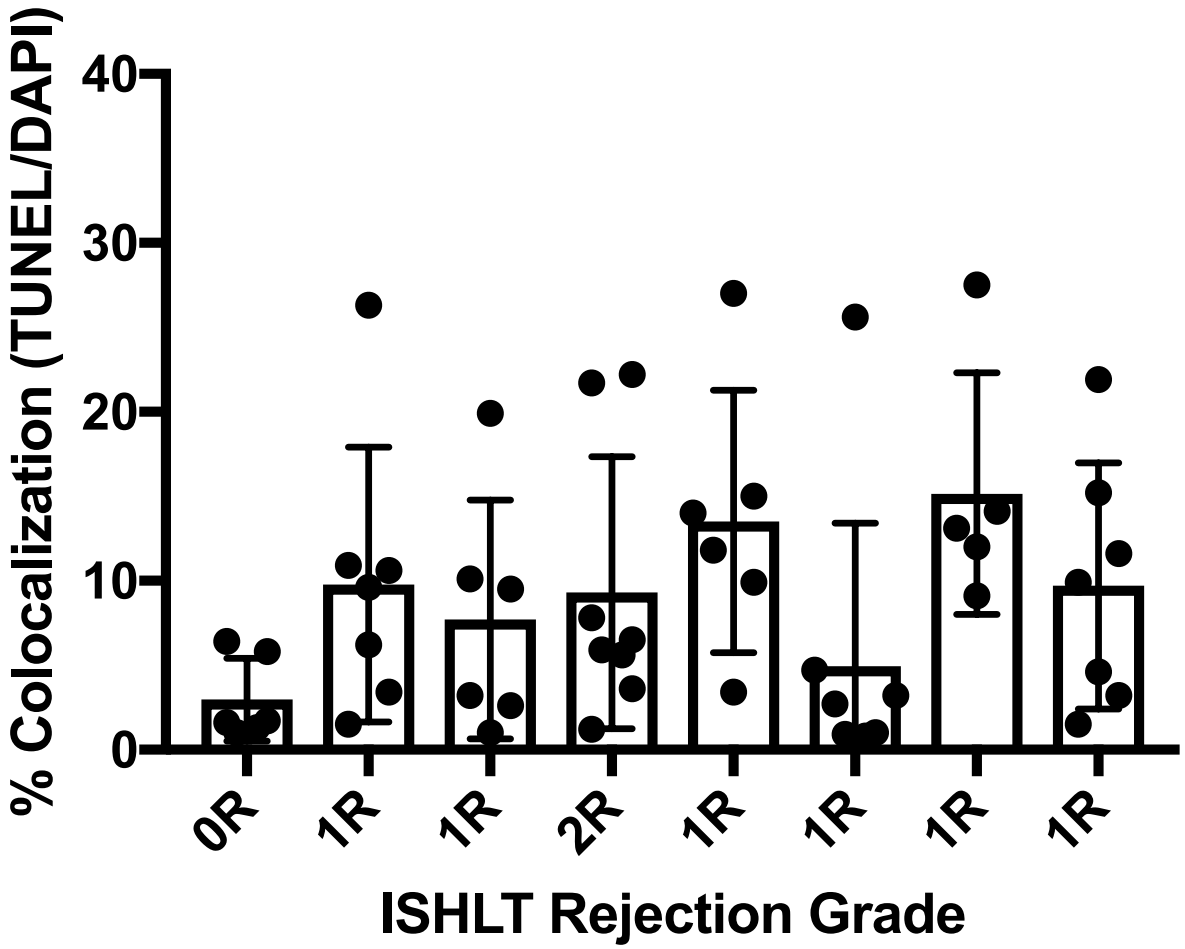

Figure 6. TUNEL/DAPI ratio for samples from patient 1025. The proportion of myocardial cells within a given area of the ventricular tissue slides that had stained positively for both TUNEL and DAPI, represented by each individual data point. Associated ISHLT rejection grades are listed for each routine biopsy in which the tissues were obtained from patient 1025. Bars represent standard deviation of the mean.

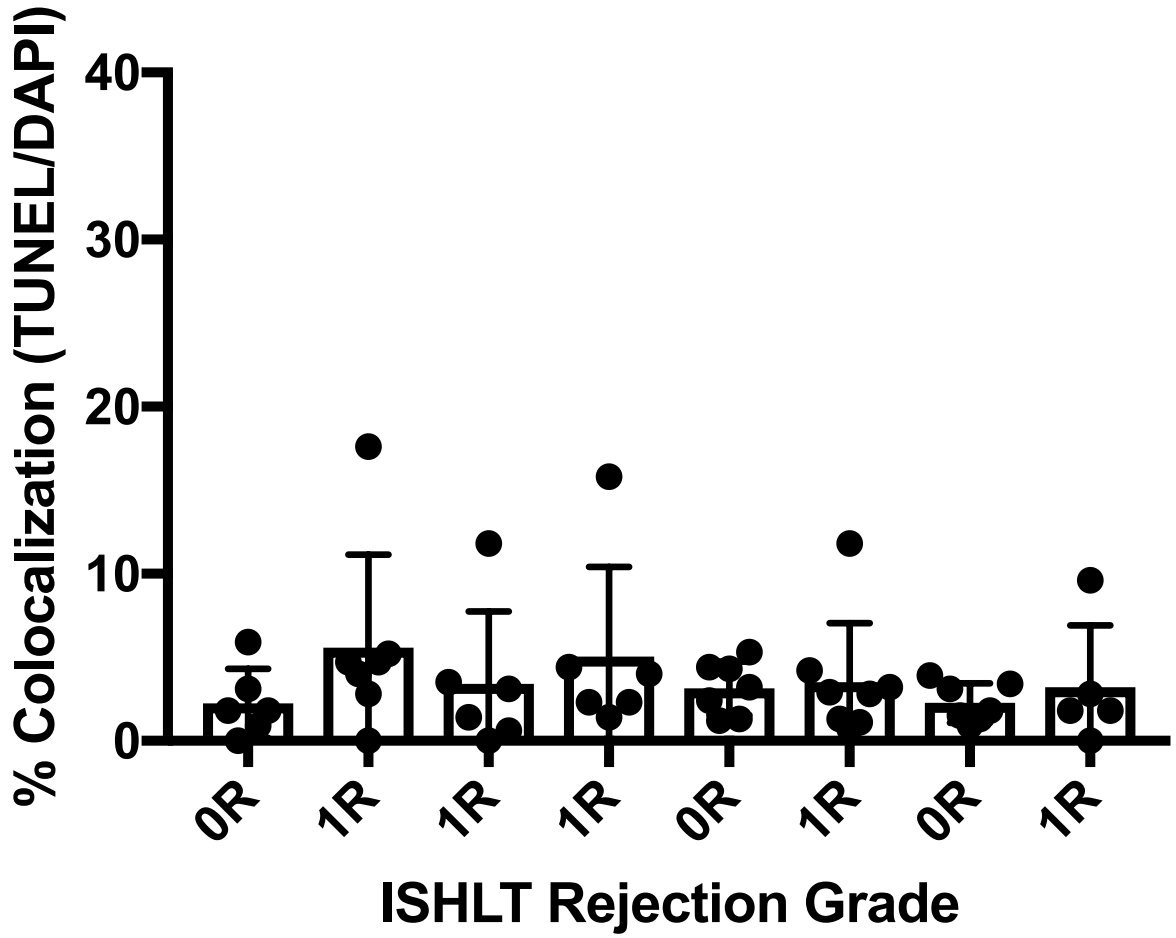

Figure 7. **TUNEL/DAPI ratio for samples from patient 1021.** The proportion of myocardial cells within a given area of the ventricular tissue slides that had stained positively for both TUNEL and DAPI, represented by each individual data point. Associated ISHLT rejection grades are listed for each routine biopsy in which the tissues were obtained from patient 1021. Bars represent standard deviation of the mean.

2.4.3 Degree of Tissue Apoptosis at Each Rejection Grade

A total of 222 samples (0R: n=49, 1R: n=112, 2R: n=61) comprised in 33 separate biopsies (0R: n=8, 1R: n=17, 2R: n=8) from 6 patients were included in the final analyses. Patients underwent a median of three biopsies. Each biopsy was divided in multiple samples for a median of 19 samples per patients. The adjusted mean percentage of myocardial cells that stained positively for TUNEL, and therefore, underwent apoptosis or necrosis, was observed to be 2.4%, 4.4% and 10.0% for rejection grade 0R, 1R, and 2R, respectively (Figure 8). Thus, the mean percentage of myocardial cells that stained positively for TUNEL increased as the severity of rejection increased (Figure 8). In addition to this, the differences in the mean percentage of TUNEL positive cells observed between 0R and 1R ($p=0.01$), 1R and 2R ($p=0.0004$), and 0R and 2R ($p<0.0001$) were found to be statistically significant.

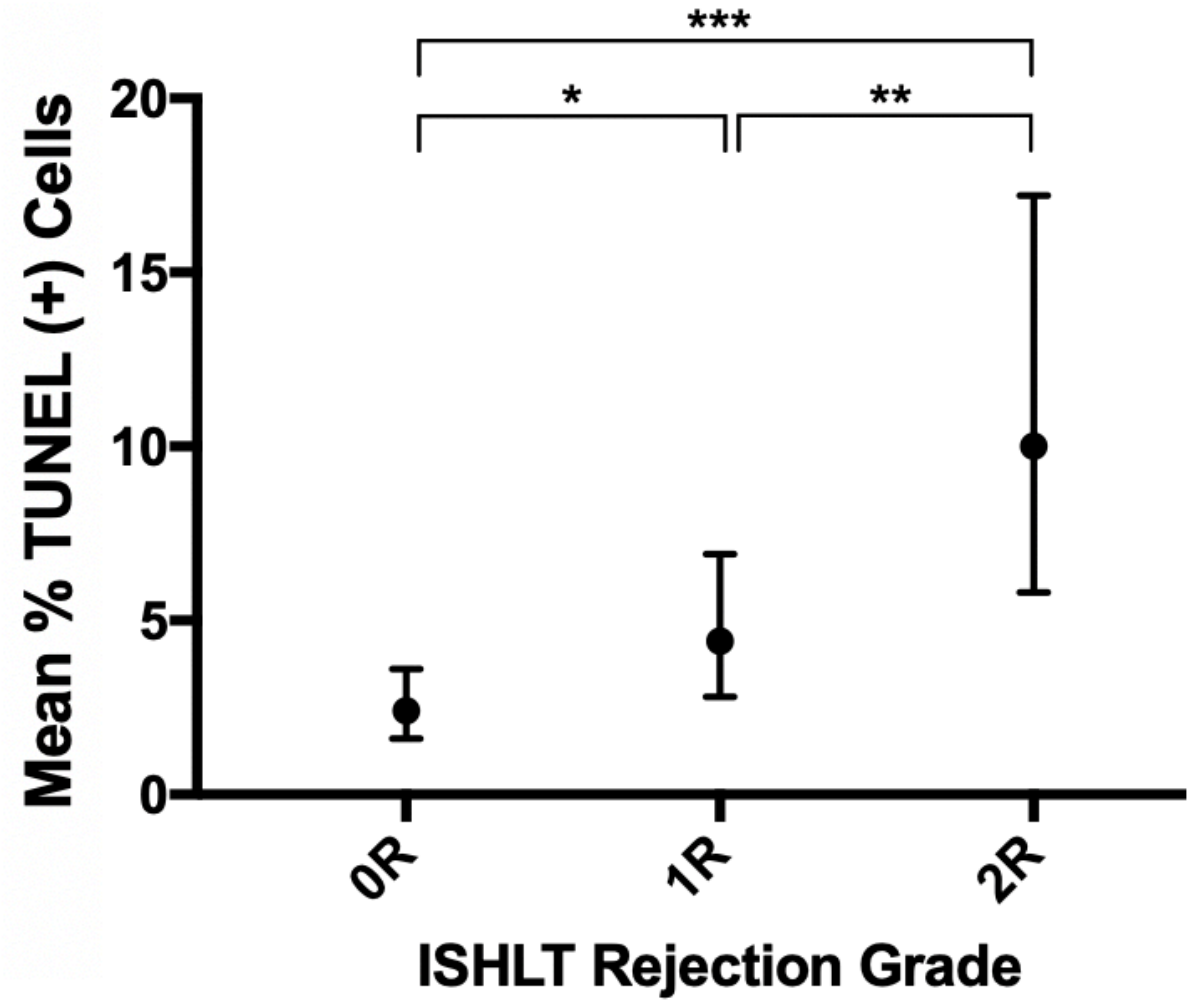

Figure 8. **The mean percentage of TUNEL positive myocardial cells at each rejection grade.** The adjusted mean proportion of myocardial cells that stained positively for TUNEL within ventricular tissues that were obtained during routine EMBs from total of 222 samples (0R: n=49, 1R: n=112, 2R: n=61) comprised in 33 separate biopsies (0R: n=8, 1R: n=17, 2R: n=8) from 6 patients (*p=0.01, **p=0.004, ***p<0.0001). Bars represent 95% confidence intervals.

2.5 Discussion

The process of apoptosis can be characterized by the fragmentation of genomic DNA and the release of this DNA into the circulation. It has been assumed that acute cellular rejection results in the death of cells within the allografted tissue through the accumulation of CD4+ and CD8+ T-cells in the interstitial space of the allograft, which initiates one of two apoptotic pathways (*6*). The first being the release of cytotoxic granules, while the other pathway involves the expression of FasL on the surface of the T cell, which binds to the FasR on the surface of the "target" cell, thereby triggering apoptosis through the classical caspase cascade (*6*). Thus, while the immune-mediated process of cellular apoptosis within an allografted tissue is well understood, the quantification of this process during rejection had not been previously completed. As such, by obtaining ventricular tissue from 33 separate EMBs (0R: n=8, 1R: n=17, 2R: n=8) from 6 consented HT patients, we were able to quantify the proportion of ventricular myocardial cells that had undergone apoptosis during varying severities of rejection.

Based on the ISHLT guidelines, a rejection grade of 0R would be assigned to a sample if the tissue appeared to be completely healthy, with no signs of lymphocyte infiltration or associated damage following H&E staining (*10*). In the case of mild rejection, or a grade of 1R, the biopsied sample would be expected to display interstitial infiltration by lymphocytes and macrophages and a single region of myocyte damage (*10*). Moderate rejection, or a grade of 2R, has been characterized by a given sample displaying two or more regions of infiltration with accompanying myocyte damage of the donated ventricular tissue (*10*). As such, the number of areas of damage associated with each rejection grade were consistent with the number of areas with elevated apoptosis within the TUNEL stained ventricular tissue samples. More specifically, samples taken from a patient's donated heart during a routine EMB that was assigned a rejection grade of 0R

after histological analysis also displayed minimal TUNEL staining across the entirety of the tissue (Figures 2, 3, 6, and 7). Samples that were assigned a rejection grade of 1R following histological analysis of the biopsied tissue also displayed a single area of elevated apoptosis, relative to the levels observed in all other regions of the interrogated tissue (Figures 2, 4-7). This was also reiterated in samples taken from patients who had been assigned a rejection grade of 2R, whereby two areas of elevated apoptosis were observed relative to all other tissue sections (Figures 2, 4-6).

While the number of areas with elevated apoptosis corresponded well with the biopsy-proven ISHLT rejection grades, the more interesting results were found in the remaining areas of interrogated tissue. This "baseline" apoptosis that occurred outside of the areas of prominent damage and cell death was especially noteworthy in the 17 stained, imaged, and quantified 1R samples. The greatest variation within 1R samples was observed between samples taken prior to and following a moderate (2R) rejection event. These 1R samples that were taken prior to a rejection event tended to have baseline levels of apoptosis that typically did not exceed 5% (Figure 2, 4, and 5). However, samples that were taken during an EMB immediately following a 2R rejection event, and that were assigned a rejection grade of 1R, tended to contain areas of tissue where 10-15% of the cells stained positively for both TUNEL and DAPI (Figures 4-6). In some cases, certain areas of tissue from these 1R samples had higher proportions of apoptotic and necrotic cells than what was observed in the baseline of 2R samples (Figure 6). These 1R samples that following a moderate rejection event, may therefore, warrant a unique category of their own and may be referred to as "recovery" 1R samples. Furthermore, patient 1021 presented an interesting case as this patient did not experience any signs of moderate rejection throughout the period in which samples were collected. As such, the analysis of the TUNEL staining from these biopsied tissues revealed a noteworthy pattern, whereby a single area of elevated apoptosis was

observed but it was unlike the other 1R samples, as the percentage of cells that stained positively for TUNEL and DAPI did not exceed 20%. These results may have suggested an overcall in the severity of rejection, simply as a precautionary measure. It should be noted that patients who receive either a 0R or 1R diagnosis are currently treated the same clinically. Therefore, the results of the TUNEL staining may provide a more accurate and precise depiction of the severity of rejection. This is especially true for the mild rejection samples, which appear to have a range in the degree of cellular apoptosis and may suggest an oversimplification of the ISHLT guidelines for rejection grades.

Overall, the serial data that was collected for each of the six heart transplant recipients created a great deal of complexity in terms of the analysis due to the multiple biopsies per patient and the variation in the number of interrogated areas from each biopsy. Furthermore, there was a lack of statistical power that prevented analysis at the biopsy level. More specifically, a mean of the percentages of apoptosis occurring within the various areas of tissue taken during a single biopsy resulted in a loss of differentiation between biopsies from differing severities of rejection. Therefore, by combining the levels of apoptosis detected in each individual area from biopsies that was assigned the same rejection grade, we were able to develop a multilevel statistical model. As such, we determined the adjusted mean percentage of myocardial cells that stained positively for both TUNEL and DAPI, and therefore, had undergone apoptosis or necrosis when a patient experienced no (0R), mild (1R), or moderate (2R) rejection. As expected, it was found that the mean proportion of cells that were apoptotic or necrotic increased as the severity of rejection increased (Figure 8). Moreover, the differences in the mean percentage of apoptotic or necrotic cells at each rejection grade were found to be statistically significant. Notably, the confidence interval for the 0R cohort was the smallest due to the large amount of uniformity across each of

the 8 interrogated samples, as the level of apoptosis in any area did not exceed 10% for these samples. The confidence interval of the 1R cohort are slightly larger due to the variation that was noted within this group. However, this variation was offset by the relatively large sample population (n=17) that was available for analysis. Finally, we analyzed 8 sets of biopsied tissues that were assigned a rejection grade on 2R. With two areas of elevated apoptosis within each sample, this created a data set with a large range of values, and therefore, a large confidence interval. This may be addressed by increasing the number of analyzed biopsies within the 2R cohort.

Taken together, the distinction between 0R samples, 1R samples taken prior to and after a moderate rejection event, and 2R samples may be especially pertinent for the assessment of the efficacy of a cfDNA-based blood biomarker, as the release of cfDNA into the circulation is directly linked to the process of apoptosis. Therefore, in addition to the one or two sites of elevated damage, an increase in the total amount of apoptosis that occurred across the tissue was likely to have a large impact on the total amount of dd-cfDNA within the recipient's plasma. Especially in cases where we observed obvious differences in the total amount of apoptosis occurring within several samples that all fit the ISHLT guidelines for a rejection grade of 1R. As such, these results suggested that the correlation between the ISHLT rejection grade and the concentration of the cfDNA-based blood biomarker at the individual biopsy level would be flawed. Thus, a more effective correlation for the assessment of cfDNA-based blood biomarkers for the non-invasive detection of ACR would be between the concentration of dd-cfDNA and the mean proportion of cells undergoing apoptosis.

2.6 Conclusion

Traditionally, EMB samples undergo histological analysis through the use of H&E staining, which highlights lymphocyte infiltration and associated damage. Samples are then assigned a rejection grade based on the guidelines determined by ISHLT. Conversely, TUNEL staining was a much more exhaustive procedure in comparison, but provided a greater understanding of myocardial cell death within these donated hearts. Therefore, this also provided a better understanding of the expected concentration of cfDNA derived from the donated heart within the recipient's plasma. On a large scale, we were able to successfully quantify the mean percentage of apoptotic or necrotic cells within a given sample according to the severity of rejection, which had not been previously completed. Also, at the individual biopsy level, we were able to elucidate the variation present within the ISHLT rejection grade of 1R. While the ISHLT guidelines provide a simplified method for the categorization of the severity of rejection, this grading system may result in the oversight of nuances that could impact patient outcomes, especially for those who experience mild rejection. Thus, levels of apoptosis may provide a more accurate representation of the range in the severity of rejection within an allografted heart, as opposed to the broad categories defined by ISHLT.

CHAPTER THREE: IDENTIFICATION & VALIDATION OF VENTRICLE-SPECIFIC DIFFERENTIALLY-METHYLATED REGIONS

3.1 Introduction

Epigenetics refers to all heritable changes in gene expression that are independent of nucleotide sequence and chromatin organization (*42*, *43*). These heritable changes are essential for maintaining the level of activity of a given gene during the propagation of one generation of cells to the next (*44*). Epigenetic features have been implicated in modulating chromatin to ensure that specific genes are expressed in a time-dependent manner to promote development into the appropriate cell types (*45*, *46*). These major epigenetic features of human cells include post-translational histone modifications, DNA methylation, and RNA-based mechanisms such as small noncoding micro-RNAs (*47*, *48*). All of these mechanisms work synergistically to dictate the transcriptional activity of a genome (*49*).

DNA methylation is typically observed at CpG dinucleotide sites, whereby methyl groups are added to the C5 position of cytosine bases that are followed by a guanine residue. This process of methylation and the maintenance of these patterns in mammals is carried out by three major DNA methyltransferases, DNMT1, DNMT3a, and DNMT3b (*49*, *50*). DNMT1 was the first characterized DNA methyltransferase, and it has been noted that this enzyme preferentially catalyzes hemi-methylated DNA (*51*). Therefore, DNMT1 is believed to be the primary enzyme responsible for copying methylation patterns from the parental to the daughter strand following DNA replication, making it the "maintenance methyltransferase" (*51*). Moreover, DNMT1 is heavily involved during S-phase, as it is integral for the preservation of methylation patterns across generations of cells (*51*). Much like DNMT1, DNMT3a and DNMT3b are responsible for the establishment of DNA methylation patterns early in mammalian development; however, these enzymes are also involved in methylating the DNA of germ cells (*49*). Furthermore, DNMT3a and

DNMT3b are regarded as *de novo* DNA methyltransferases, as they do not exhibit any significant preference between hemimethylated and unmethylated DNA (*52*). It should be noted that 40% of genes are rich with CpG clusters, known as CpG islands, and 70% of the CpG sites within an island are methylated (*48*, *53*). Upon investigating the role of methylated CpGs, it has been found that these islands act as docking sites for methyl binding proteins (*48*, *54*). These bound proteins then come together in order to recruit chromatin remodeling complexes that promote chromatin condensation and therefore, gene inactivation (*48*, *54*). Given the role of methylation in the silencing of gene expression, which can be used to dictate the fate of a cell, differentially methylated regions can be exploited to indicate the origin of circulating cfDNA.

In order to analyze single-cytosine methylation levels, and therefore, differentially methylated regions within the human genome, the technique of whole genome bisulfite sequencing (WGBS) can be employed. This process begins with the bisulfite conversion of the DNA of interest, whereby unmethylated cytosines are converted to uracil bases and read as thymine when sequenced, while methylated cytosines are protected and remain intact (*55*). Several algorithms are then employed to computationally map the bisulfite converted reads to the reference genome, which allows for the methylated and unmethylated cytosine to be identified to create "methylomes" for various cell types (*55*). These methylomes have since been employed as a unique identification tool that can allow cfDNA to be mapped back to the cell or organ type that it originated from, prior to its fragmentation and release into the circulation due to apoptosis (*23*). This was demonstrated in type-1 diabetes and islet-graft recipients, whereby pancreatic β-cell cfDNA was identified and quantified in the circulation of these patients using the differentially hypomethylated *INS* promoter region (*23*). In addition to this, regions that were differentially methylated in oligodendrocyte were used to detect elevated levels of cfDNA derived from the

increasing number of oligodendrocytes undergoing apoptosis within relapsing multiple sclerosis patients (*23*). Moreover, glial-specific DMRs were utilized to identify and quantify the increased concentration of cfDNA derived from the brain, within the circulation of patients who had suffered from severe traumatic brain injuries (*23*). Thus, this proof-of-concept study demonstrated that the organ from which cfDNA originated and the rate at which the given cell type undergoes apoptosis could be determined in humans. Furthermore, this approach could theoretically be adapted to identify cfDNA derived from any cell type in the body, on the basis of identifying DMRs specific to the organ of interest. This provides an alternative and minimally invasive method for diagnosing and monitoring a broad spectrum of human pathologies, such as acute cellular rejection following heart transplantation.

3.2 Hypothesis and Specific Aims for Chapter Four

Current cfDNA-based assays that have been developed for the non-invasive detection of ACR following HT have focused on the use of informative and donor-specific SNPs. However, as previously mentioned, the utility of these assays has been compromised by either the requirement of *a priori* knowledge of both the donor and recipient's genomes or the use of algorithms that estimate the concentration of dd-cfDNA on the basis of theoretical SNP frequencies. Thus, an alternative to quantifying the donor's "genetic fingerprint" would be to quantifying the donated organ's "fingerprint", which in this case would be its organ-specific methylation patterns. As such, we **hypothesize** that ventricle-specific DMRs, which can be detected on cfDNA released from ventricular cells undergoing apoptosis due to ACR, could be a useful and potentially superior non-invasive method for the quantification of dd-cfDNA and assessment of the severity of rejection.

Specific Aims:

1) To identify candidate ventricle-specific DMRs *in silico.*
2) To retrospectively validate candidate ventricle-specific DMRs *in vitro* using blood samples taken from heart transplant recipients during biopsy-proven rejection and quiescence.
3) To correlate the quantity of the candidate ventricle-specific DMRs within the recipient's plasma to both the ISHLT rejection grade and level of myocardial apoptosis.

3.3 Materials and Methods

3.3.1 Patient Data

Adult heart transplant recipients undergoing routine endomyocardial biopsies at the Foothills Medical Centre were recruited to provide 8-10 mL of whole blood immediately prior to the biopsy. All patients provided informed written consent for participation in this study which was approved by the CHREB (REB14-1244). Blood samples were taken from the jugular vein, the same point of entry for the EMB, which limited the invasiveness of the sample collection process. These samples were utilized for the *in vitro* validation of the utility of ventricle-specific differentially methylated regions for the identification and quantification of cfDNA released from the donated heart due to ACR. Of the 47 patients recruited, four patients were selected for analysis (Table 2). These patients had no signs of antibody-mediated rejection, were over two weeks post-HT, and had at least five serial samples with a range in the severity of rejection over time.

Table 2. The demographics of four heart transplant recipients selected for the *in vitro* validation of candidate ventricle-specific differentially methylated regions as a cfDNA-based blood biomarker for the detection of ACR.

Parameter	Patient Fraction
Sex (Male:Female)	1:3
Mean Age	62.25
Race (%)	
Caucasian	100
Mean Days Post-HT at Recruitment	54

3.3.2 *In Silico* Identification of Candidate Ventricle-Specific DMRs

Publicly available datasets from the NIH Roadmap Epigenomics (*56*) and the Blueprint Epigenome (*57*) projects were used to obtain methylomes from various tissues and cells within the human body (Appendix III). From these datasets, the University of Calgary's computing cluster Helix was used to convert each file from a BigWig or Wig format into sorted bedgraph files (Appendix IV). From there, the software package Metilene (*58*) was used to create input files for the comparison of the methylomes of the ventricular tissue to both non-ventricular tissues in the human body, as well as, the various hematopoietic cells. The methylomes of the various hematopoietic cells were not pooled with the methylomes of various other tissues during the comparison with ventricular methylomes. This was because of the importance of developing an assay that had the capacity to distinguish between cfDNA derived from the ventricles and hematopoietic cells, as the natural turnover of these cells was the primary contributor to the total cfDNA pool within the recipients' plasma and source of background noise.

Metilene compared the assembled methylomes by removing all non-informative segments and identified regions within the genome that had significant differential methylation, and were therefore, potential DMRs (*58*). Essentially, DMRs were identified on the basis of a mean methylation level of all CpG sites within the given region, measured as a percentage (*58*). As such, an initial filtering step was used to ensure that the mean methylation differences were greater than 10%. From here, additional parameters were established, whereby a minimum of 3 CpG sites must be present within each DMR, with no more than 25 bp separating each of the CpG sites. This was followed by a second filtering step that identified DMRs with a mean methylation difference of 50-80%. Metilene incorporated a Mann-Whitney U test at each filtering step to assesses the statistical significance of the mean methylation differences of the compared groups using an alpha

value of 0.05. This improved the likelihood that the selected regions were in fact differentially methylated when tested *in vitro*. Notably, the DMRs were constrained to a total length of no more than 100 bp so that the DMR could be detectable within a single fragment of cfDNA. Also, DMRs on sex chromosomes were omitted to avoid any dosage variation across HT patients. Thus, common DMRs found on autosomal chromosomes from the comparison of both the ventricular tissues versus non-ventricular tissue methylomes and ventricular tissue versus hematopoietic cell methylomes provided the list of candidate DMRs for further validation (Table 3). Details regarding the scripts used to perform these steps are outlined in section IV of the Appendix.

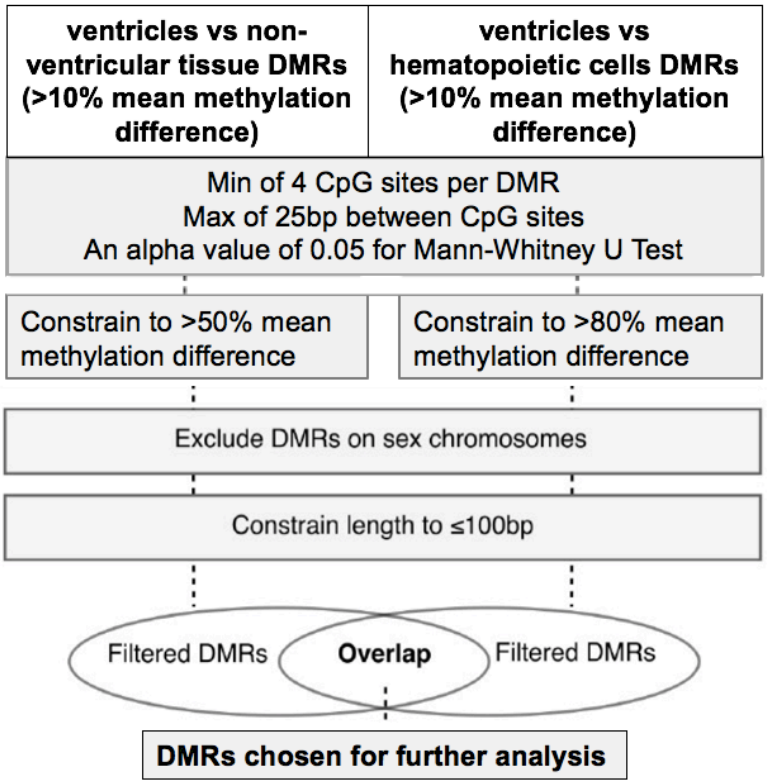

Figure 9. The workflow for the *in silico* identification of ventricle-specific DMRs. The process of separately interrogating publicly available methylomes of human non-ventricular tissues and hematopoietic cells against ventricular methylomes using the software Metilene for the identification of ventricle-specific DMRs.

3.3.3 Primer Design

The resulting sequences of the candidate DMRs, as well as, approximately 100 bp upstream and downstream of these regions, were determined by referring back to the ventricular tissue methylome (GSM1010978) from the NIH Roadmap Epigenomics project. These sequences then acted as the input for the software MethPrimer (*59*), which was utilized to generate primers (Table 4) for the amplification of the candidate DMRs from bisulfite converted DNA. Specific parameters were used to ensure that the primers did not contain CpG islands so that no preferential amplification would occur between methylated and unmethylated regions of template DNA. Furthermore, each primer contained at least two non-CpG cytosines, which allowed for enhanced amplification of bisulfite converted fragments. In addition to this, we ensured that the target melting temperatures of the primers were kept within 55^0 C - 65^0C. Finally, the total product size was constrained to no more than 150 bp, but ideally 120 bp, to allow for the amplification of these regions within the small cfDNA fragments, which are 165 bp in length, on average. The resulting primer sequences obtained from the MethPrimer software (*59*) were then submitted to the University of Calgary's Core Oligonucleotide Synthesis Laboratory to be synthesized.

3.3.4 Determining Tm of Primers

In order to determine the appropriate temperature that would allow for optimal primer annealing, a temperature gradient experiment was conducted. Each 200 µL PCR tube contained a total of 25 µL of reaction mixture. This mixture was comprised of 5 µL of 5X EpiMark® Hot Start Taq Reaction Buffer (New England BioLabs), 0.5 µL of 10 mM dNTP mix (Invitrogen), 0.5 µL of 10 µM forward primer, 0.5 µL of 10 µM reverse primer, 1.0 uL of 10 ng/µL bisulfite converted control human DNA (Qiagen), 0.125 µL of 5.00 U/mL EpiMark® Hot Start Taq DNA Polymerase

(New England BioLabs), and 17.38 μL of RNAse-free water to ensure the total volume was 25 uL. It should be noted that a master mix for each set of primers for a given DMR was created to reduce errors associated with pipetting volumes into each individual tube. Furthermore, the reagents were added in the order mentioned above. The tubes were then placed in the thermocycler and the PCR reaction was allowed to take place as follows: 3 minutes at 94^0 C, 45 seconds at 94^0 C, 45 seconds at one of eight temperatures between 55^0 C - 65^0 C, 1.5 minutes at 68^0 C, steps 2-4 were repeated 40X, 10 minutes at 68^0 C, followed by an infinite hold at 4^0 C (Appendix I).

3.3.5 Production, Running, and Imaging of the 3% Agarose Gel

Small agarose gels with a 3% concentration were created by dissolving 1.50 g of UltraPure™ Agarose (Thermo Fisher Scientific) into 50 mL of 1X TAE buffer. For the purpose of imaging, 5 μL of SYBR Green dye (10,000X in DMSO) (Invitrogen) was mixed into the dissolved agarose solution prior to pouring the gel into the casting tray. Then, 2 μL of 6X DNA loading dye was added to 10 μL of the PCR products and 7 μL of the dyed products were loaded into the wells of the gel while immersed in 1X TAE buffer within the chamber. The gels were allowed to run for 45 minutes at 105 V. The gels were then imaged immediately after using the BioRad ChemiDoc Gel Imaging System under UV light.

3.3.6 Extraction of Cell-Free DNA from Whole Blood

Prior to each routine EMB, consented heart transplant recipients provided 8-10 mL of whole blood, which was extracted from the right jugular vein, the same point of entry for the biopsy, and transferred to Streck BCT tubes. These tubes contained a preservative that limited cell lysis, thereby minimizing contamination of the plasma from genomic DNA of hematopoietic cells. From

there, the whole blood was centrifuged at 1900 x g at room temperature for 10 minutes to fractionate the blood. Then, the entire plasma layer was transferred into 2-3 2.0 mL Eppendorf tubes, which were then centrifuged at maximum speed (13,000 RPM) for 16 minutes at 4^{o}C. The resulting supernatant was then transferred into new 2.0 mL Eppendorf tubes and stored at -80^{o}C until the cfDNA was ready for isolation. Isolation was performed using the semi-automated MagNA Pure 24 System (Roche), which allowed 23 samples from four patients (patient 1002: n=5; patient 1017: n=8; patient 1021: n=5; patient 1025: n=5) to be processed in a single run (Appendix I). These served as samples for testing the utility of ventricle-specific differentially-methylated regions for the detection and quantification of cfDNA released from the donated heart due to varying degrees of acute cellular rejection.

3.3.7 Bisulfite Conversion

This process began with the bisulfite conversion of the DNA of interest, whereby unmethylated cytosines were converted to uracil bases and read as thymine when sequenced, while methylated cytosines were protected and remained intact. The protocol outlined in the Epitect Bisulfite Kit (Qiagen) was used to bisulfite convert the extracted cfDNA samples. However, modification to the procedure were made to improve the final yield. As such, the buffer EB was warmed to 56^{0}C prior to elution in step 17. In addition to this, step 17 was carried out twice using 20 µL of the warmed EB buffer each time to obtain one elution with a high concertation of cfDNA, followed by a second elution, which contained the remaining cfDNA not obtained in the first elution.

3.3.8 Genomic DNA Panel

Commercially available genomic DNA obtained from various human tissues (Zyagen), each of which was derived from one of the three germ layers, was purchased in order to create a panel. This panel was comprised of gDNA from the brain, colon, esophagus, intestine, kidney, liver, lung, pancreas, stomach, skin, spinal cord, skeletal muscle, spleen, and thymus. As such, we were able to compare the methylation levels at each of the three regions of interest within gDNA derived from not only the ventricles but the other diverse tissues as well. This was done by bisulfite converting each gDNA sample, PCR amplifying the regions of interest, and sequencing the resulting amplicons. This ultimately allowed us to determine whether the methylation patterns within the two regions on chromosome 9 and the single region on chromosome 12 were in fact ventricle specific.

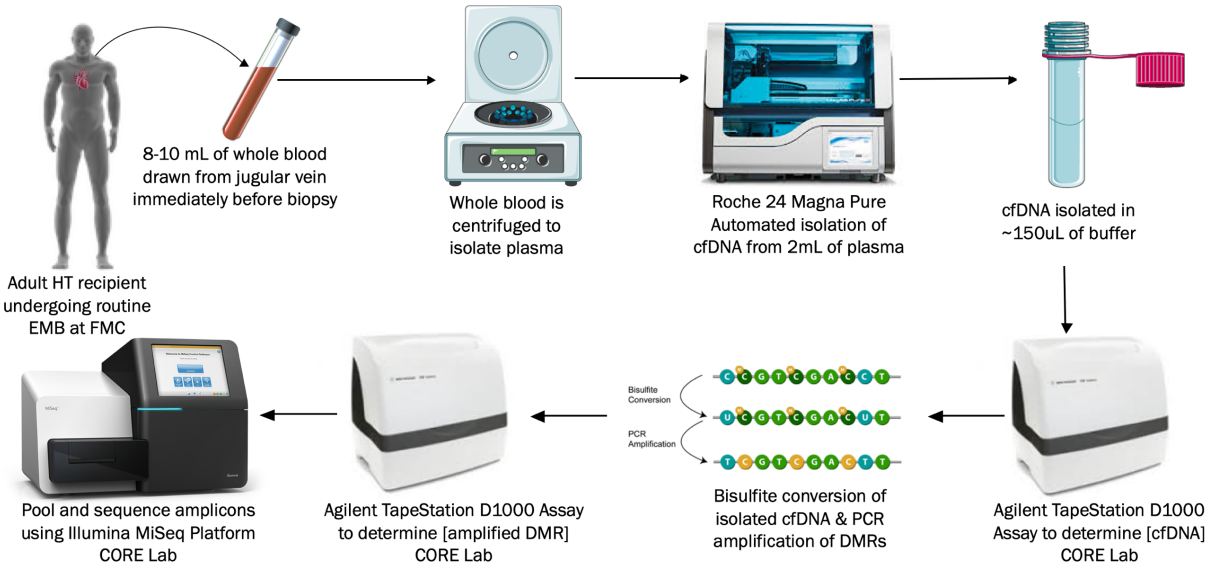

Figure 10. The workflow for DMR validation. A schematic of the process of obtaining cfDNA from HT patients in order to identify and quantify the amount of dd-cfDNA within the recipients' plasma.

3.3.9 PCR Amplification of DMRs from Patient Samples

Following the extraction of cfDNA from patient plasma samples, the cfDNA from each was then bisulfite converted and functioned as the template DNA for the PCR amplification of the three DMRs of interest. More specifically, a master mix that contained the general reagents for each PCR reaction was created to ensure minimal pipetting errors associated with the use of small volumes. Overall, each 200 μL PCR tube contained 5 μL of 5X EpiMark® Hot Start Taq Reaction Buffer (New England BioLabs), 0.5 μL of 10 mM dNTP mix (Invitrogen), 0.5 μL of 10 μM forward primer, 0.5 μL of 10 μM reverse primer, 1.0 uL of 10 ng/μL bisulfite converted control human DNA (Qiagen), 0.125 μL of 5.00 U/mL EpiMark® Hot Start Taq DNA Polymerase (New England BioLabs), and 17.38 μL of RNAse-free water to ensure the total volume was 25 uL. The tubes were then vortexed and centrifuged to ensure all reagents were sufficiently incorporated at the bottom of each tube. Finally, the tubes were then placed in the thermocycler and the PCR reaction was allowed to take place as follows: 3 minutes at 94^0 C – 3 minutes, 45 seconds at 94^0 C, 45 seconds at the determined Tm of the given primer, 1.5 minutes at 68^0 C, steps 2-4 were repeated 40X, 10 minutes at 68° C, followed by an infinite hold at 4^0 C.

3.3.10 Amplicon Pooling

In order to maximize the efficiency of the sequencing runs performed on the Illumina MiSeq sequencing platform, amplicons of each of the three DMRs amplified from the same template DNA were pooled together in equimolar amounts. The molarity of each PCR product was determined through a high sensitivity TapeStation performed by the Core Laboratory at the University of Calgary. Overall 63 μL of total solution was submitted in each tube. Therefore, 21 μL the amplicon with the lowest molarity was added to the pool while the remaining two amplicons were diluted

with pure water to the same molarity within 21 μL of solution to produce an equimolar mixture. For example, when amplifying Chr 9-2 within the bisulfite converted cfDNA obtained from the plasma of patient 1002 prior to the 11th biopsy, the molarity of the amplicon was 4.38 nM (Appendix V, Table 25), while the amplicon of Chr 9-1 had a molarity of 19.7 nM (Appendix V, Table 24), and the amplicon of Chr 12 had a molarity of 6.37 nM (Appendix V, Table 26). Therefore, 21 μL of the Chr 9-2 amplicon solution was added to the pool (Appendix V, Table 25), while 4.67 μL of the Chr 9-1 amplicon solution (Appendix V, Table 24), diluted with 16.33 μL of pure water, was added along with 14.44 μL of the Chr 12 amplicon solution (Appendix V, Table 26), which was diluted with 6.56 μL of pure water. This resulted in a 63 μL solution with a molarity of 4.38 nM. The volume of each amplicon required to obtain the desired molarity within 21 μL of solution was determined using the $C_1V_1=C_2V_2$ equation.

3.3.11 Amplicon Sequencing Using Illumina MiSeq

The Illumina MiSeq sequencing platform was implemented as it had the capacity to perform deep sequencing of PCR amplicons and allowed for cost-effective analysis of several genomic regions in a single run. The pooled samples were given to the University of Calgary Core Laboratory where sequencing libraries were prepared using the Illumina MiSeq library preparation kit. Libraries were then sequenced using the v3 MiSeq reagent kit v3 (150 cycles) to produce 2x75 bp paired-end reads. The results of the run, provided in .fastq format, were then accessed through the BaseSpace Sequencing Hub. The quality of each sequenced pool was assessed by generating a FastQC (*60*) report for each file, where a Q score ≥30 was used as a threshold.

3.3.12 Analysis of Bisulfite-Sequenced Runs

The bisulfite sequencing plugin for the CLC genomics workbench (Qiagen) was utilized to analyze the bisulfite sequenced reads. Reads were mapped such that the entire length of the read aligned with no less than 80% similarity to the hg19 reference genome. Therefore, all non-specific reads and broken pairs were discarded. Methylation levels were determined for each individual CpG site within each of the DMRs on chromosome 9 and 12 using the methylation caller of the bisulfite sequencing plugin. Mean methylation levels were then calculated based on the methylation levels of the individual CpG sites within each of the three DMRs of interest.

3.3.13 Determination of Concentration of Total cfDNA & DMRs within Recipients' Plasma

The total concentration of cfDNA, in copies/mL, within the heart transplant recipients' plasma was determined by multiplying the concentration of total cfDNA extracted from 2 mL of patient plasma in ng/μL, as determined by a high sensitivity TapeStation, by 1000 μL/mL to obtain the concentration of cfDNA in ng/mL. This concentration was then divided by 0.00303 ng, which is the approximate mass of a single human genome, and provided the total copies of cfDNA per millilitre of plasma (*23*, *61*). In order to determine the absolute concentration of each DMR within the recipients' plasma in copies/mL, the fraction of unmethylated molecules within the given pool of amplicons, as determined from the analysis of the bisulfite sequenced reads, was multiplied by the total concentration of cfDNA extracted from the initial plasma sample in ng/mL, then divided by 0.00303 ng. Sample calculations are provided in Appendix V.

3.4 Results

3.4.1 Ventricle-Specific DMRs Identified *In Silico*

Publicly available methylomes were obtained from both the NIH Roadmap Epigenomics (*56*) and the Blueprint Epigenome (*57*) projects. This included methylomes from hematopoietic cells (n=14), non-ventriclular tissues (n=19), as well as left and right ventricles (n=3) (Appendix III). Interestingly, *in silico* analysis of 6 right ventricle and 6 left ventricle methylomes curated within the lab by Dimple Prasher using RRBS indicated that the left and right ventricles were epigenetically similar, as only 4 regions were found to be differentially methylated amongst the interrogated methylomes (Figure 11). It should also be noted that one region was found to be hypomethylated in the left ventricle, relative to the right ventricle, by approximately 20% (Figure 11). The mean methylation difference of another two regions that were hypermethylated in the left ventricle were just over 20%, while the remaining region was also hypermethylated in the left ventricles and had a mean methylation difference of nearly 40% (Figure 11). Therefore, the three publicly available ventricular datasets were combined during the comparison of ventricular methylomes and all other tissue or cellular methylomes. After comparing the ventricular methylomes to the 19 tissue methylomes, with a minimum mean methylation difference of 50%, 255 DMRs were identified, majority of which were hypomethylated in the ventricles relative to the other tissues (Figure 12A). The comparison of the ventricular methylomes to the 14 methylomes of hematopoietic cells, with a minimum mean methylation difference of 80%, 2,060 DMRs were identified, with a more even distribution between hypomethylated and hypermethylated regions (Figure 12B). Of these datasets, 24 DMRs were common to both and located on autosomal chromosomes. From these 24 ventricle-specific DMRs, 10 with the highest mean methylation differences were selected for further interrogation (Table 3).

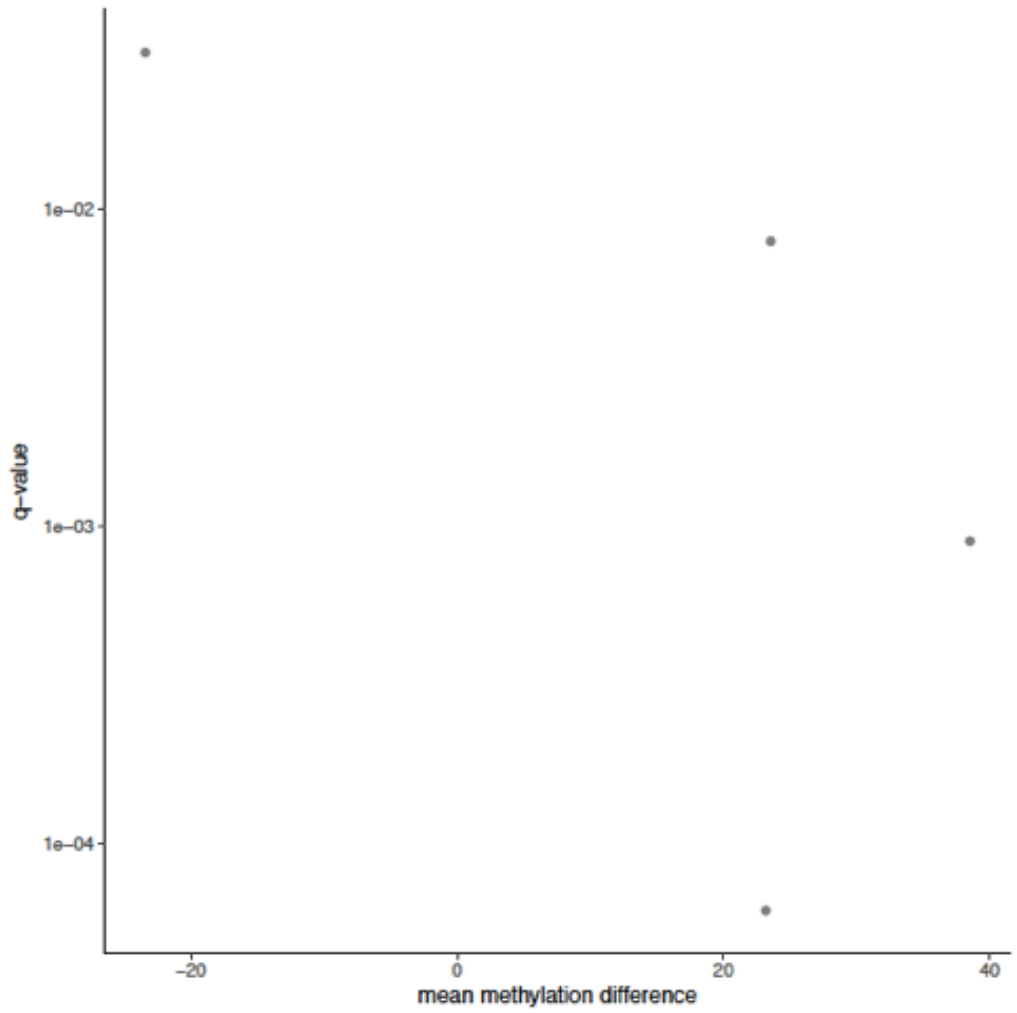

Figure 11. The DMRs identified *in silico* from the comparison of left and right ventricle methylomes. The mean methylation difference and associated q-value, which is a measure of significance in terms of the false discovery rate rather than the false positive rate, of four DMRs identified from the comparison of 6 human left ventricle methylomes and 6 human right ventricle methylomes using the software Metilene. The mean methylation differences below zero represent regions that are hypomethylated in the left ventricle, relative to the right ventricle. Conversely, positive mean methylation differences represent regions that are hypermethylated in the left ventricle, relative to the right ventricle. The ventricular methylomes were generated in the Greenway Lab by Dimple Prasher using gDNA from human left and right ventricle tissue samples and RRBS.

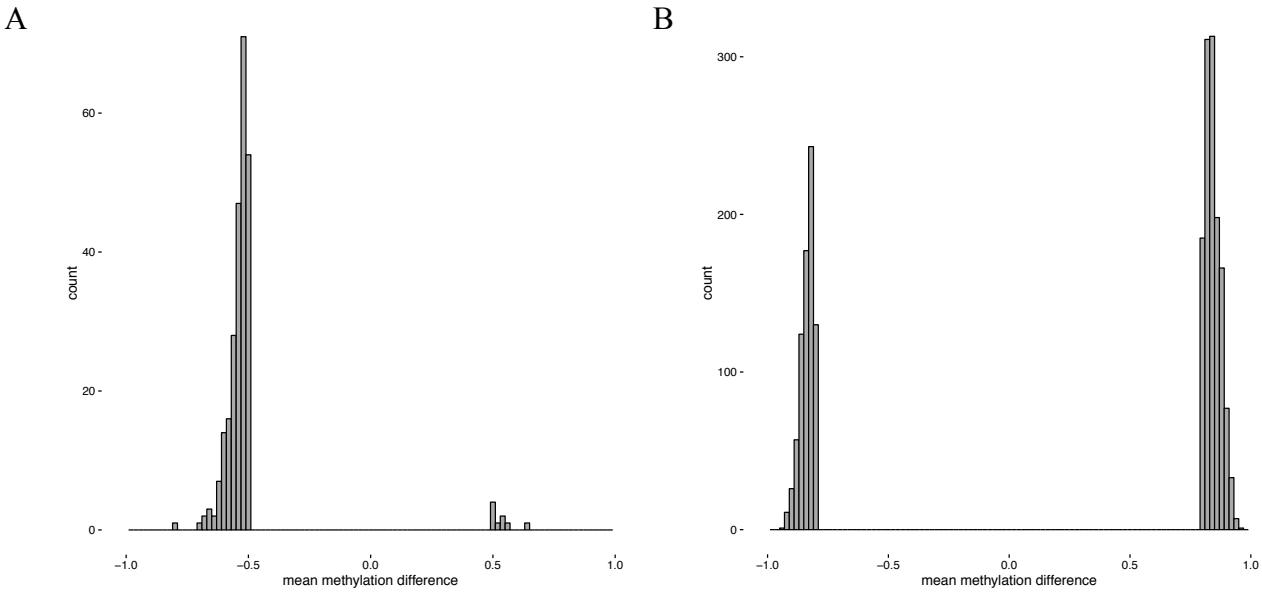

Figure 12. The DMRs identified *in silico* from the comparison of ventricular methylomes to other tissues and hematopoietic cells within the human body. The number of DMRs and associated mean methylation differences obtained from the comparison of publicly available human ventricular tissue methylomes (n=3) and human non-ventricular tissue methylomes (n=19) (A). The number of DMRs and associated mean methylation differences obtained from the comparison of publicly available human ventricular tissue methylomes (n=3) and human hematopoietic cell methylomes (n=14) (B).

Table 3. Candidate DMRs chosen for further validation, including DMR position and length, number of CpG sites within each DMR, and mean methylation difference as a percentage. The bolded and starred DMRs indicate the three regions that were selected for complete validation.

Chr	Start Position	End Position	DMR Length	# of CpG Sites	Mean Methylation Difference (%)	
					Ventricles vs. Non-Ventricle Tissue	Ventricles vs. Hematopoietic Cells
1	98233085	98233139	54	4	57.43	80.95
2	86256014	86256083	69	6	55.94	82.21
5	14806789	14806833	44	5	51.00	81.98
9*	**101595534**	**101595574**	**40**	**3**	**56.90**	**81.89**
9	127014429	127014496	67	6	50.74	80.66
9*	**130622579**	**130622629**	**50**	**5**	**60.65**	**82.11**
12*	**106132052**	**106132096**	**44**	**6**	**55.29**	**80.10**
14	105618787	105618853	66	7	54.08	81.10
15	77265443	77265483	40	4	50.03	81.67
19	17193075	17193123	48	4	52.33	80.95

3.4.2 Primer Validation for Amplifying Ventricular DMRs

Using the software MethPrimer, and the sequences of regions that included the candidate DMRs, potential primer sets were identified for each DMR (Table 4). The specificity and optimal melting temperature of the generated primers was determined by PCR using a temperature gradient; the resulting products were visualized on a 3% agarose gel. As such, the primers generated for the amplification of the DMRs on chromosome 1, 2, and 9:127,014,429-127,014,496 were not successful as no bands were visible on the agarose gel (data not shown). In contrast to this, the primer set generated for the amplification of the DMR on chromosome 5 produced bands of DNA in lanes 7, 8, and 9 with a length of approximately 150 bp (Figure 13). However, it should also be noted that a clear band of contamination, approximately 75 bp in length, was also seen in those lanes (Figure 13). Therefore, this specific primer set lacked specificity and resulted in unwanted off-target amplification. This was also the case for the primer sets that were generated for the amplification of the DMRs on chromosome 14 and 19, whereby a strong band of DNA with a length of approximately 130 bp was visible. However, due to off-target amplification, contaminating bands of DNA approximately 60 bp in length were also observed (data not shown).

The forward and reverse primers generated by MethPrimer for the DMRs on Chr 9-1, 9-2, as well as, Chr 12 and chromosome 15 successfully resulted in the amplification of a single strong band with no off-target amplification observed. The expected product size for the amplification of the DMR on chromosome 15 from bisulfite converted control human DNA was 105 bp (Table 4) and upon amplification, the actual product size was 108 bp with an optimal melting temperature of 58.5°C (data not shown). Interestingly, when the same forward and reverse primers were used to amplify the DMR on chromosome 15 from cfDNA extracted from the plasma of HT patient 1025, amplification was not successful as the gel did not display any visible bands (data not

shown). The expected product size for the amplification of the DMR on Chr 9-1 from bisulfite converted control human DNA was 127 bp (Table 4) and upon amplification, the actual product size was 151 bp with an optimal melting temperature of 56.9°C (Figure 14A). The expected product size for the amplification of the DMR on Chr 9-2 from bisulfite converted control human DNA was 105 bp (Table 4) and upon amplification, the actual product size was 102 bp with an optimal melting temperature of 61.1°C (Figure 14B). The expected product size for the amplification of the DMR on Chr 12 from bisulfite converted control human DNA was 145 bp (Table 4) and upon amplification, the actual product size was 155 bp with an optimal melting temperature of 58.5°C (Figure 14C). Once again as a preliminary test, cfDNA extracted from the plasma of heart transplant patient 1025 was used as template DNA for the PCR reaction to confirm that these DMRs could be amplified from cfDNA using the associated primers. As such, these three DMRs were successfully amplified from the cfDNA extracted from patient 1028 and therefore, became the three DMRs of interest for further testing within other HT patients.

Table 4. Forward and reverse bisulfite PCR primer sequences designed using MethPrimer for each DMR of interest, and the associated melting temperature of the primer sets. Dashes denote an inability to determine a successful melting temperature for the amplification of the given DMR without off-target amplification.

DMR (Chr)	Position	Expected Product Size (bp)	Forward Primer (5' → 3')	Reverse Primer (5' → 3')	Tm (°C)
1	98233085-98233139	129	ATTTTGTATGTT TTGTTTTTTTT	ATAATCTAATAA ATTTACTCCATC	-
2	86256014-86256083	148	GAAATGGTTAGG TAGAGTTGTTGA	AATCTCAATTTAAA AATAAAAAAAA	-
5	14806789-14806833	140	GTGGATTATTAG GAGAAGAGTAGG	TCACAAAAAAACAA TTAAAACTAATA	-
9-2*	**101595534-101595574**	**105**	**GGAGTTGGGTAG GAGGAGGTTAGG**	**TTCAAAAACCCAAC TACCAAATATAA**	**61.1**
9	127014429-127014496	119	AATAAAAAGAAATT AAATTTTTAGGTTTTG	CAAAATTACCTAAA ACAAACCTTCTC	-
9-1*	**130622579-130622629**	**127**	**GGAGTTGGGTAG GAGGAGGTTAGG**	**TTCAAAAACCCAA CTACCAAATATAA**	**56.9**
12*	**106132052-106132096**	**145**	**TGTGTTATTTTGTAT TTTAAAGTTTAGTAT**	**AAATAACTAAAACT ACTTTTTATTAACTTA**	**58.5**
14	105618787-105618853	123	TTTAGTTAGGTAG GGGTTGTAGTTTTG	AAATCCCAAAAT AACTCAAAAAAAA	-
15	77265443-77265483	105	TATTTGTTTTGG GAGAAGTTATTT	ACTATACAAAAAAA ACAAACTTAATATACA	-
19	17193075-17193123	116	ATAGTTTAGTGG GGTTTGTGAAGG	CTAACTAAAAAAA CTCTCAAATCTCCC	-

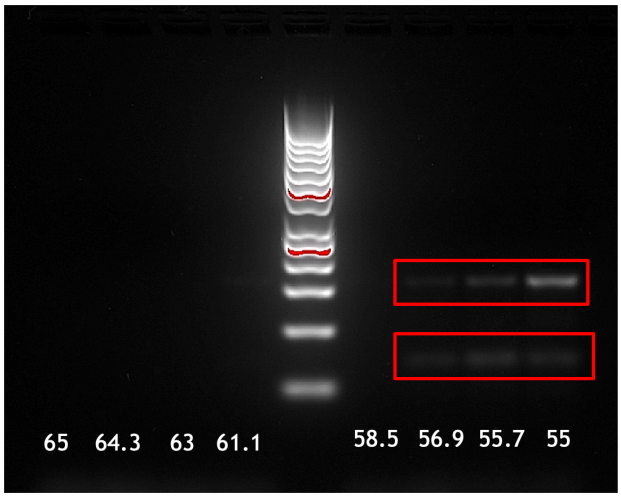

Figure 13. The identification of the optimal melting temperature for the amplification of the candidate ventricle-specific DMR at chromosome 5. The resulting gel from the optimization of the melting temperature for the DMR at chromosome 5. Each well contained 7μL the same reaction mixture, however, the melting temperature ranged from 65°C (lane 1) to 55°C (lane 9). A 50 bp ladder was used for reference (lane 5). The PCR products amplified from bisulfite converted control human DNA were combined with 6X DNA loading dye and the gel contained SYBR Green dye (10,000X in DMSO) to allow for visualization of the bands under UV light.

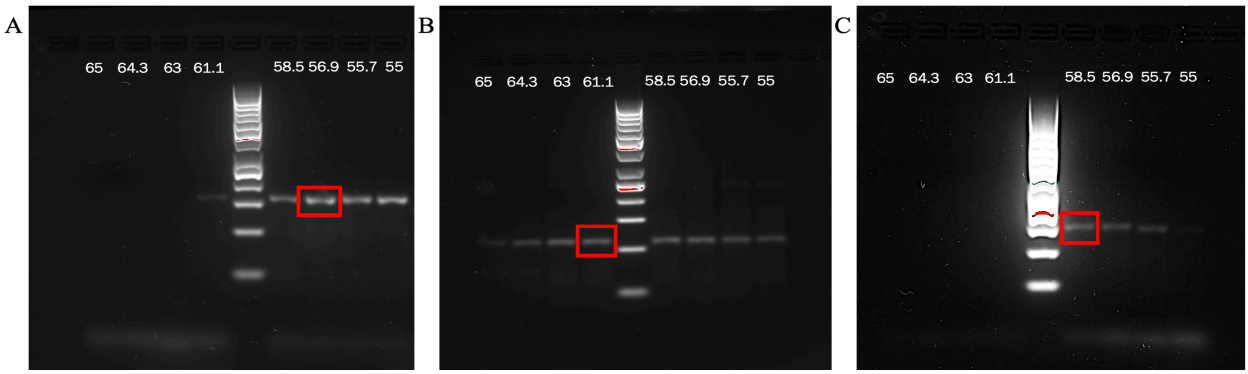

Figure 14. The identification of the optimal melting temperature for the candidate ventricle-specific DMRs at chromosome 9 and 12. The resulting gel from the optimization of the melting temperature for the DMRs at Chr 9-1 (A), Chr 9-2 (B), and Chr 12 (C). Each well contained 7µL the same reaction mixture, however, the melting temperature ranged from 65ºC (lane 1) to 55ºC (lane 9). A 50 bp ladder was used for reference (lane 5). The PCR products amplified from bisulfite converted control human DNA were combined with 6X DNA loading dye and the gel contained SYBR Green dye (10,000X in DMSO) to allow for visualization of the bands under UV light. The red box denoted the optimal melting temperature selected for further PCR reactions of each DMR.

3.4.3 Methylation Levels of Each DMR in Ventricular gDNA

Upon amplification of the DMR on Chr 9-1 and sequencing the resulting amplicons from bisulfite converted gDNA derived from left ventricle tissue, the five individual CpG sites within this DMR were found to be methylated in only 10-20% of the sequenced amplicons, with an overall average methylation level of 14.28% across the entire region (Table 5). The three individual CpG sites within the DMR on Chr 9-2 were found to be methylated in 18-26% of the sequenced amplicons from bisulfite converted gDNA derived from left ventricle tissue, with an overall average methylation level of 32.81% across the entire region (Table 6). Finally, the six individual CpG sites within the DMR on Chr 12 were found to the methylated in 16-22% of the sequenced amplicons from bisulfite converted gDNA derived from left ventricle tissue, with an overall average methylation level of 20.95% across the entire region (Table 7).

Table 5. Total sequencing coverage, methylation levels at each CpG site, and the overall methylation level within Chr 9-1 in gDNA extracted from human left ventricle tissue.

CpG Position	Total Coverage	Methylation Level (%)	Overall Methylation (%)
130622580	260174	15	**14.28**
130622588	260174	13	
130622614	259912	20	
130622622	259906	13	
130622628	259838	10	

Table 6. Total sequencing coverage, methylation levels at each CpG site, and the overall methylation level within Chr 9-2 in gDNA extracted from human left ventricle tissue.

CpG Position	Total Coverage	Methylation Level (%)	Overall Methylation (%)
101595535	121753	26	**22.67**
101595551	121640	24	
101595573	121524	18	

Table 7. Total sequencing coverage, methylation levels at each CpG site, and the overall methylation level within Chr 12 in gDNA extracted from human left ventricle tissue.

CpG Position	Total Coverage	Methylation Level (%)	Overall Methylation (%)
106132053	61079	19	**20.95**
106132055	61289	22	
106132057	61287	21	
106132059	61243	21	
106132071	61222	16	
106132095	61342	21	

3.4.4 *In Vitro* Validation of Ventricular DMRs - Genomic DNA Panel

In order to confirm that the three selected DMRs were in fact ventricle specific, we obtained genomic DNA from a variety of tissues within the human body, which encompassed all three developmental germ layers. All three regions of interest were the most unmethylated within the gDNA of the ventricles, whereby 85.8% of the reads were unmethylated within the region at Chr 9-1 (Figure 15A), 77.3% were unmethylated within the region at Chr 9-2 (Figure 15B), and 80.0% were unmethylated within the region at Chr 12 (Figure 15C). The largest methylation differences were observed in the region at Chr 9-1 when comparing the methylation level of this region in the ventricles and in the various other tissues within the human body (Figure 15A). More specifically, this region tended to be an average of 62.2% more unmethylated in the ventricles when compared to the other tissues. In contrast to this, the region at Chr 9-2 showed the smallest methylation difference when the levels observed in the ventricles at this region were compared to those in the gDNA from other tissues within the human body (Figure 15B). Notably, the methylation level at this region within gDNA from the pancreas and lungs was only found to be approximately 10% and 15% more methylated than in the ventricles, respectively (Figure 15B). Finally, the region of interest on Chr 12 was an average of 52.3% more unmethylated in the ventricles when compared to the methylation levels observed at this region in the other tissues within the human body (Figure 15C).

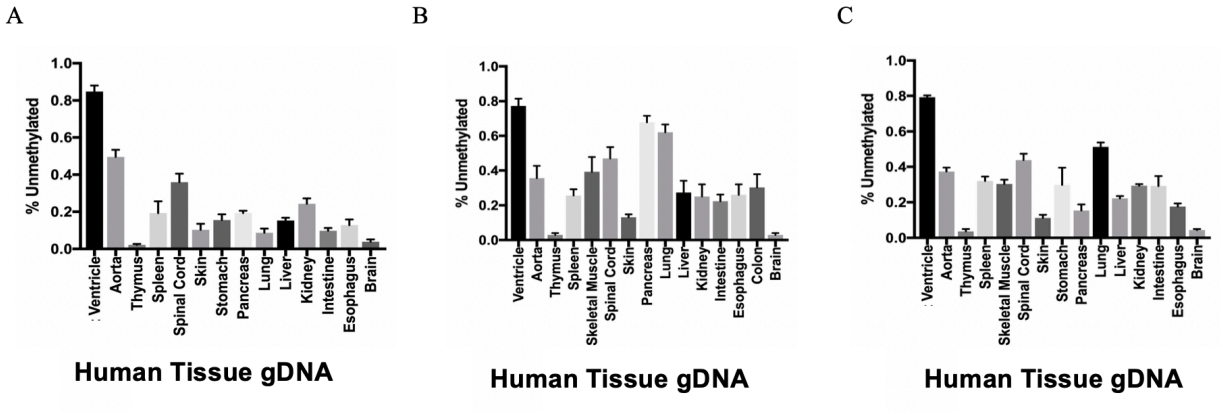

Figure 15. The methylation levels at the candidate ventricle-specific DMRs at chromosome 9 and 12 within bisulfite converted gDNA from various tissues in the human body. The percentage of unmethylated CpG sites within Chr 9-1 (A), Chr 9-2 (B), and Chr 12 (C) in genomic DNA obtained from the ventricles, highlighted in the red box, and various other tissues in the human body. Methylation levels were determined using bisulfite sequencing on the Illumina MiSeq sequencing platform. Bars represent standard deviation of the mean methylation difference.

3.4.5 Total cfDNA levels in Recipient Plasma During Varying Degrees of Rejection

The total concentration of cfDNA, in copies/mL, within the plasma of heart transplant patients 1002, 1017, 1021, and 1025 at each routine EMB was clustered based on the associated biopsy-proven ISHLT rejection grade. It was found that patient 1021 had a very high concentration of cfDNA during the 8th biopsy despite being assigned an ISHLT rejection grade of 0R, whereby 336,600 copies/mL of cfDNA were extracted from this recipient's plasma (Figure 16). In addition to this, patient 1021 also had an incredibly high concentration of cfDNA within their plasma during the third biopsy, which was assigned an ISHLT rejection grade of 1R, with 415,800 copies/mL of cfDNA present within this recipient's plasma (Figure 16). As such, the median concentration of cfDNA for these four patients when assigned an ISHLT rejection grade of 0R was found to be 41,696 copies/mL, while a median concentration of 63,030 copies/mL was observed at 1R, and 76,890 copies/mL when assigned an ISHLT rejection grade of 2R (Figure 16). However, when these two abnormally high samples were omitted the median concentration of cfDNA for these four patients when assigned an ISHLT rejection grade of 0R was found to be 25,311 copies/mL, while a median concentration of 53,130 copies/mL was observed at an ISHLT rejection grade of 1R (Figure 17). In general, the average total concentration of cfDNA within the plasma of these recipients increased as the severity of rejection increased. However, these differences in total cfDNA concentrations at each rejection grade were not found to be statistically significant as each cohort had a great deal of overlap in the total amount of cfDNA extracted from the recipients' plasma (Figures 16 and 17).

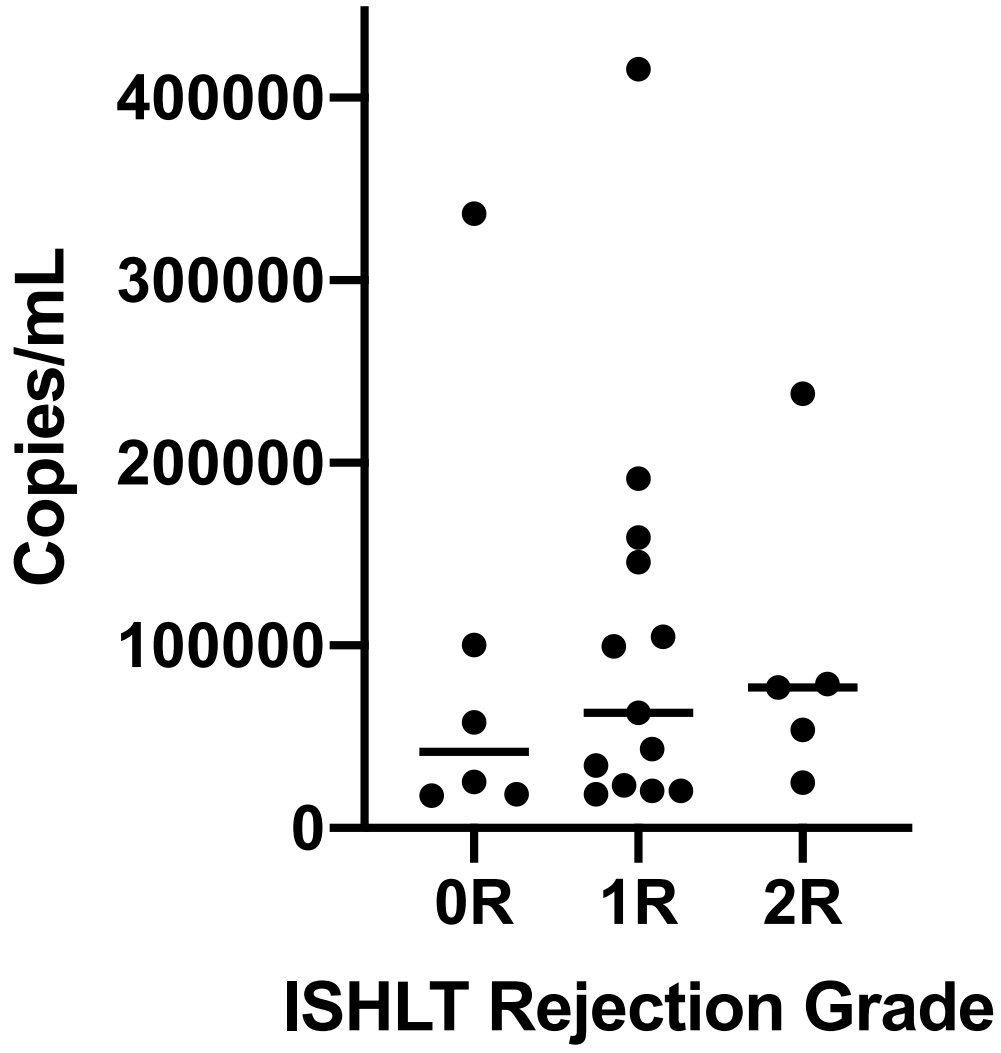

Figure 16. The total concentration of cfDNA within the plasma of patients 1002, 1017, 1021, and 1025 obtained immediately prior to routine EMBs. The total concentration (copies/mL) of cfDNA within the plasma of heart transplant patients 1002, 1017, 1021, and 1025 obtained immediately prior to each routine EMB, along with the associated biopsy proven ISHLT rejection grade. Median concentration is indicated by the line. No statistically significant difference was observed between each of the rejection grades when analyzed using a Mann-Whitney *U* test.

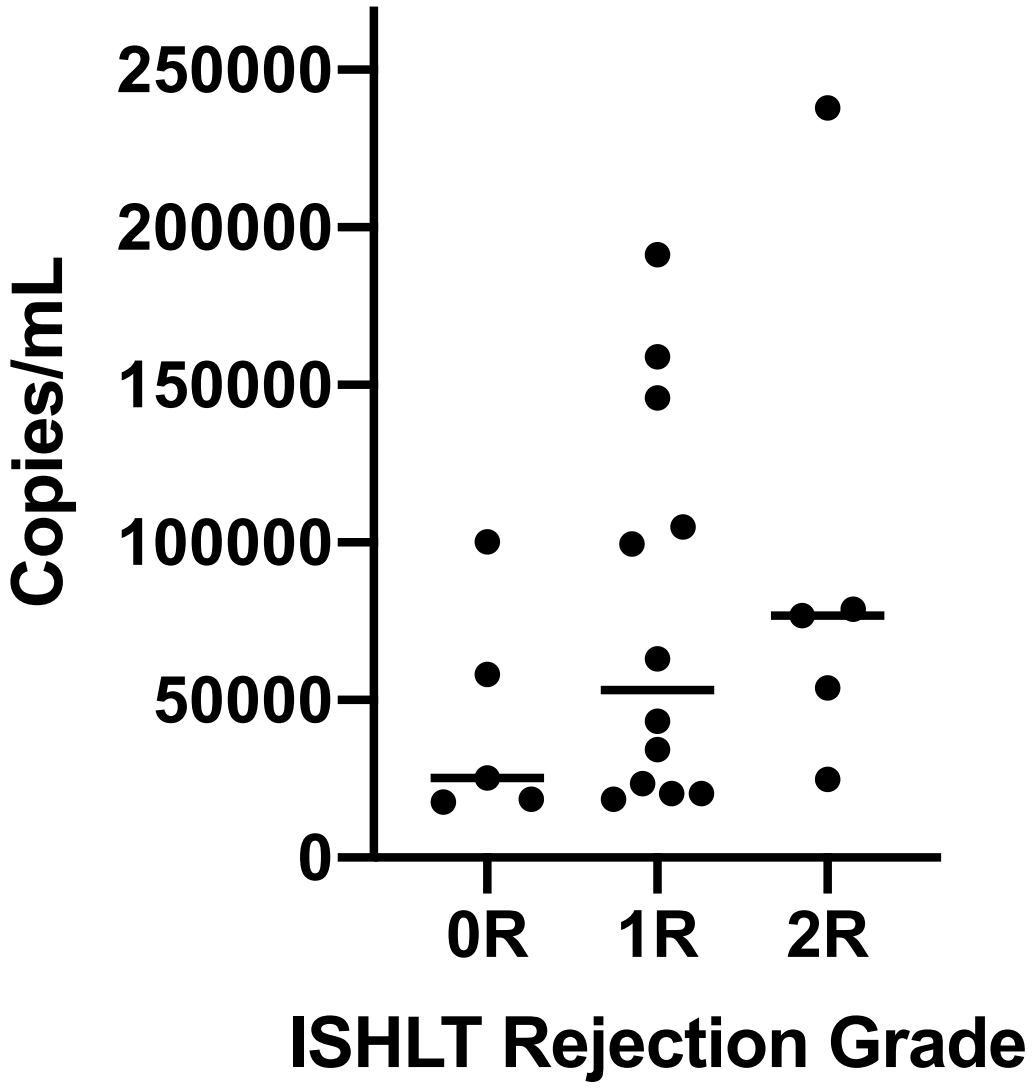

Figure 17. The total concentration of cfDNA within the plasma of patients 1002, 1017, 1021, and 1025 obtained immediately prior to routine EMBs with outliers omitted. The total concentration (copies/mL) of cfDNA within the plasma of heart transplant patients 1002, 1017, 1021, and 1025 obtained immediately prior to each routine EMB, along with the associated biopsy proven ISHLT rejection grade. Plasma samples with abnormally high concentrations of cfDNA were omitted. Median concentration is indicated by the line. No statistically significant difference was observed between each of the rejection grades when analyzed using a Mann-Whitney *U* test.

3.4.6 Characteristics of Input Materials for Each Patient

The total amount of cfDNA extracted from each plasma sample was determined using a high sensitivity TapeStation assay and ranged from 0.0415 ng/μL, which was obtained from patient 1017's 7th biopsy (Appendix V, Tables 30-32), to 1.26 ng/μL and was obtained from patient 1021's 3rd biopsy (Appendix V, Tables 27-29). The average total concentration of cfDNA extracted from the 23 plasma samples from patients 1002, 1021, 1017, and 1025 was 0.299 ng/μL. The concentration of the amplified DMR at Chr 9-1 ranged from 0.133-1.9 ng/μL, with an average concentration of 0.935 ng/μL (Appendix V, Tables 24, 27, 30, and 33). The concentration of the amplified DMR at Chr 9-2 ranged from 0.271-0.868 ng/μL, with an average concentration of 0.506 ng/μL (Appendix V, Tables 25, 28, 31, and 34). The concentration of the amplified DMR at Chr 12 ranged from 0.266-1.46 ng/μL, with an average concentration of 0.721 ng/μL (Appendix V, Tables 26, 29, 32, and 35). The peak molarity of the amplified DMR at Chr 9-1 ranged from 1.78-22.0 nM, with an average molarity of 11.0 nM (Appendix V, Tables 24, 27, 30, and 33). The peak molarity of the amplified DMR at Chr 9-2 ranged from 4.26-13.8 nM, with an average molarity of 8.02 nM (Appendix V, Tables 25, 28, 31, and 34). The peak molarity of the amplified DMR at Chr 12 ranged from 0.605-15.2 nM, with an average concentration of 7.11 nM (Appendix V, Tables 26, 29, 32, and 35).

3.4.6.1 DMR #1 – Chr 9-1

Plasma samples from patient 1002 were collected during the 11-15th biopsies, which took place 760-858 days post-HT. Interestingly, the cfDNA extracted from biopsies 11 and 12, which were both assigned rejection grades of 2R, resulted in very low proportions of unmethylated cfDNA that mapped to the region of Chr 9-1 (Table 8). More specifically, only 9% of the sequenced amplicons from this region were found to be unmethylated in both samples, and therefore, derived from the ventricles of the donated heart (Table 8). Conversely, the cfDNA extracted from the plasma samples taken at the 13th and 14th biopsies had relatively large amounts of unmethylated cfDNA from the region of Chr 9-1, despite having been assigned a rejection grade of 1R (Table 8). The region at Chr 9-1 that was amplified from the cfDNA extracted from patient 1002's 15th biopsy failed to be sequenced within the pool of amplicons, and therefore, no data could be collected for this DMR for this biopsy. Furthermore, the total amount of cfDNA extracted from patient 1002's plasma during the 11th and 12th biopsies was substantially lower than the total amount of cfDNA obtained from the 14th and 15th biopsies, despite the greater severity in rejection observed (Figure 18A). As such, the concentration of the DMR at Chr 9-1 was only 2,240 copies/mL and 4,840 copies/mL during the 11th and 12th biopsies, respectively, despite the assignment of a 2R rejection grade (Figure 18B). Conversely, the concentration of the DMR at Chr 9-1 was found to be 26,110 copies/mL during the 14th biopsy, when only mild rejection was suspected based on the histological analysis of the biopsied tissue samples (Figure 18B).

Plasma samples from patient 1021 were collected during the 1st, 3rd, and 6-8th biopsies, which took place 22-190 days post-HT. Once again, despite only having experienced mild or no rejection during these biopsies, the total amount of cfDNA extracted from this patient's plasma tended to be quite high (Figure 19A). This was particularly evident in the 3rd and 8th biopsies, in which a

rejection grade of 1R and 0R were assigned respectively (Figure 19A). As such, 13.2% of the amplicons from the region at Chr 9-1 were found to be unmethylated in the sample obtained from the 3rd biopsy, while and 22.4% of the amplicons were found to be unmethylated in the sample obtained from the 8th biopsy (Table 9). The region at Chr 9-1 that was amplified from the cfDNA extracted from patient 1021's 7th biopsy failed to be sequenced within the pool of amplicons, and therefore, no data could be collected for this DMR at this biopsy. Most notably, despite having been assigned a rejection grade of 0R at the 8th biopsy, patient 1021 was found to have 75,400 copies/mL of the DMR at Chr 9-1 in their plasma (Figure 19B). This was in sharp contrast to the 8,630 copies/mL and 5,110 copies/mL of this DMR detected in patient 1021's plasma during the 1st and 6th biopsies, respectively, which were also assigned rejection grades of 0R.

Plasma samples from patient 1017 were collected during the 6th-11th biopsies, as well as the 13th and 15th biopsies, which took place between 94-374 days post-HT. Notably, the fraction of unmethylated molecules detected from the amplification of the DMR at Chr 9-1 was quite high for all of the cfDNA samples extracted from the biopsies in which a rejection grade of 1R was assigned (Table 10). More specifically, 24.0-29.4% of the amplicons were found to be unmethylated at Chr 9-1 when mild rejection was experienced by this patient (Table 10). In contrast to this, only 8.4% and 15.0% of the amplicons of this DMR were found to be unmethylated within the plasma samples taken during moderate to severe rejection events at days 269 and 374, respectively (Table 10). As such, cfDNA derived from the ventricles of the donated heart accounted for a large fraction of the total amount of cfDNA within the recipient's plasma in these samples taken during each biopsy in which a rejection grade of 1R was assigned (Figure 20A). However, an increase in the total cfDNA within the recipient's plasma was also observed during the moderate to severe rejection episodes at days 269 and 374 post-HT (Figure 20A). Thus, a spike in the concentration

of this DMR at Chr 9-1 within the recipient's plasma was observed at day 374 post-HT during the moderate rejection event, with 11,830 copies/mL within the recipient's plasma (Figure 20B). However, this was not the case for the sample taken at day 269 post-HT, in which a rejection grade of 2R-3R was assigned following the biopsy (Figure 20B). Markedly, the cfDNA samples obtained at days 206 and 290 post-HT, where the patient experienced mild rejection, contained 6,830 copies/mL and 8,170 copies/mL of the DMR at Chr 9-1, respectively (Figure 20B). This was slightly higher than the concentration of this DMR within patient 1017's plasma at day 269 post-HT, which was found to be 6,460 copies/mL, despite having experienced moderate to severe rejection (Figure 20B). Another discrepancy that was observed occurred at days 150 and 178 post-HT, whereby patient 1017 was assigned a rejection grade of 1R and 0R, respectively. Despite this, the concentration of the DMR at Chr 9-1 within the recipient's plasma was higher at day 178 with 6,075 copies/mL, when no rejection was observed, than at day 150 when the patient experienced mild rejection but only 3,310 copies/mL of this DMR were detected (Figure 20B).

Plasma samples from patient 1025 were obtained during the 1st, 4th-7th, and 9th routine biopsies, which took place 40-236 days post-HT. The region at Chr 9-1 that was amplified from the cfDNA extracted from patient 1025's 1st biopsy failed to be sequenced within the pool of amplicons, and therefore, no data could be collected for this DMR for this biopsy. Strikingly, the amplification of the DMR at Chr 9-1 from the cfDNA obtained during the 5th and 9th biopsies resulted in 32.6% and 24.4% of the amplicons being unmethylated in this area, respectively, despite only having experienced mild rejection according to the biopsy (Table 11). In contrast to this, the amplification of this DMR from the cfDNA obtained during the 6th biopsy, in which a rejection grade of 2R was assigned, resulted in only 5.4% of the amplicons being unmethylated in this region (Table 11). Interestingly, while the concentration of total cfDNA extracted from the

plasma of patient 1025 at day 145 was highest when moderate rejection was experienced, the concentration of total cfDNA varied considerably across each of the biopsies that resulted in a diagnosis of mild rejection (Figure 21A). As a result, cfDNA that was unmethylated at Chr 9-1, and was therefore, derived from the ventricles of the donated heart, accounted for a large fraction of the total amount of cfDNA within the recipient's plasma in the samples taken during the 5th and 9th biopsies in which a rejection grade of 1R was assigned (Figure 21A). Thus, we did not observe a spike in the concentration of the DMR at Chr 9-1 within patient 1025's plasma at day 145, despite having experienced moderate rejection, as only 12,850 copies/mL of the DMR was detected (Figure 21B). Rather, at days 131 and 236 we observed 34,210 copies/mL and 46,700 copies/mL, respectively, of this DMR within the recipient's plasma despite the patient only having experienced mild rejection, according to histological analysis of the biopsied tissue samples (Figure 21B).

Table 8. Routine serial EMBs and associated biopsy-proven rejection grades, as well as, the total coverage, methylation levels at the individual CpG sites, and the overall methylation percentages, as determined from the amplification and bisulfite sequencing of Chr 9-1 from cfDNA obtained from patient 1002. Dashes indicate unsuccessfully sequenced amplicons.

Biopsy #	Biopsy-Proven Rejection Grade	CpG Position	Total Reads	Methylation Level	Overall % Methylation	Overall % Unmethylated
11	2R	130622580	15949	0.96	**91.0**	**9.0**
		130622588	15948	0.96		
		130622614	15929	0.97		
		130622622	15909	0.94		
		130622628	15902	0.72		
12	2R	130622580	17759	0.96	**91.0**	**9.0**
		130622588	17759	0.95		
		130622614	17743	0.98		
		130622622	17721	0.94		
		130622628	17699	0.72		
13	1R	130622580	6801	0.65	**67.8**	**32.2**
		130622588	6805	0.70		
		130622614	6801	0.70		
		130622622	6795	0.70		
		130622628	6793	0.64		
14	1R	130622580	17893	0.67	**73.8**	**26.2**
		130622588	17893	0.73		
		130622614	17888	0.73		
		130622622	17888	0.86		
		130622628	17884	0.7		
15	1R	130622580	-	-	**-**	**-**
		130622588	-	-		
		130622614	-	-		
		130622622	-	-		
		130622628	-	-		

A

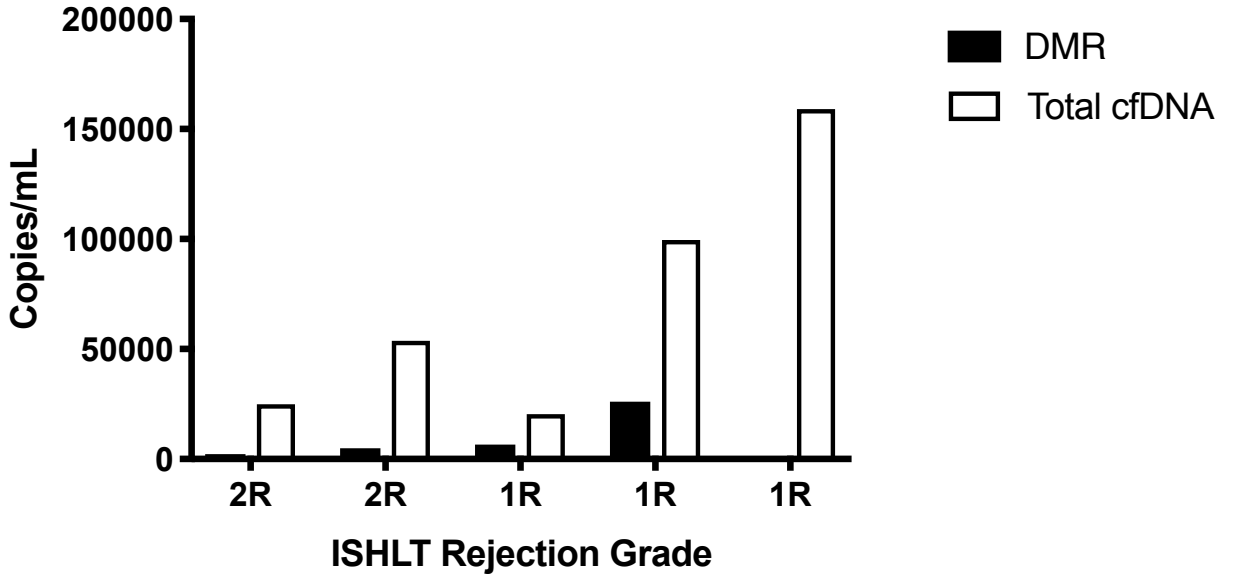

B

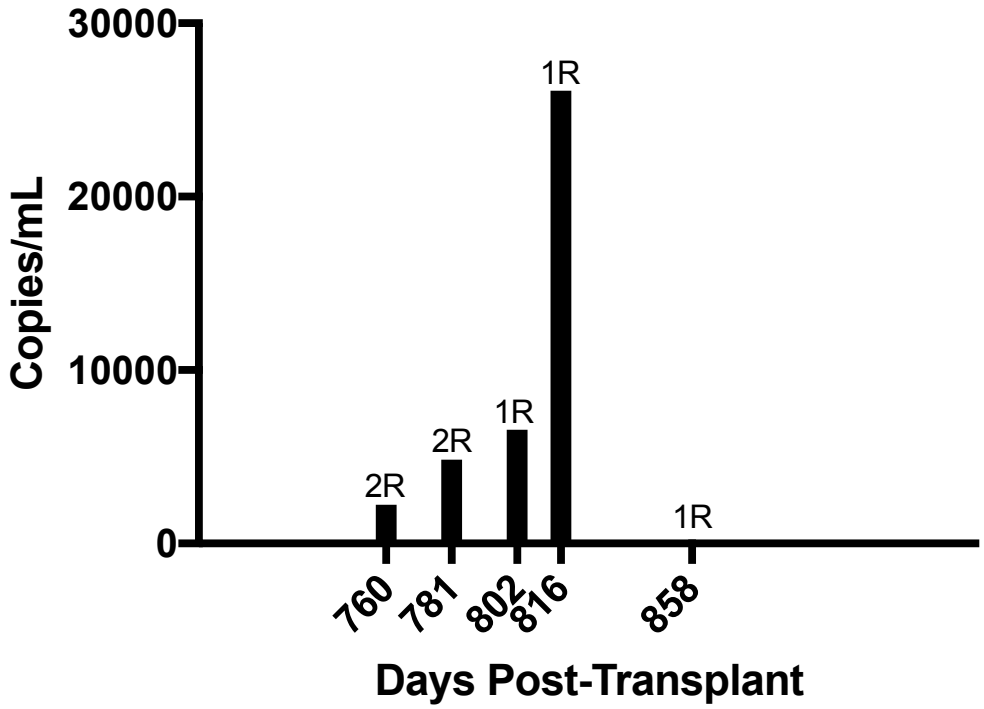

Figure 18. The concentration of the DMR at Chr 9-1 and total cfDNA within the plasma of patient 1002 over time. The concentration (copies/mL) of all cfDNA within the plasma of patient 1002 immediately before each routine EMB, with the associated biopsy-proven ISHLT rejection grades listed; along with the concentration (copies/mL) of the DMR at Chr 9-1 within the plasma of patient 1002 (A). The concentration (copies/mL) of the DMR on Chr 9-1 within the plasma of patient 1002 on the indicated day post-transplant, with the associated biopsy-proven ISHLT rejection grade (B).

Table 9. Routine serial EMBs and associated biopsy-proven rejection grades, as well as, the total coverage, methylation levels at the individual CpG sites, and the overall methylation percentages, as determined from the amplification and bisulfite sequencing of Chr 9-1 from cfDNA obtained from patient 1021. Dashes indicate unsuccessfully sequenced amplicons.

Biopsy #	Biopsy-Proven Rejection Grade	CpG Position	Total Reads	Methylation Level	Overall % Methylation	Overall % Unmethylated
1	0R	130622580	11631	0.85	**91.4**	**8.6**
		130622588	11633	0.95		
		130622614	11633	0.95		
		130622622	11631	0.9		
		130622628	11629	0.92		
3	1R	130622580	15862	0.9	**86.8**	**13.2**
		130622588	15868	0.93		
		130622614	15868	0.87		
		130622622	15868	0.91		
		130622628	15865	0.73		
6	0R	130622580	21973	0.96	**91.2**	**8.8**
		130622588	21971	0.96		
		130622614	21947	0.98		
		130622622	21928	0.94		
		130622628	21908	0.72		
7	1R	130622580	-	-	-	-
		130622588	-	-		
		130622614	-	-		
		130622622	-	-		
		130622628	-	-		
8	0R	130622580	15884	0.8	**77.6**	**22.4**
		130622588	15882	0.8		
		130622614	15872	0.8		
		130622622	15867	0.76		
		130622628	15860	0.72		

A

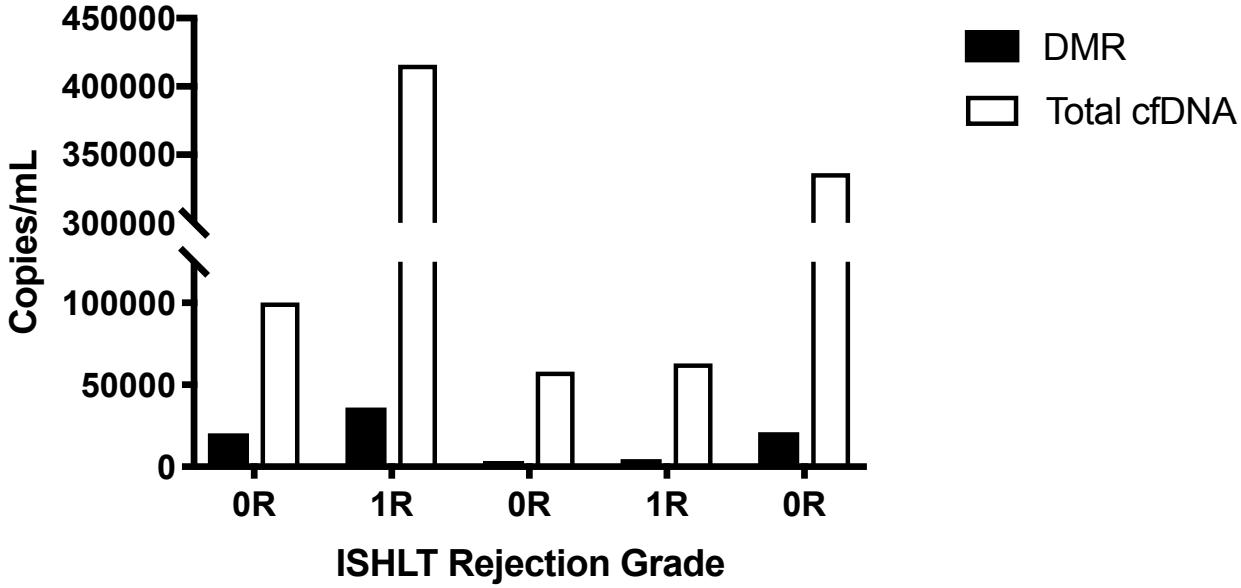

B

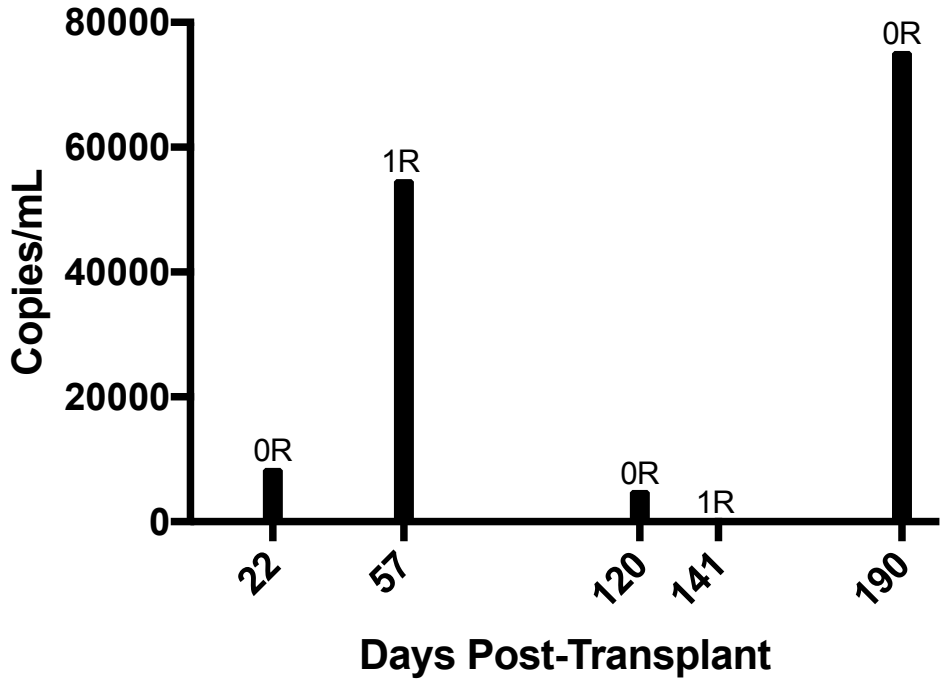

Figure 19. The concentration of the DMR at Chr 9-1 and total cfDNA within the plasma of patient 1021 over time. The concentration (copies/mL) of all cfDNA within the plasma of patient 1021 immediately before each routine EMB, with the associated biopsy-proven ISHLT rejection grades listed; along with the concentration (copies/mL) of the DMR on Chr 9-1 within the plasma of patient 1021 (A). The concentration (copies/mL) of the DMR on Chr 9-1 within the plasma of patient 1021 on the indicated day post-transplant, with the associated biopsy-proven ISHLT rejection grade (B).

Table 10. Routine serial EMBs and associated biopsy-proven rejection grades, as well as, the total coverage, methylation levels at the individual CpG sites, and the overall methylation percentages, as determined from the amplification and bisulfite sequencing of Chr 9-1 from cfDNA obtained from patient 1017.

Biopsy #	Biopsy-Proven Rejection Grade	CpG Position	Total Reads	Methylation Level	Overall % Methylation	Overall % Unmethylated
6	0R	130622580	19867	0.96	**90.6**	**9.4**
		130622588	19870	0.95		
		130622614	19871	0.97		
		130622622	19866	0.94		
		130622628	19854	0.71		
7	1R	130622580	5278	0.69	**75.8**	**24.2**
		130622588	5262	0.8		
		130622614	5258	0.84		
		130622622	5252	0.69		
		130622628	5233	0.77		
8	0R	130622580	3450	0.74	**76.0**	**24.0**
		130622588	3449	0.82		
		130622614	3447	0.92		
		130622622	3445	0.82		
		130622628	3444	0.5		
9	1R	130622580	8758	0.72	**71.0**	**29.0**
		130622588	8773	0.87		
		130622614	8772	0.71		
		130622622	8774	0.72		
		130622628	8771	0.53		
10	2-3R	130622580	18020	0.96	**91.6**	**8.4**
		130622588	18019	0.96		
		130622614	17997	0.98		
		130622622	17986	0.95		
		130622628	17977	0.73		
11	1R	130622580	13000	0.75	**76.2**	**23.8**
		130622588	13000	0.76		
		130622614	12996	0.75		
		130622622	12994	0.79		
		130622628	12987	0.76		
13	1R	130622580	8559	0.64	**70.6**	**29.4**
		130622588	8560	0.74		
		130622614	8552	0.74		
		130622622	8547	0.74		
		130622628	8534	0.67		
15	2R	130622580	10747	0.83	**85.0**	**15.0**
		130622588	10746	0.87		
		130622614	10745	0.88		
		130622622	10741	0.83		
		130622628	10734	0.84		

A

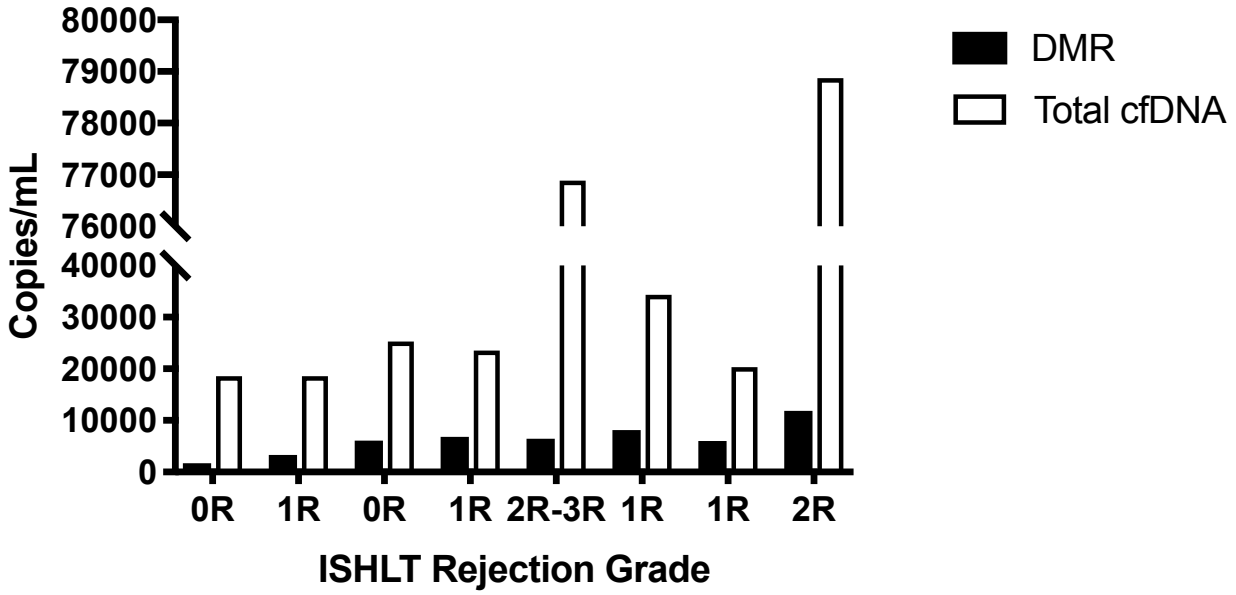

B

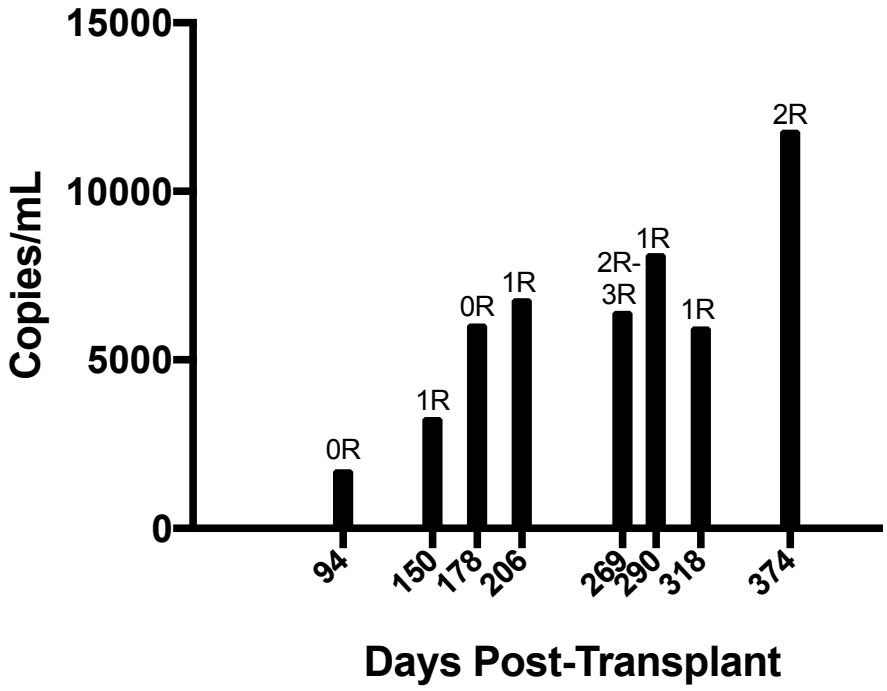

Figure 20. The concentration of the DMR at Chr 9-1 and total cfDNA within the plasma of patient 1017 over time. The concentration (copies/mL) of all cfDNA within the plasma of patient 1017 immediately before each routine EMB, with the associated biopsy-proven ISHLT rejection grades listed; along with the concentration (copies/mL) of the DMR on Chr 9-1 within the plasma of patient 1017 (A). The concentration (copies/mL) of the DMR on Chr 9-1 within the plasma of patient 1017 on the indicated day post-transplant, with the associated biopsy-proven ISHLT rejection grade (B).

Table 11. Routine serial EMBs and associated biopsy-proven rejection grades, as well as, the total coverage, methylation levels at the individual CpG sites, and the overall methylation percentages, as determined from the amplification and bisulfite sequencing of Chr 9-1 from cfDNA obtained from patient 1025. Dashes indicate unsuccessfully sequenced amplicons.

Biopsy #	Biopsy-Proven Rejection Grade	CpG Position	Total Reads	Methylation Level	Overall % Methylation	Overall % Unmethylated
1	0R	130622580	-	-	**-**	**-**
		130622588	-	-		
		130622614	-	-		
		130622622	-	-		
		130622628	-	-		
4	1R	130622580	10768	0.96	**90.8**	**9.2**
		130622588	10769	0.95		
		130622614	10756	0.97		
		130622622	10748	0.94		
		130622628	10740	0.72		
5	1R	130622580	8352	0.66	**67.4**	**32.6**
		130622588	8354	0.65		
		130622614	8353	0.75		
		130622622	8349	0.66		
		130622628	8347	0.65		
6	2R	130622580	6080	0.93	**94.6**	**5.4**
		130622588	6082	1		
		130622614	6080	1		
		130622622	6076	0.99		
		130622628	6074	0.81		
7	1R	130622580	59116	0.88	**95.0**	**5.0**
		130622588	59122	0.98		
		130622614	59127	0.98		
		130622622	59119	0.94		
		130622628	59105	0.97		
9	1R	130622580	8193	0.75	**75.6**	**24.4**
		130622588	8194	0.77		
		130622614	8175	0.79		
		130622622	8158	0.81		
		130622628	8150	0.66		

A

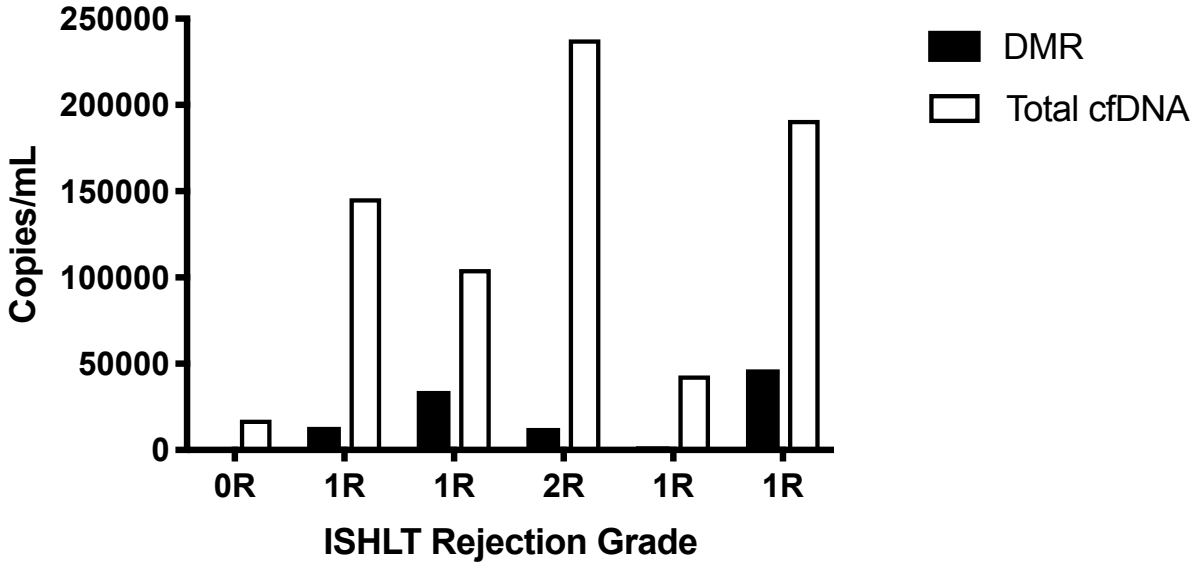

B

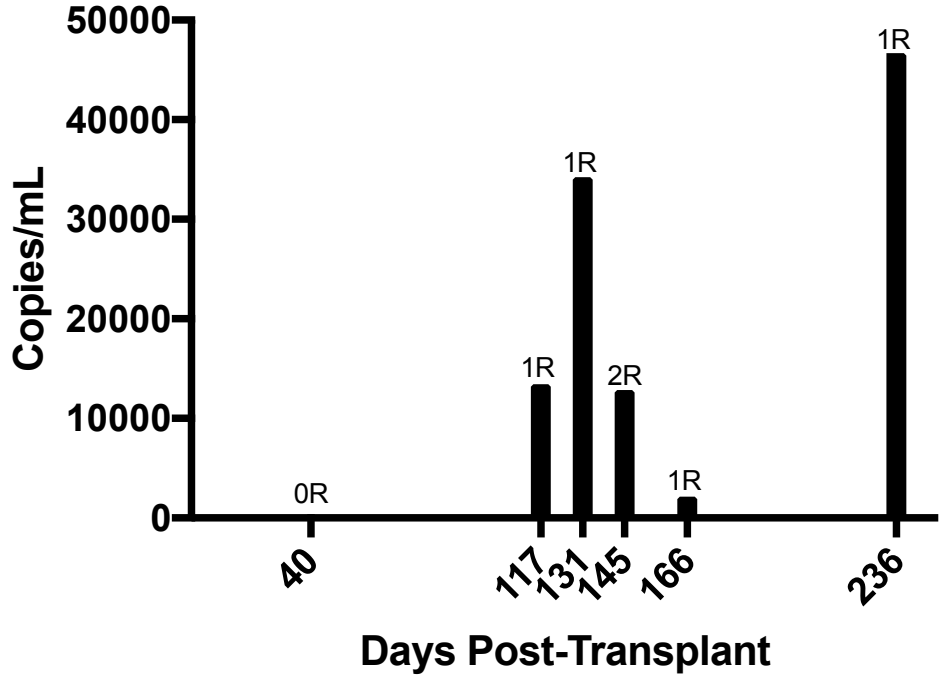

Figure 21. The concentration of the DMR at Chr 9-1 and total cfDNA within the plasma of patient 1025 over time. The concentration (copies/mL) of all cfDNA within the plasma of patient 1025 immediately before each routine EMB, with the associated biopsy-proven ISHLT rejection grades listed; along with the concentration (copies/mL) of the DMR on Chr 9-1 within the plasma of patient 1025 (A). The concentration (copies/mL) of the DMR on Chr 9-1 within the plasma of patient 1025 on the indicated day post-transplant, with the associated biopsy-proven ISHLT rejection grade (B).

3.4.6.2 DMR #2 – Chr 9-2

Plasma samples from patient 1002 were collected during the 11-15th biopsies, which took place 760-858 days post-HT. Notably, the cfDNA extracted from biopsies 11 and 12, which were both assigned rejection grades of 2R, resulted in very low proportions of unmethylated amplicons within the region of Chr 9-2 (Table 12). More specifically, only 6.3% and 4.4% of the sequenced amplicons that mapped to this region were found to be unmethylated in the samples taken during the 11th and 12th biopsies, respectively (Table 12). Conversely, relatively large amounts of cfDNA were found to be unmethylated within the region of Chr 9-2 and were therefore, derived from the ventricles of the donated heart, despite having been assigned a rejection grade of 1R at the 14th and 15th biopsies (Table 12). Furthermore, the fraction of this DMR on chromosome 9 within the total pool of cfDNA was quite small in the samples taken from biopsies 11 and 12, but relatively large in the samples taken from biopsies 14 and 15 (Figure 22A). As such, the concentration of the DMR at Chr 9-2 was only 1,570 copies/mL and 2,310 copies/mL during the 11th and 12th biopsies, respectively, despite the assignment of a 2R rejection grade (Figure 22B). Conversely, the concentration of this DMR was found to be 12,660 copies/mL and 17,020 copies/mL during the 14th and 15th biopsies, respectively, when the patient experienced only mild rejection (Figure 22B).

Plasma samples from patient 1021 were collected during the 1st, 3rd, and 6-8th biopsies, which took place 22-190 days post-HT. This patient had only experienced mild or no rejection during these biopsies. As such, the fraction of unmethylated amplicons of Chr 9-2 generally remained low, whereby 6.0-8.7% of the amplicons were found to be unmethylated in this region (Table 13). However, the first biopsy was an exception as 20.3% of the amplicons were unmethylated in this region despite having been assigned a rejection grade of 0R (Table 13). Interestingly, upon determination of the concentration of this DMR within the recipient's plasma, it was found that

cfDNA derived from the ventricles of the donated heart accounted for a relatively large fraction of the total cfDNA present within the recipient's plasma during the 1st, 3rd, and 8th biopsies (Figure 23A). As such, 20,360 copies/mL of the DMR at Chr 9-2 were observed in the first biopsy, despite patient 1021 having been assigned a rejection grade of 0R following the biopsy (Figure 23B). Moreover, 36,170 copies/mL of this DMR were observed in the recipient's plasma at day 57 post-HT, when diagnosed with mild rejection (Figure 23B). Finally, 21,210 copies/mL of the DMR at Chr 9-2 were detected in the plasma of patient 1021 at day 190 post-HT despite displaying no signs of rejection, according to the histological analysis of the tissue samples taken during the 8th EMB (Figure 23B).

Plasma samples from patient 1017 were collected during the 6th-11th biopsies, as well as the 13th and 15th biopsies, which took place between 94-374 days post-HT. Notably, the fraction of unmethylated molecules detected from the amplification of the DMR at Chr 9-2 remained relatively consistent across each biopsy with no more than 10% of the amplicons being unmethylated within this region (Table 14). However, the sequencing results of the 6th biopsy were an exception this, as 18% of the amplicons were found to be unmethylated at Chr 9-2 (Table 14). Notably, the fraction of cfDNA that was unmethylated region at Chr 9-2, and therefore, derived from the ventricles of the donated heart, accounted for a relatively large proportion of the total cfDNA within patient 1017's plasma during the 10th and 15th biopsies, when moderate to severe rejection was experienced (Figure 24A). As such, we observed a striking increase in the concentration of this DMR within the recipient's plasma at days 269 and 374 post-HT, with 5,150 copies/mL and 4,500 copies/mL detected, respectively (Figure 24B). Following the moderate rejection event at day 269 post-HT we observed a steady decline in the concentration of the DMR at Chr 9-2 within the recipient's plasma (Figure 24B). Finally, despite the absence of any signs of

rejection at days 94 and 178 post-HT, 3,400 copies/mL and 1,595 copies/mL were detected in the plasma of patient 1017, respectively (Figure 24B).

Plasma samples from patient 1025 were obtained during the 1st, 4th-7th, and 9th routine biopsies, which took place 40-236 days post-HT. The fraction of unmethylated amplicons of Chr 9-2 generally remained low across each biopsy, whereby 5.7-9.0% of the amplicons were found to be unmethylated in this region (Table 15). However, the first biopsy was an exception as 15.7% of the amplicons were unmethylated in this region, despite having been assigned a rejection grade of 0R (Table 15). Interestingly, at the 6th biopsy in which patient 1025 was diagnosed with moderate rejection, the sequencing data indicated that only 5.7% of the amplicons that mapped to Chr 9-2 were unmethylated, which was the lowest fraction observed across all of the biopsies (Table 15). Despite this, we observed a steady increase in the concentration of this DMR starting at 117 days post-HT and peaked at the moderate rejection event at day 145 post-HT, whereby 13,560 copies/mL were detected in the plasma of patient 1025 (Figure 25B). Following the 2R rejection event, at the biopsy on day 166 post-HT when the recipient showed mild rejection, only 3,890 copies/mL of this DMR were detected in the plasma of patient 1025 (Figure 25B). In contrast to this, we observed another spike in the concentration of the DMR at Chr 9-2 at day 236 post-HT, whereby 11,480 copies/mL of this DMR were detected in the plasma of patient 1025, despite the biopsy results having suggested only mild rejection in this case as well (Figure 25B).

Table 12. Routine serial EMBs and associated biopsy-proven rejection grades, as well as, the total coverage, methylation levels at the individual CpG sites, and the overall methylation percentages, as determined from the amplification and bisulfite sequencing of Chr 9-2 from cfDNA obtained from patient 1002.

Biopsy #	Biopsy-Proven Rejection Grade	CpG Position	Total Reads	Methylation Level	Overall % Methylation	Overall % Unmethylated
11	2R	101595535	3319	0.84	**93.7**	**6.3**
		101595551	3309	0.97		
		101595573	3306	1		
12	2R	101595535	2326	0.87	**95.7**	**4.3**
		101595551	2310	1		
		101595573	2308	1		
13	1R	101595535	2771	0.98	**97.3**	**2.7**
		101595551	2767	0.95		
		101595573	2761	0.99		
14	1R	101595535	2225	0.81	**87.3**	**12.7**
		101595551	2221	0.84		
		101595573	2211	0.97		
15	1R	101595535	4299	0.82	**89.3**	**10.7**
		101595551	4277	0.86		
		101595573	4268	1		

A

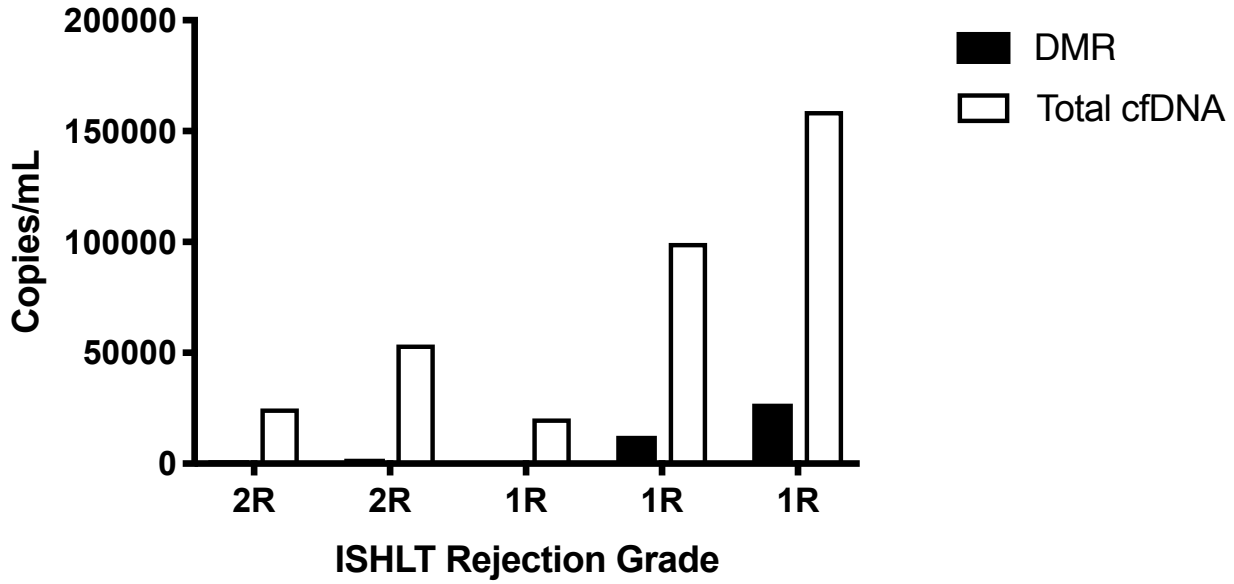

B

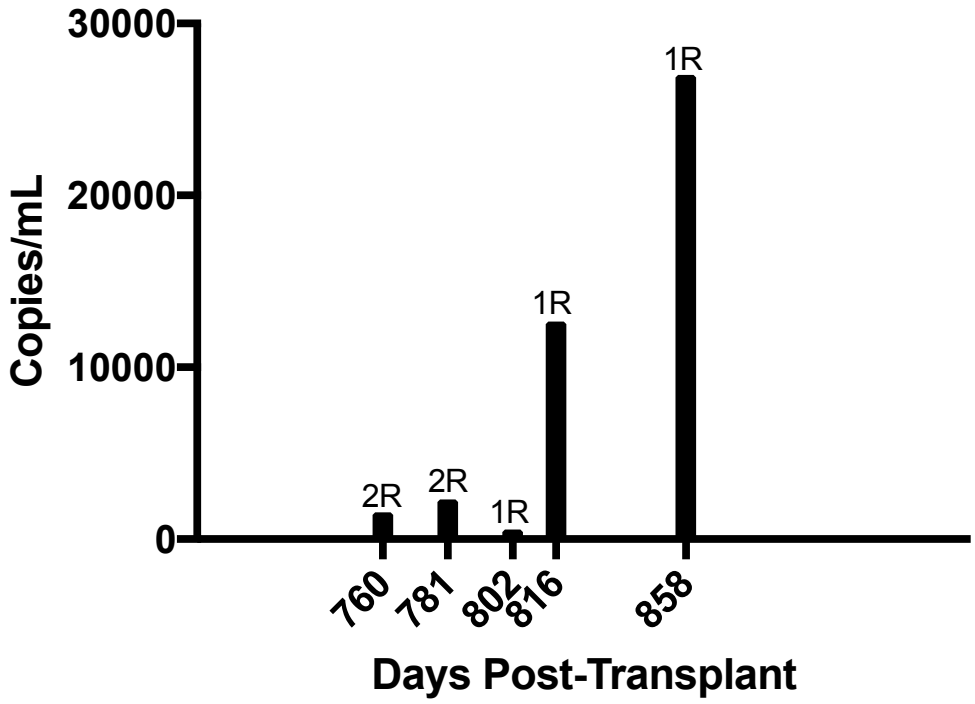

Figure 22. The concentration of the DMR at Chr 9-2 and total cfDNA within the plasma of patient 1002 over time. The concentration (copies/mL) of all cfDNA within the plasma of patient 1002 immediately before each routine EMB, with the associated biopsy-proven ISHLT rejection grades listed; along with the concentration (copies/mL) of the DMR on Chr 9-2 within the plasma of patient 1002 (A). The concentration (copies/mL) of the DMR on Chr 9-2 within the plasma of patient 1002 on the indicated day post-transplant, with the associated biopsy-proven ISHLT rejection grade (B).

Table 13. Routine serial EMBs and associated biopsy-proven rejection grades, as well as, the total coverage, methylation levels at the individual CpG sites, and the overall methylation percentages, as determined from the amplification and bisulfite sequencing of Chr 9-2 from cfDNA obtained from patient 1021.

Biopsy #	Biopsy-Proven Rejection Grade	CpG Position	Total Reads	Methylation Level	Overall % Methylation	Overall % Unmethylated
1	0R	101595535	2003	0.81	**79.7**	**20.3**
		101595551	2001	0.7		
		101595573	2003	0.88		
3	1R	101595535	3350	0.95	**91.3**	**8.7**
		101595551	3323	0.87		
		101595573	3293	0.92		
6	0R	101595535	2998	0.9	**94.0**	**6.0**
		101595551	2985	0.96		
		101595573	2980	0.96		
7	1R	101595535	12409	0.85	**92.7**	**7.3**
		101595551	12387	1		
		101595573	12388	0.93		
9	0R	101595535	3019	0.96	**93.7**	**6.3**
		101595551	3009	0.95		
		101595573	3004	0.9		

A

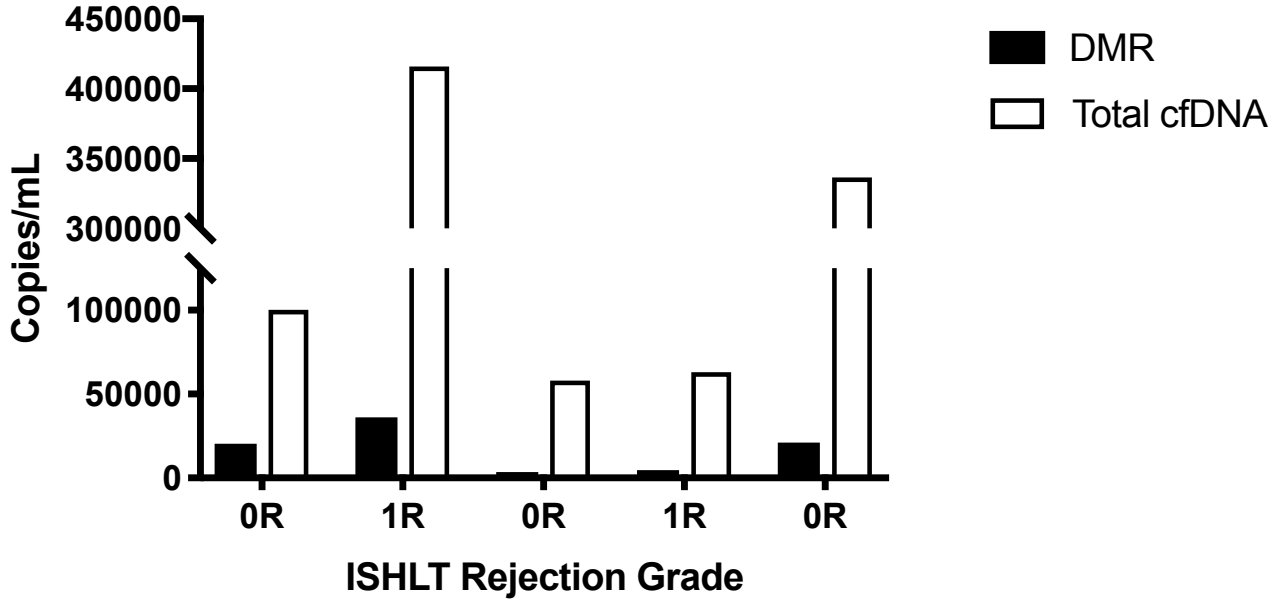

B

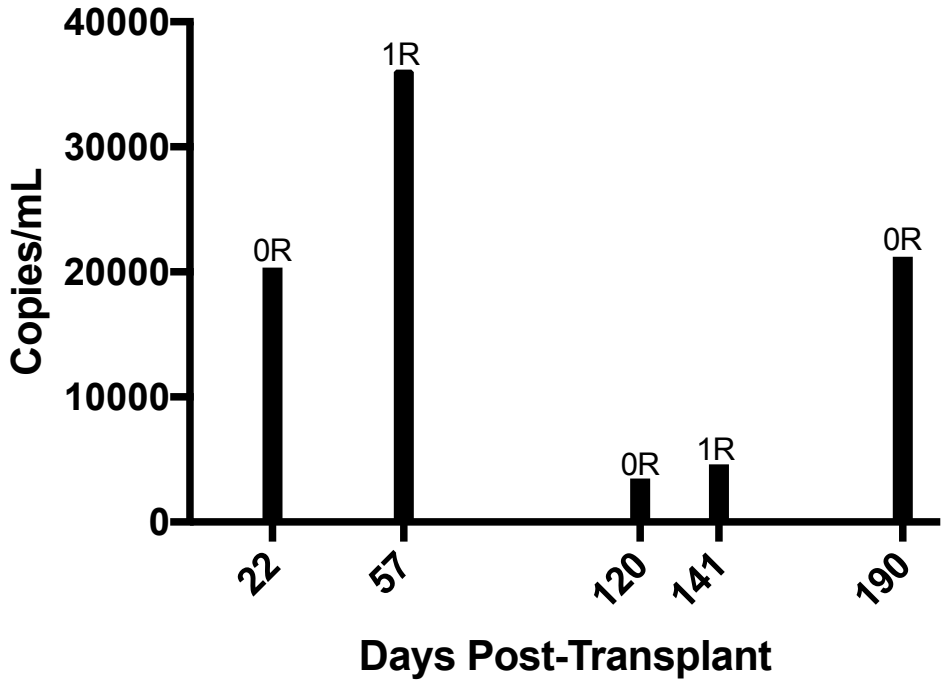

Figure 23. The concentration of the DMR at Chr 9-2 and total cfDNA within the plasma of patient 1021 over time. The concentration (copies/mL) of all cfDNA within the plasma of patient 1021 immediately before each routine EMB, with the associated biopsy-proven ISHLT rejection grades listed; along with the concentration (copies/mL) of the DMR on Chr 9-2 within the plasma of patient 1021 (A). The concentration (copies/mL) of the DMR on Chr 9-2 within the plasma of patient 1021 on the indicated day post-transplant, with the associated biopsy-proven ISHLT rejection grade (B).

Table 14. Routine serial EMBs and associated biopsy-proven rejection grades, as well as, the total coverage, methylation levels at the individual CpG sites, and the overall methylation percentages, as determined from the amplification and bisulfite sequencing of Chr 9-2 from cfDNA obtained from patient 1017.

Biopsy #	Biopsy-Proven Rejection Grade	CpG Position	Total Reads	Methylation Level	Overall % Methylation	Overall % Unmethylated
6	0R	101595535	2211	0.78	**82.0**	**18.0**
		101595551	2207	0.76		
		101595573	2202	0.92		
7	1R	101595535	4414	0.98	**97.3**	**2.7**
		101595551	4388	0.96		
		101595573	4387	0.98		
8	0R	101595535	3646	0.9	**93.7**	**6.3**
		101595551	3623	0.91		
		101595573	3618	1		
9	1R	101595535	3673	0.9	**92.7**	**7.3**
		101595551	3655	0.96		
		101595573	3653	0.92		
10	2-3R	101595535	3579	0.91	**93.3**	**6.7**
		101595551	3564	0.91		
		101595573	3565	0.98		
11	1R	101595535	1668	0.93	**92.7**	**7.3**
		101595551	1664	0.9		
		101595573	1661	0.95		
13	1R	101595535	4082	0.93	**95.7**	**4.3**
		101595551	4052	0.94		
		101595573	4046	1		
15	2R	101595535	1982	0.91	**94.3**	**5.7**
		101595551	1971	0.95		
		101595573	1972	0.97		

A

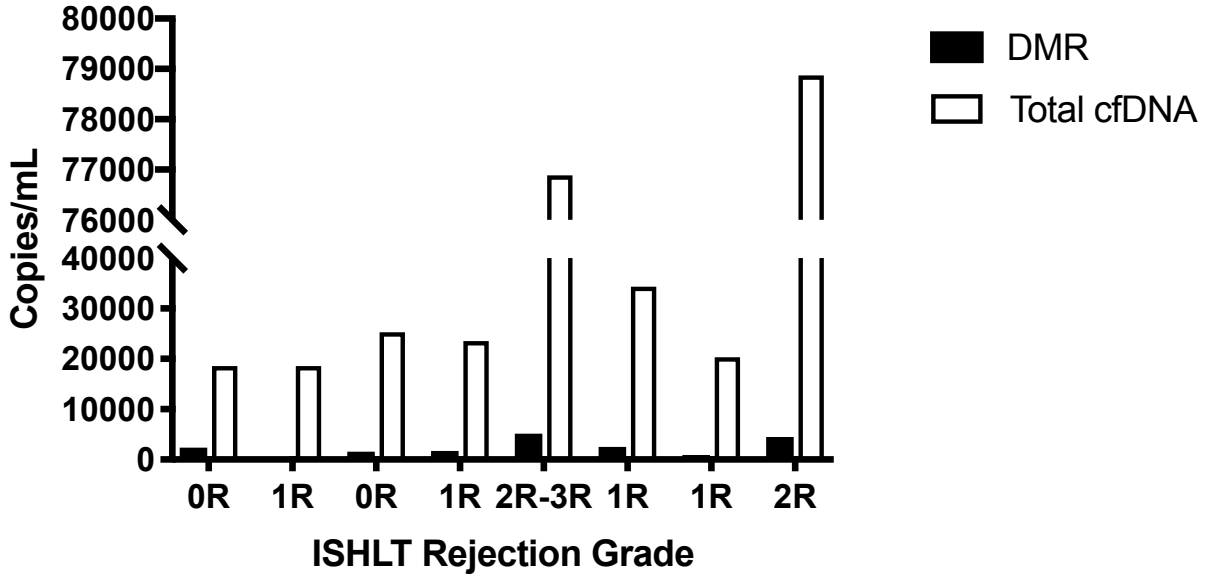

B

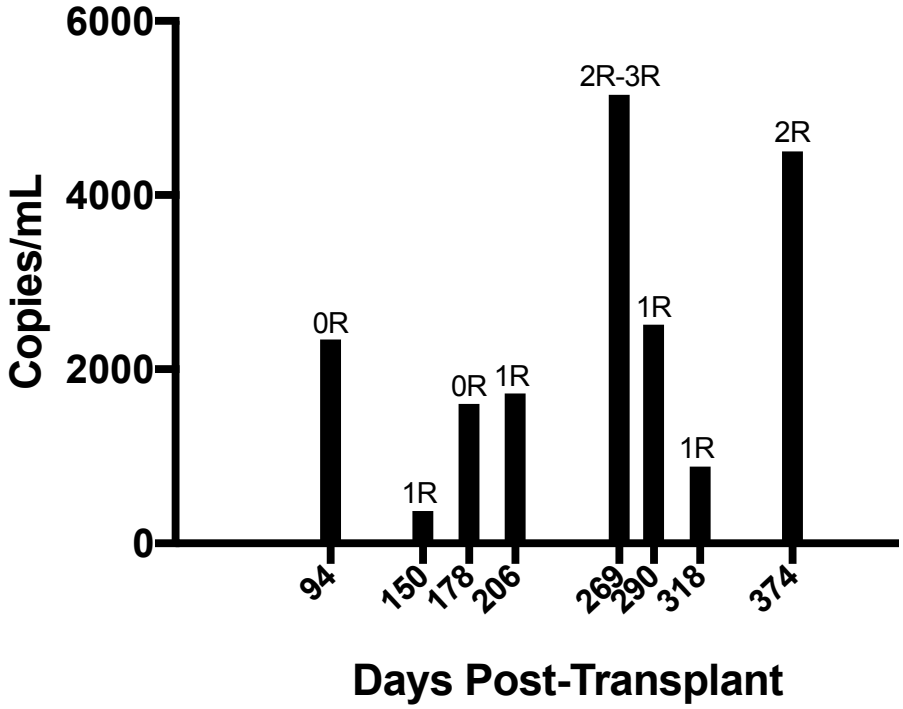

Figure 24. The concentration of the DMR at Chr 9-2 and total cfDNA within the plasma of patient 1017 over time. The concentration (copies/mL) of all cfDNA within the plasma of patient 1017 immediately before each routine EMB, with the associated biopsy-proven ISHLT rejection grades listed; along with the concentration (copies/mL) of the DMR on Chr 9-2 within the plasma of patient 1017 (A). The concentration (copies/mL) of the DMR on Chr 9-2 within the plasma of patient 1017 on the indicated day post-transplant, with the associated biopsy-proven ISHLT rejection grade (B).

Table 15. Routine serial EMBs and associated biopsy-proven rejection grades, as well as, the total coverage, methylation levels at the individual CpG sites, and the overall methylation percentages, as determined from the amplification and bisulfite sequencing of Chr 9-2 from cfDNA obtained from patient 1025.

Biopsy #	Biopsy-Proven Rejection Grade	CpG Position	Total Reads	Methylation Level	Overall % Methylation	Overall % Unmethylated
1	0R	101595535	6177	0.83	**84.3**	**15.7**
		101595551	6159	0.8		
		101595573	6152	0.9		
4	1R	101595535	4480	0.9	**91.7**	**8.3**
		101595551	4484	0.85		
		101595573	4483	1		
5	1R	101595535	6595	0.94	**93.0**	**7.0**
		101595551	6598	0.95		
		101595573	6599	0.9		
6	2R	101595535	3792	0.95	**94.3**	**5.7**
		101595551	3782	0.93		
		101595573	3779	0.95		
7	1R	101595535	35897	0.86	**91.0**	**9.0**
		101595551	35777	0.91		
		101595573	35735	0.96		
9	1R	101595535	3014	0.92	**94.0**	**6.0**
		101595551	3016	0.92		
		101595573	3015	0.98		

A

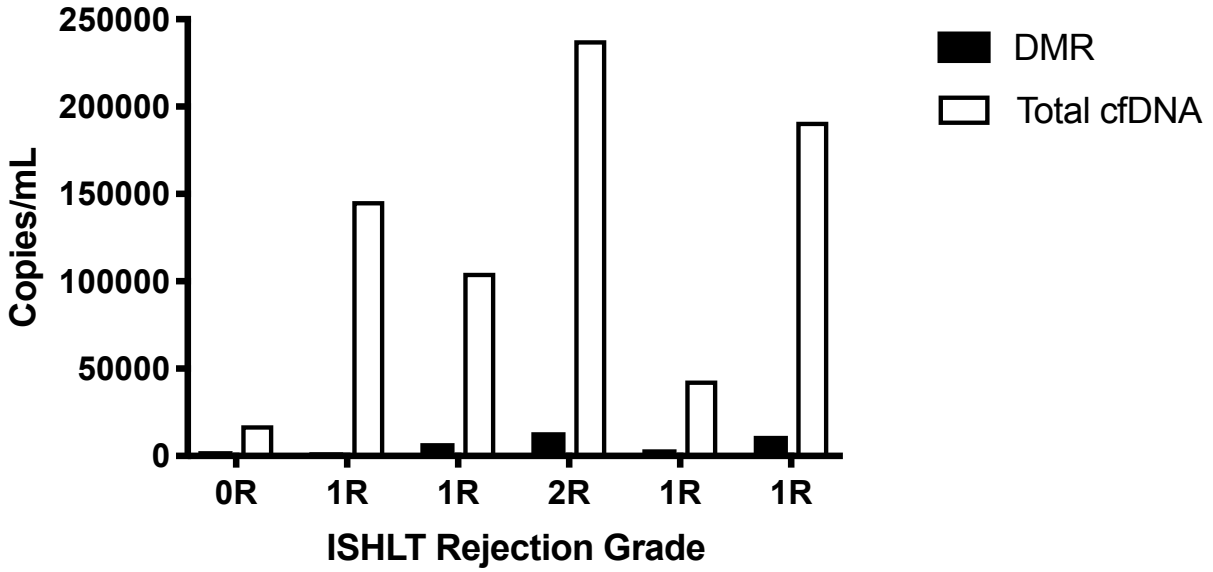

B

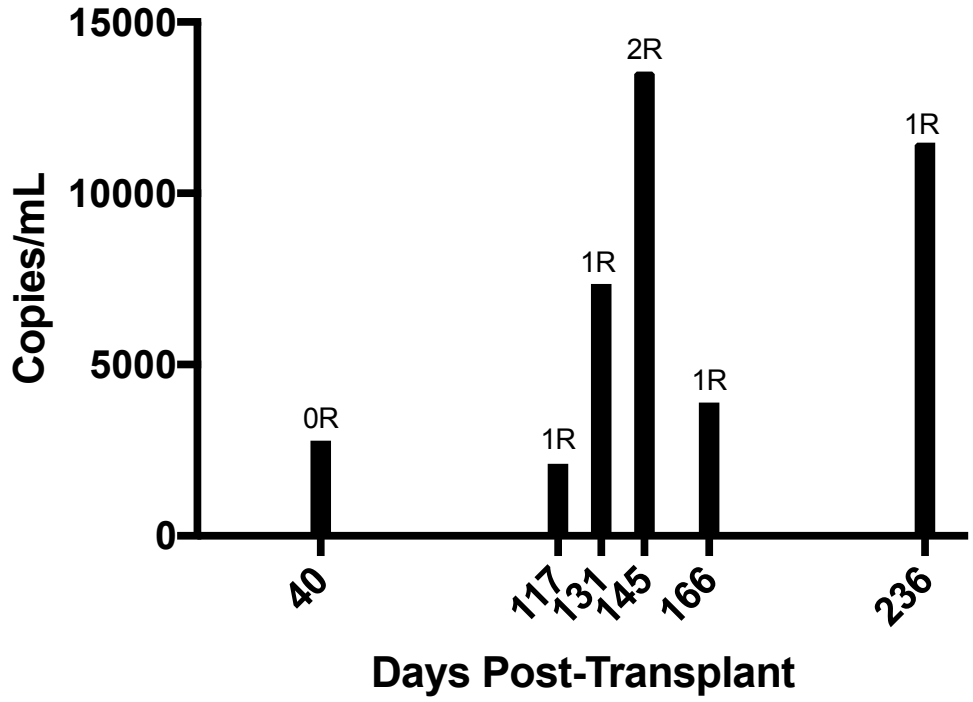

Figure 25. The concentration of the DMR at Chr 9-2 and total cfDNA within the plasma of patient 1025 over time. The concentration (copies/mL) of all cfDNA within the plasma of patient 1025 immediately before each routine EMB, with the associated biopsy-proven ISHLT rejection grades listed; along with the concentration (copies/mL) of the DMR on Chr 9-2 within the plasma of patient 1025 (A). The concentration (copies/mL) of the DMR on Chr 9-2 within the plasma of patient 1025 on the indicated day post-transplant, with the associated biopsy-proven ISHLT rejection grade (B).

3.4.6.3 DMR #3 – Chr 12

Plasma samples from patient 1002 were collected during the 11-15th biopsies, which took place 760-858 days post-HT. Notably, the cfDNA extracted from biopsies 11 and 12, which were both assigned rejection grades of 2R, resulted in very low proportions of unmethylated cfDNA, specifically within the region of Chr 12 (Table 16). More specifically, only 10.0% and 10.8% of the sequenced amplicons that mapped to this region were found to be unmethylated in the samples taken during the 11th and 12th biopsies, respectively (Table 16). Conversely, the cfDNA extracted from the plasma sample taken at the 15th biopsy had a relatively large fraction of unmethylated cfDNA within this region on chromosome 12, despite having been assigned a rejection grade of 1R (Table 16). Furthermore, the fraction of cfDNA that was unmethylated at Chr 12, and therefore, derived from the ventricles of the donated heart, within the total pool of cfDNA was quite small in the samples taken from biopsies 11 and 12, but relatively large in the sample taken from biopsy 15 (Figure 26A). As such, the concentration of the DMR at Chr 12 was only 2,490 copies/mL and 5,810 copies/mL during the 11th and 12th biopsies, respectively, despite the assignment of a 2R rejection grade (Figure 26B). Conversely, the concentration of this DMR within the plasma of patient 1002 was found to be 29,740 copies/mL during the 15th biopsy, despite having been diagnosed with mild rejection (Figure 26B).

Plasma samples from patient 1021 were collected during the 1st, 3rd, and 6-8th biopsies, which took place 22-190 days post-HT. This patient had only experienced mild or no rejection during these biopsies. The region at Chr 12 that was amplified from the cfDNA extracted from patient 1021's 6th and 9th biopsies failed to be sequenced within the pool of amplicons, and therefore, no data could be collected for this DMR at these biopsies. Based on the sequencing results, 9.8% of the amplicons that mapped to Chr 12 were found to be unmethylated in cfDNA extracted from the

first biopsy, when patient 1021 displayed no rejection (Table 17). At the third biopsy the recipient was diagnosed with mild rejection and 11.5% of the amplicons that mapped to the region of interest on chromosome 12 were found to be unmethylated (Table 17). Finally, the sequencing results from the 7th biopsy, in which patient 1021 had experienced mild rejection, indicated that only 6.0% of the amplicons that mapped to Chr 12 were unmethylated (Table 17). Notably, the fraction of cfDNA that was unmethylated at Chr 12, and was therefore, derived from the ventricles of the donated heart, accounted for a relatively large portion of the total cfDNA extracted from the third biopsy (Figure 27A). Therefore, a prominent increase in the concentration of this DMR was observed at day 57 post-HT within the plasma of patient 1021, with 47,820 copies/mL detected, despite having only experienced mild rejection (Figure 27B). In contrast to this, patient 1021 was once again diagnosed with mild rejection at day 141 post-HT but only 3,780 copies/mL were detected within this recipient's plasma (Figure 27B).

Plasma samples from patient 1017 were collected during the 6^{th}-11^{th} biopsies, as well as the 13^{th} and 15^{th} biopsies, which took place between 94-374 days post-HT. Notably, the fraction of amplicons that were found to be unmethylated at Chr 12 ranged between 4.8-14.2% across each of the biopsies (Table 18). Interestingly, the sequencing results of the 15^{th} biopsy indicated that only 5.7% of the amplicons that mapped to Chr 12 were unmethylated, despite having been diagnosed with moderate rejection (Table 18). Most notably, cfDNA that was unmethylated at Chr 12, and was therefore, derived from the ventricles of the donated heart, accounted for a large fraction of the total cfDNA within the recipient's plasma in the samples taken during the 10^{th} biopsy, when a rejection grade of 2R-3R was assigned (Figure 28A). As such, a noticeable spike in the concentration of the DMR at Chr 12 within the plasma of patient 1017 was observed at day 269 post-HT with 9,460 copies/mL detected (Figure 28B). Then at day 374, this patient was once

again diagnosed with moderate rejection and 4,500 copies/mL were detected within the recipient's plasma (Figure 28B). The other biopsies in which patient 1017 experienced no or mild rejection, approximately 3,000 copies/mL of this DMR were detected in the recipient's plasma (Figure 28B).

Plasma samples from patient 1025 were obtained during the 1st, 4th-7th, and 9th routine biopsies, which took place 40-236 days post-HT. The fraction of unmethylated amplicons that mapped to Chr 12 generally remained consistent across each biopsy, whereby 10.0-14.7% of the amplicons were found to be unmethylated (Table 19). However, the first biopsy when the patient displayed no rejection was an exception as 6.2% of the amplicons that mapped to this region were unmethylated; along with the 7th biopsy, whereby 18.2% of the amplicons were found to be unmethylated at Chr 12 (Table 19). Interestingly, the 6th biopsy in which patient 1025 was diagnosed with moderate rejection, the sequencing data indicated that only 10.0% of the amplicons that mapped to Chr 12 were unmethylated, which was the lowest fraction observed across all of the biopsies (Table 19). In addition to this, while the concentration of total cfDNA extracted from the plasma of patient 1025 at day 145 was highest when moderate rejection was experienced, the concentration of total cfDNA varied considerably across each of the mild rejection cases (Figure 29A). Despite this, we observed a steady increase in the concentration of the DMR at Chr 12 starting at 117 days post-HT and peaked at the moderate rejection event at day 145 post-HT, whereby 23,790 copies/mL were detected in the plasma of patient 1025 (Figure 29B). Following the 2R rejection event, the biopsy at day 166 post-HT where the recipient showed signs of mild rejection, only 7,870 copies/mL of this DMR were detected in the plasma of patient 1025 (Figure 29B). In contrast to this, we observed another spike in the concentration of this DMR at day 236 post-HT, whereby 19,710 copies/mL were detected in patient 1025's plasma, despite histological analysis of the biopsied tissue having suggested only mild rejection (Figure 29B).

Table 16. Routine serial EMBs and associated biopsy-proven rejection grades, as well as, the total coverage, methylation levels at the individual CpG sites, and the overall methylation percentages, as determined from the amplification and bisulfite sequencing of Chr 12 from cfDNA obtained from patient 1002.

Biopsy #	Biopsy-Proven Rejection Grade	CpG Position	Total Reads	Methylation Level	Overall % Methylation	Overall % Unmethylated
11	2R	106132053	11346	0.93	**90.0**	**10.0**
		106132055	11369	0.91		
		106132057	11371	0.94		
		106132059	11372	0.94		
		106132071	11379	0.79		
		106132095	11369	0.89		
12	2R	106132053	9371	0.91	**89.2**	**10.8**
		106132055	9380	0.9		
		106132057	9383	0.94		
		106132059	9384	0.97		
		106132071	9389	0.75		
		106132095	9385	0.88		
13	1R	106132053	6462	0.92	**92.2**	**7.8**
		106132055	6468	0.94		
		106132057	6467	0.98		
		106132059	6469	0.95		
		106132071	6463	0.82		
		106132095	6464	0.92		
14	1R	106132053	7406	0.95	**93.8**	**6.2**
		106132055	7415	0.96		
		106132057	7415	0.95		
		106132059	7414	0.97		
		106132071	7416	0.89		
		106132095	7421	0.91		
15	1R	106132053	8691	0.77	**81.3**	**18.7**
		106132055	8698	0.87		
		106132057	8698	0.87		
		106132059	8699	0.86		
		106132071	8708	0.7		
		106132095	8713	0.81		

A

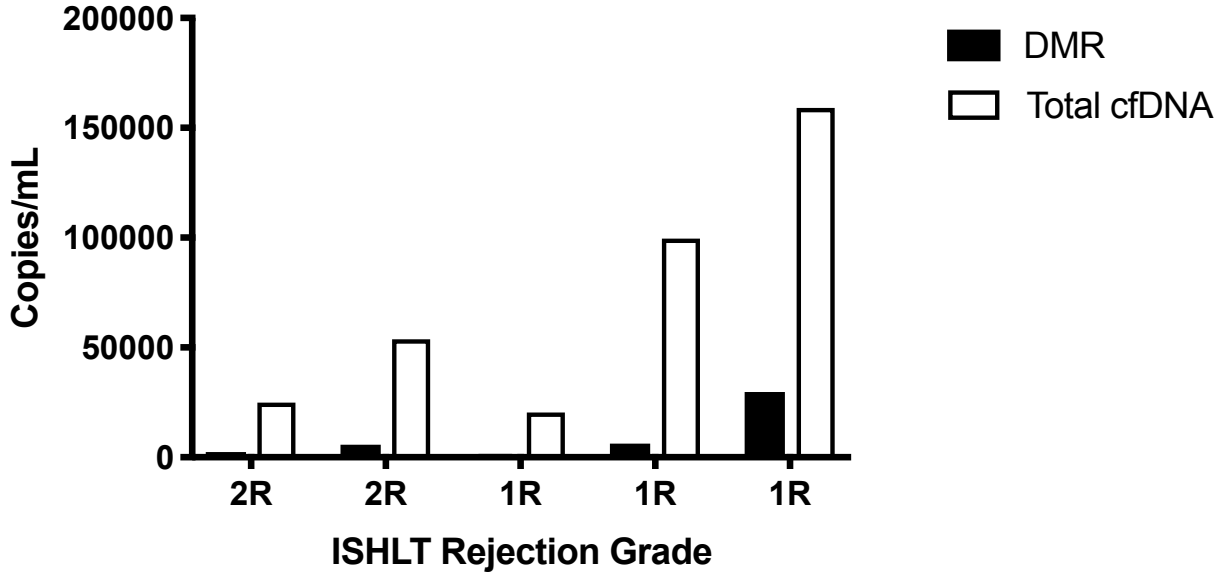

B

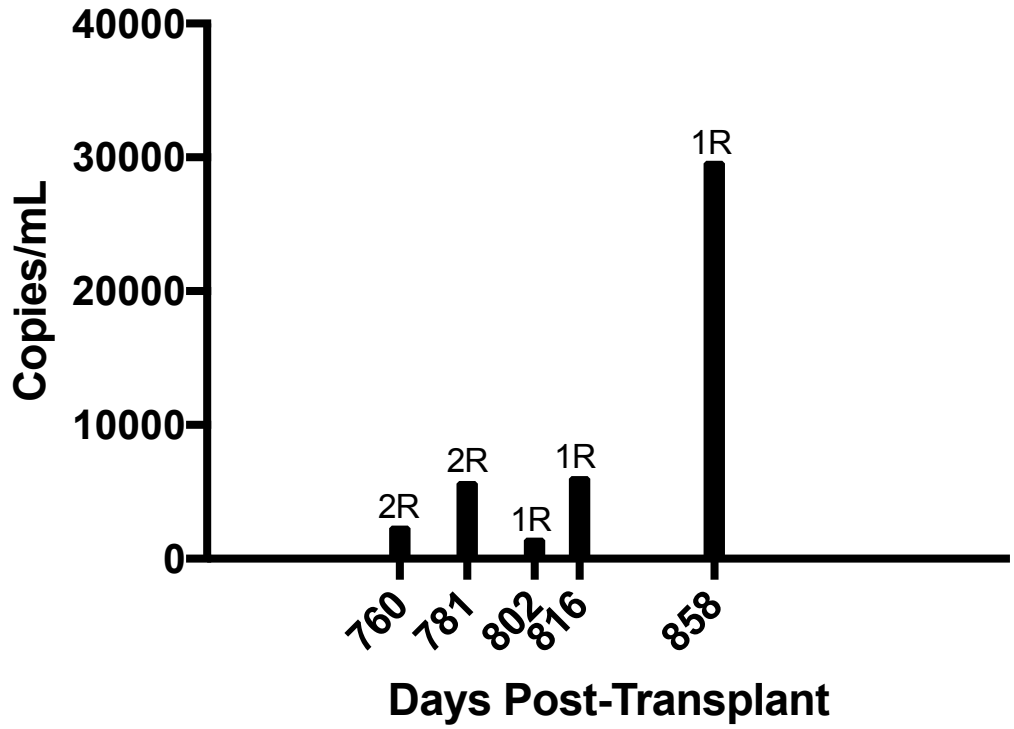

Figure 26. The concentration of the DMR at Chr 12 and total cfDNA within the plasma of patient 1002 over time. The concentration (copies/mL) of all cfDNA within the plasma of patient 1002 immediately before each routine EMB, with the associated biopsy-proven ISHLT rejection grades listed; along with the concentration (copies/mL) of the DMR on Chr 12 within the plasma of patient 1002 (A). The concentration (copies/mL) of the DMR on Chr 12 within the plasma of patient 1002 on the indicated day post-transplant, with the associated biopsy-proven ISHLT rejection grade (B).

Table 17. Routine serial EMBs and associated biopsy-proven rejection grades, as well as, the total coverage, methylation levels at the individual CpG sites, and the overall methylation percentages, as determined from the amplification and bisulfite sequencing of Chr 12 from cfDNA obtained from patient 1021. Dashes indicate unsuccessfully sequenced amplicons.

Biopsy #	Biopsy-Proven Rejection Grade	CpG Position	Total Reads	Methylation Level	Overall % Methylation	Overall % Unmethylated
1	0R	106132053	6470	0.93	**90.2**	**9.8**
		106132055	6488	0.93		
		106132057	6488	0.97		
		106132059	6492	0.94		
		106132071	6501	0.78		
		106132095	6491	0.86		
3	1R	106132053	8266	0.88	**88.5**	**11.5**
		106132055	8437	0.88		
		106132057	8441	0.93		
		106132059	8443	0.9		
		106132071	8446	0.82		
		106132095	8434	0.9		
6	0R	106132053	-	-	**-**	**-**
		106132055	-	-		
		106132057	-	-		
		106132059	-	-		
		106132071	-	-		
		106132095	-	-		
7	1R	106132053	3624	0.95	**94.0**	**6.0**
		106132055	3624	0.93		
		106132057	3635	0.98		
		106132059	3635	0.98		
		106132071	3635	0.9		
		106132095	3623	0.9		
8	0R	106132053	-	-	-	-
		106132055	-	-		
		106132057	-	-		
		106132059	-	-		
		106132071	-	-		
		106132095	-	-		

A

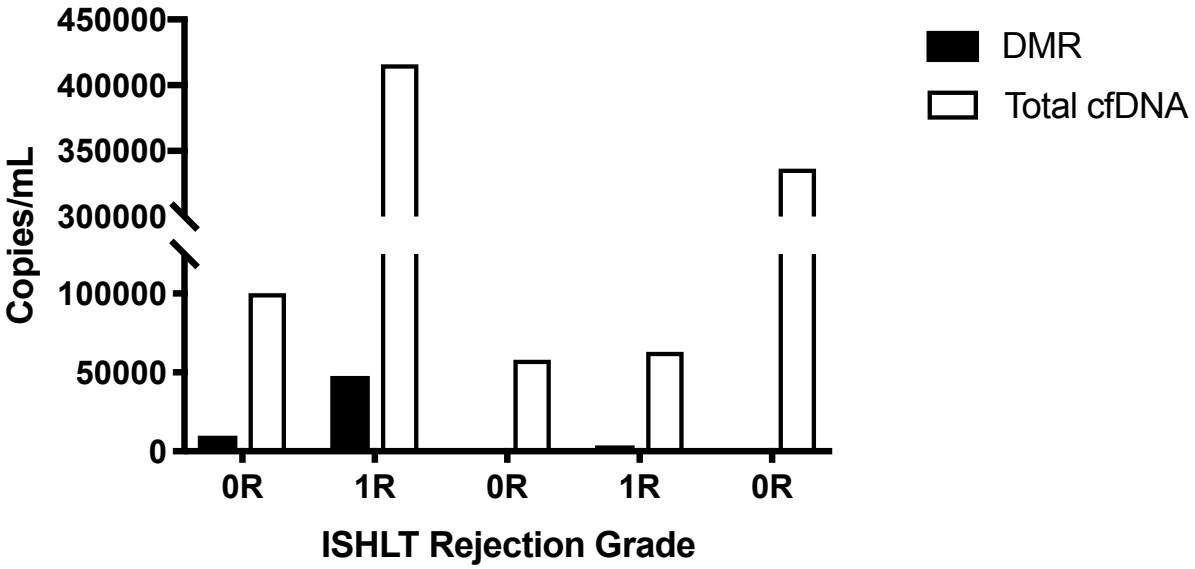

B

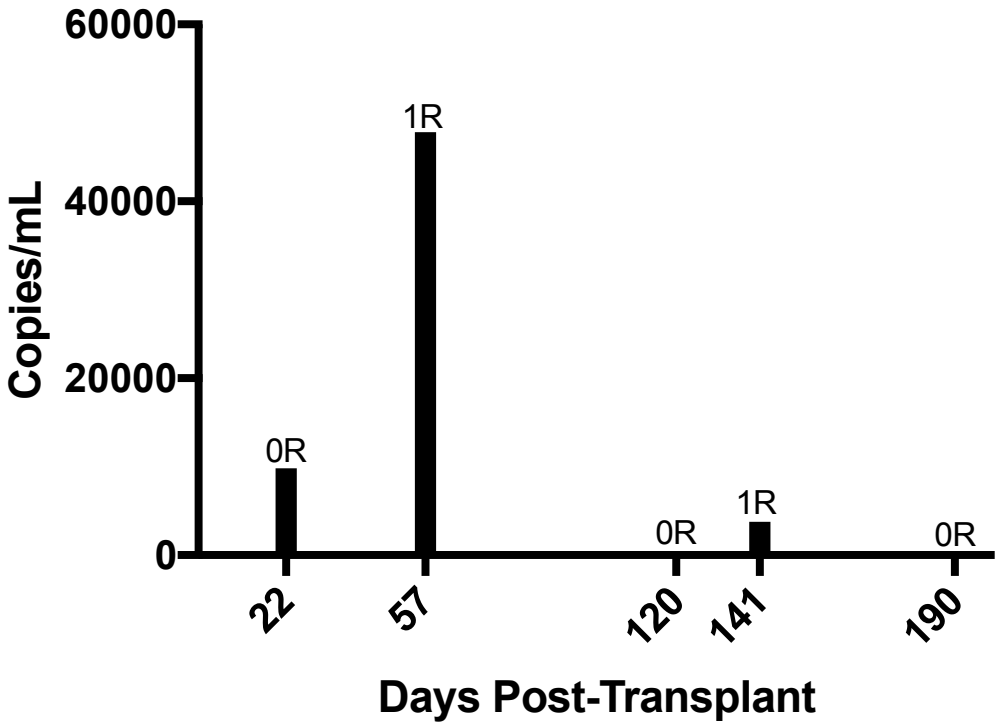

Figure 27. The concentration of the DMR at Chr 12 and total cfDNA within the plasma of patient 1021 over time. The concentration (copies/mL) of all cfDNA within the plasma of patient 1021 immediately before each routine EMB, with the associated biopsy-proven ISHLT rejection grades listed; along with the concentration (copies/mL) of the DMR on Chr 12 within the plasma of patient 1021 (A). The concentration (copies/mL) of the DMR on Chr 12 within the plasma of patient 1021 on the indicated day post-transplant, with the associated biopsy-proven ISHLT rejection grade (B).

Table 18. Routine serial EMBs and associated biopsy-proven rejection grades, as well as, the total coverage, methylation levels at the individual CpG sites, and the overall methylation percentages, as determined from the amplification and bisulfite sequencing of Chr 12 from cfDNA obtained from patient 1017.

Biopsy #	Biopsy-Proven Rejection Grade	CpG Position	Total Reads	Methylation Level	Overall % Methylation	Overall % Unmethylated
6	0R	106132053	4610	0.87	**89.0**	**11.0**
		106132055	4593	0.9		
		106132057	4593	0.95		
		106132059	4595	0.91		
		106132071	4595	0.79		
		106132095	4594	0.92		
7	1R	106132053	6176	0.95	**95.2**	**4.8**
		106132055	6181	0.97		
		106132057	6183	0.99		
		106132059	6183	0.97		
		106132071	6177	0.87		
		106132095	6187	0.96		
8	0R	106132053	5987	0.91	**88.2**	**11.8**
		106132055	5991	0.92		
		106132057	5990	0.95		
		106132059	5992	0.92		
		106132071	5990	0.76		
		106132095	5990	0.83		
9	1R	106132053	7461	0.88	**87.7**	**12.3**
		106132055	7462	0.89		
		106132057	7462	0.92		
		106132059	7463	0.91		
		106132071	7463	0.77		
		106132095	7469	0.89		
10	2-3R	106132053	6471	0.87	**87.7**	**12.3**
		106132055	6477	0.9		
		106132057	6477	0.9		
		106132059	6477	0.87		
		106132071	6476	0.83		
		106132095	6477	0.89		
11	1R	106132053	7450	0.92	**92.0**	**8.0**
		106132055	7452	0.96		
		106132057	7453	0.91		
		106132059	7455	0.96		
		106132071	7450	0.87		
		106132095	7455	0.9		

13	1R	106132053	5689	0.87	**85.8**	**14.2**
		106132055	5693	0.88		
		106132057	5694	0.89		
		106132059	5696	0.92		
		106132071	5701	0.75		
		106132095	5689	0.84		
15	2R	106132053	7488	0.95	**94.3**	**5.7**
		106132055	7499	0.95		
		106132057	7502	0.96		
		106132059	7501	0.95		
		106132071	7502	0.9		
		106132095	7502	0.95		

A

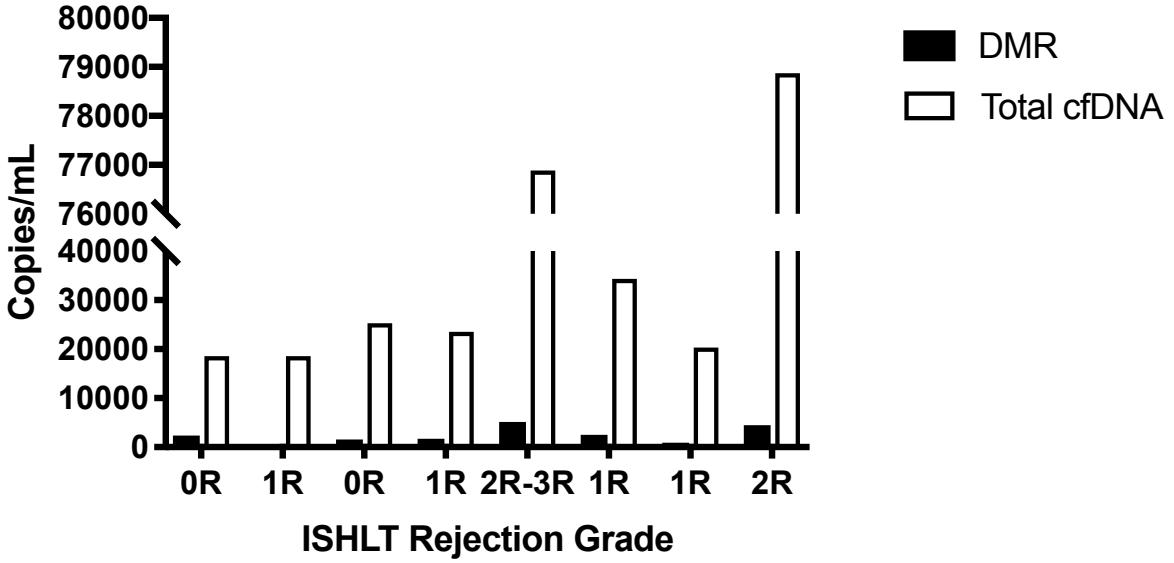

B

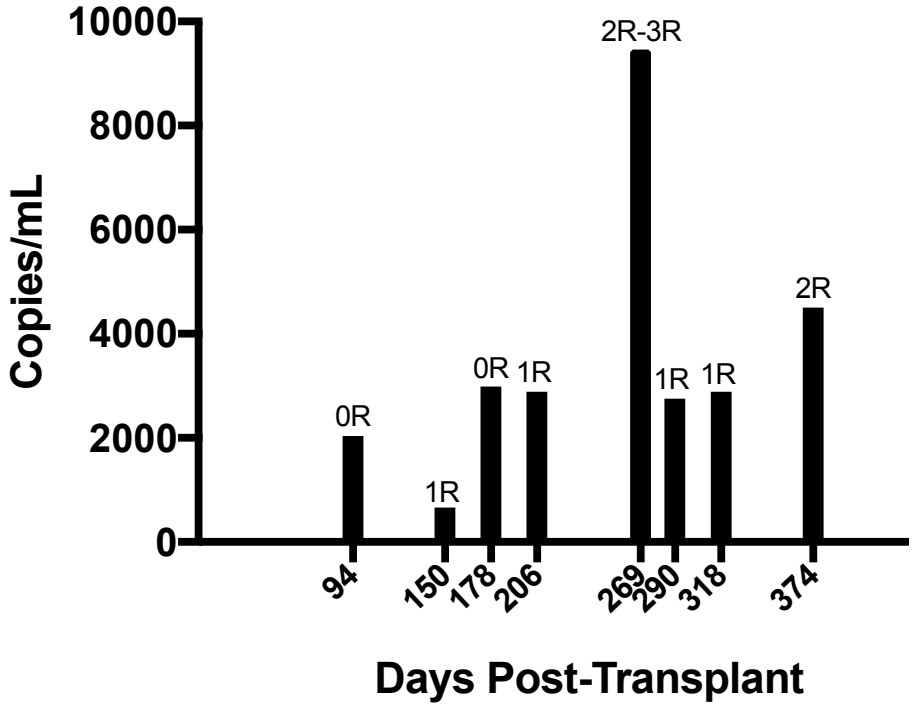

Figure 28. The concentration of the DMR at Chr 12 and total cfDNA within the plasma of patient 1017 over time. The concentration (copies/mL) of all cfDNA within the plasma of patient 1017 immediately before each routine EMB, with the associated biopsy-proven ISHLT rejection grades listed; along with the concentration (copies/mL) of the DMR on Chr 12 within the plasma of patient 1017 (A). The concentration (copies/mL) of the DMR on Chr 12 within the plasma of patient 1017 on the indicated day post-transplant, with the associated biopsy-proven ISHLT rejection grade (B).

Table 19. Routine serial EMBs and associated biopsy-proven rejection grades, as well as, the total coverage, methylation levels at the individual CpG sites, and the overall methylation percentages, as determined from the amplification and bisulfite sequencing of Chr 12 from cfDNA obtained from patient 1025.

Biopsy #	Biopsy-Proven Rejection Grade	CpG Position	Total Reads	Methylation Level	Overall % Methylation	% Unmethylated
1	0R	106132053	7003	0.96	**93.8**	**6.2**
		106132055	7004	0.95		
		106132057	7004	0.95		
		106132059	7005	0.97		
		106132071	7005	0.85		
		106132095	7008	0.95		
4	1R	106132053	6946	0.89	**85.3**	**14.7**
		106132055	6953	0.89		
		106132057	6959	0.94		
		106132059	6962	0.9		
		106132071	6973	0.67		
		106132095	6954	0.83		
5	1R	106132053	11106	0.87	**85.3**	**14.7**
		106132055	11125	0.85		
		106132057	11130	0.9		
		106132059	11135	0.95		
		106132071	11141	0.71		
		106132095	11001	0.84		
6	2R	106132053	8753	0.87	**90.0**	**10.0**
		106132055	8761	0.89		
		106132057	8765	0.95		
		106132059	8771	0.93		
		106132071	8779	0.85		
		106132095	8772	0.91		
7	1R	106132053	64374	0.78	**81.8**	**18.2**
		106132055	64441	0.7		
		106132057	64446	0.86		
		106132059	64443	0.84		
		106132071	64400	0.76		
		106132095	64486	0.97		
9	1R	106132053	8661	0.89	**89.7**	**10.3**
		106132055	8675	0.9		
		106132057	8680	0.96		
		106132059	8681	0.92		
		106132071	8688	0.87		
		106132095	8667	0.84		

A

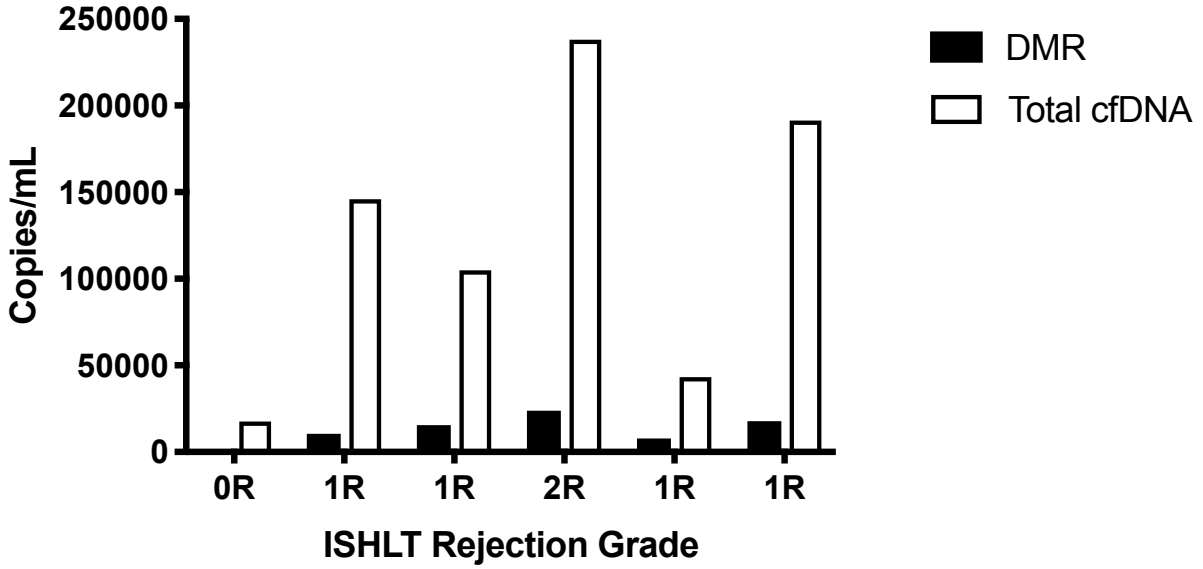

B

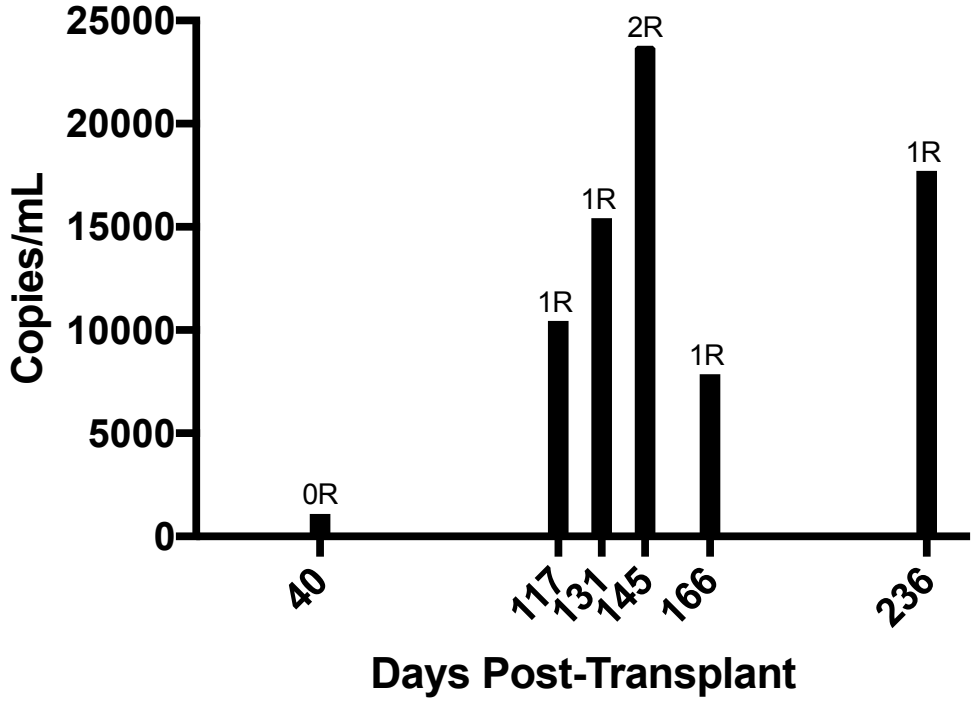

Figure 29. The concentration of the DMR at Chr 12 and total cfDNA within the plasma of patient 1025 over time. The concentration (copies/mL) of all cfDNA within the plasma of patient 1025 immediately before each routine EMB, with the associated biopsy-proven ISHLT rejection grades listed; along with the concentration (copies/mL) of the DMR on Chr 12 within the plasma of patient 1025 (A). The concentration (copies/mL) of the DMR on Chr 12 within the plasma of patient 1025 on the indicated day post-transplant, with the associated biopsy-proven ISHLT rejection grade (B).

3.4.7 Correlation of Concentration of DMR and Degree of Tissue Apoptosis

3.4.7.1 DMR #1 – Chr 9-1

An obvious negative correlation was observed between the concentration of the DMR at Chr 9-1 and the mean percentage of myocardial cells that stained positively for both TUNEL and DAPI at a given biopsy-proven rejection grade for the matched blood and tissue samples obtained from patient 1002 (Figure 30A). This negative correlation was also observed between the stained tissue samples and corresponding cfDNA samples obtained from patient 1021, however, the negative trend was not as drastic (Figure 30B). Finally, the correlation between the mean percentage of myocardial cells that stained positively for both TUNEL and DAPI at a given biopsy-proven rejection grade and the concentration of this DMR for the associated samples obtained from patient 1025 was found to only be slightly positive (Figure 30C).

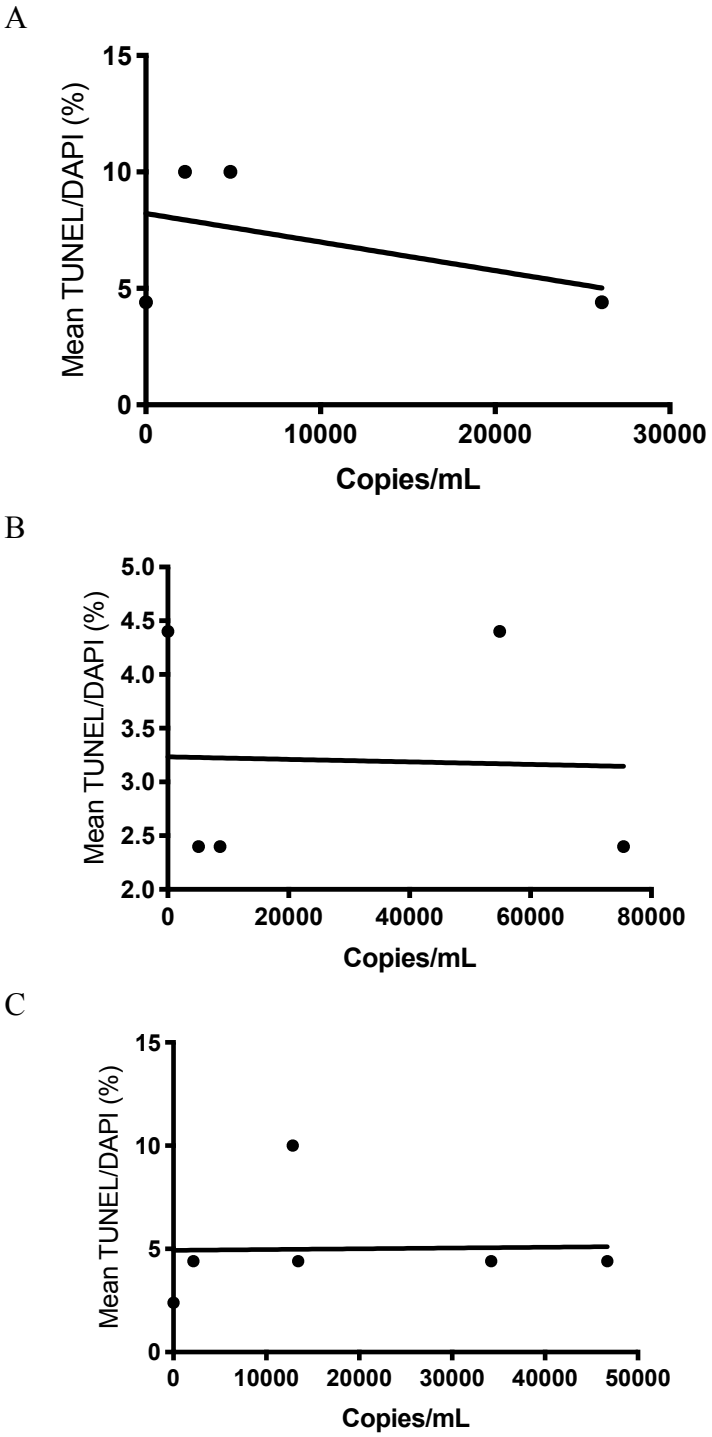

Figure 30. The correlation between myocardial apoptosis and the concentration of the DMR at Chr 9-1. The correlation between the mean proportion of cells that stained positively for both TUNEL and DAPI for the associated biopsy-proven rejection grade and the concentration (copies/mL) of the DMR at Chr 9-1 within each corresponding plasma sample from patient 1002 (A), 1021 (B), and 1025 (C).

3.4.7.2 DMR #2 – Chr 9-2

An obvious negative correlation was observed between the concentration of the DMR at Chr 9-2 and the mean percentage of myocardial cells that stained positively for both TUNEL and DAPI at a given biopsy-proven rejection grade for the matched blood and tissue samples obtained from patient 1002 (Figure 31A). In contrast to this, the correlation between the mean percentage of myocardial cells that had undergone apoptosis or necrosis at a given biopsy-proven rejection grade and the concentration of this DMR for the associated blood and tissue samples obtained from patient 1021 was found to be positive (Figure 31B). Similarly, the correlation between the results of the stained tissue samples and the concentration of the DMR at chr 9-2 within the corresponding cfDNA samples was also found to be strongly positive (Figure 31C).

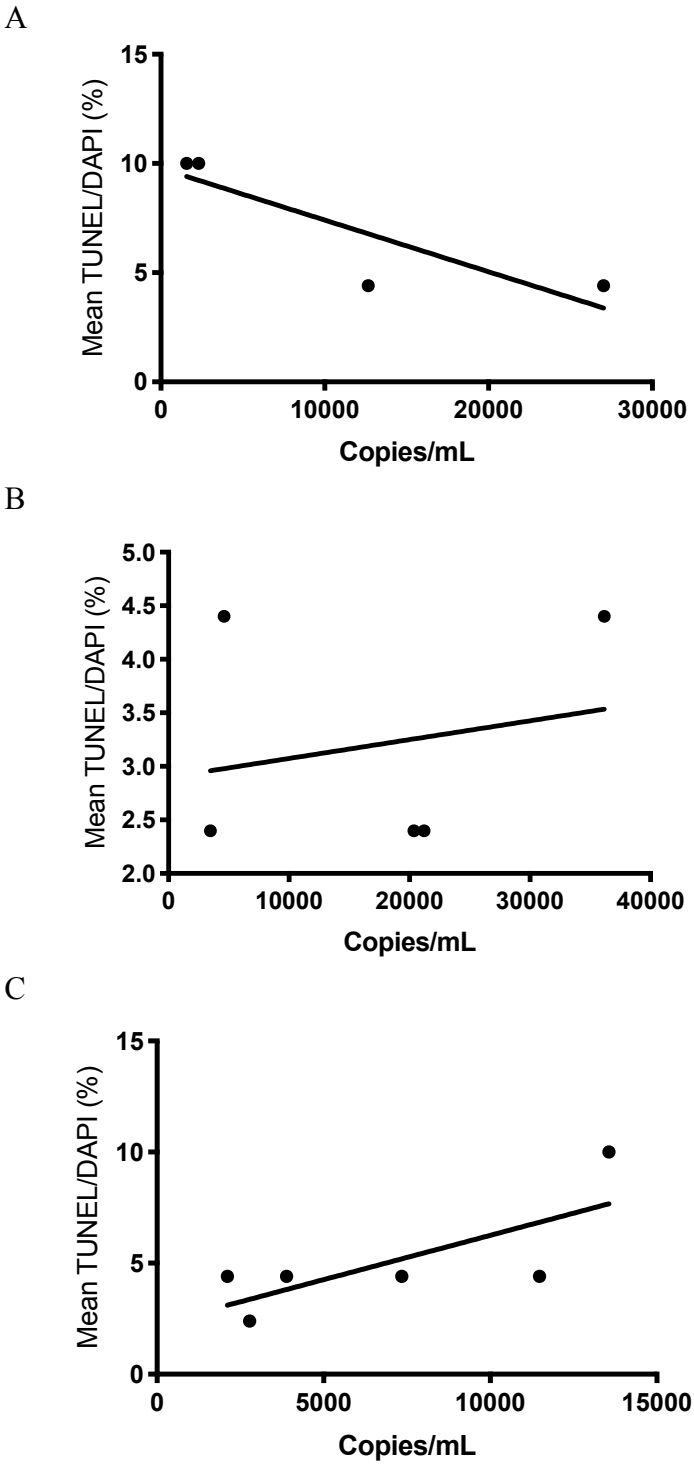

Figure 31. The correlation between myocardial apoptosis and the concentration of the DMR at Chr 9-2. The correlation between the mean proportion of cells that stained positively for both TUNEL and DAPI for the associated biopsy-proven rejection grade and the concentration (copies/mL) of the DMR at Chr 9-2 within each corresponding plasma sample from patient 1002 (A), 1021 (B), and 1025 (C).

3.4.7.3 DMR #3 – Chr 12

An obvious negative correlation was observed between the concentration of the DMR at Chr 12 and the mean percentage of myocardial cells that stained positively for both TUNEL and DAPI at a given biopsy-proven rejection grade for the matched blood and tissue samples obtained from patient 1002 (Figure 32A). In contrast to this, the correlation between the mean percentage of myocardial cells that had undergone apoptosis or necrosis at a given biopsy-proven rejection grade and the concentration of this DMR for the associated blood and tissue samples obtained from patient 1021 was found to be positive (Figure 32B). Similarly, the correlation between the results of the stained tissue samples and the concentration of the DMR at Chr 12 within the corresponding cfDNA samples obtained from patient 1025 was also found to be strongly positive (Figure 32C).

A

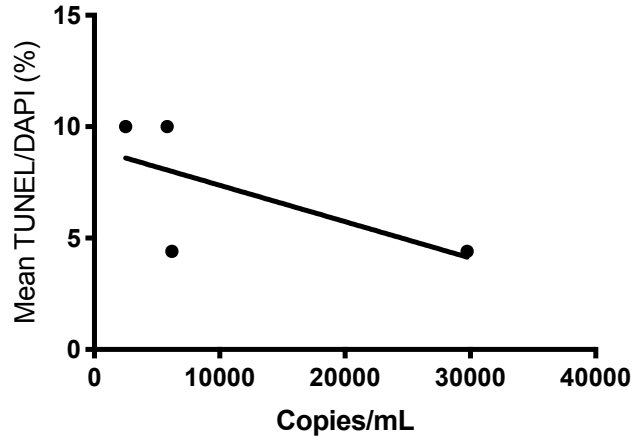

B

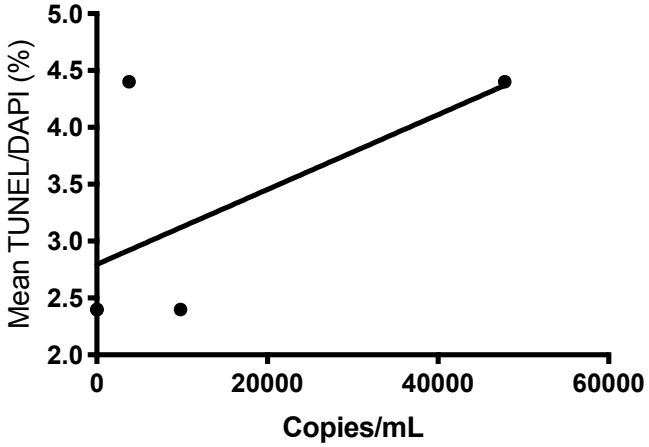

C

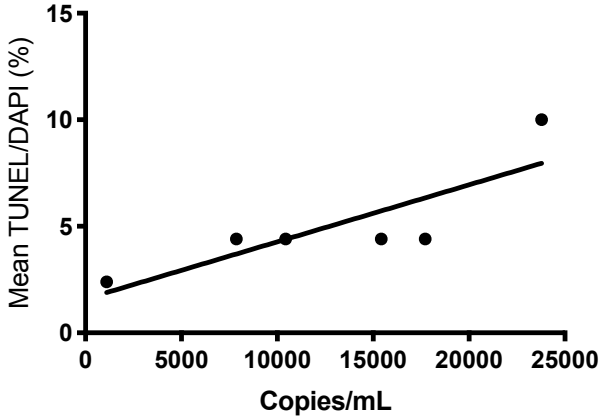

Figure 32. The correlation between myocardial apoptosis and the concentration of the DMR at Chr 12. The correlation between the mean proportion of cells that stained positively for both TUNEL and DAPI for the associated biopsy-proven rejection grade and the concentration (copies/mL) of the DMR at Chr 12 within each corresponding plasma sample from patient 1002 (A), 1021 (B), and 1025 (C).

3.5 Discussion

DNA methylation plays a critical role in dictating gene expression and therefore, the differentiation of a cell into a specific cell type (*62*). It has been noted that DNA methylation patterns differ across tissues and these differences are sufficient for distinguishing between tissue types (*63*, *64*). Tissue specific methylation patterns are conserved within a tissue type and, to a large degree, across individuals (*64*). This was critical for the development of this universal non-invasive cfDNA-based assay using the limited number of publicly available methylomes (*56*, *57*). The use of all publicly available methylomes of tissues and hematopoietic cells within the human body and the software Metilene (*58*) allowed for an unbiased approach for the identification of potential ventricle-specific DMRs. This was in contrast to previously established protocols, which used regions of genes that were known to play a specific role in the unique function of an organ of interest and where therefore, differentially methylated in comparison to the methylomes of all other tissues and cells (*23*, *63*). Thus, the process of successfully identifying a robust and organ-specific DMR was contingent on its methylation pattern being unique to the organ of interest.

The 255 DMRs (Figure 12A) that were identified from the comparison of the methylomes of the ventricles and the methylomes of various tissues in the human body, and the 2,060 DMRs (Figure 12B) that were identified from the comparison of the ventricular methylomes to those of hematopoietic cells suggested that ventricular cells were much more epigenetically similar to other tissues in the body than to hematopoietic cells. It should be noted that these comparisons were made separately due to the fact that the natural turnover of hematopoietic cells within the circulation accounted for a majority of the background noise when extracting cfDNA from the plasma of HT patients (*65*). Therefore, in order to identity the most robust possible DMRs, the regions must be unique to the ventricles not only in comparison to other tissues in the body, but

even more so in comparison to hematopoietic cells. Taken together, only 24 regions were found to be common among the two sets of data. This provided an adequate foundation for potential ventricle-specific DMRs that could function as blood biomarkers for the non-invasive identification and quantification of cfDNA derived from the ventricles of the donated heart due to ACR-mediated tissue injury following HT. However, it must be noted that typically only one methylome for each non-ventricular tissue type was available for analysis. Therefore, this hindered the confidence in not only the universality of these DMRs, but also the specificity of these DMRs. As more methylomes become publicly available, this will allow for a more stringent analysis of differential methylation amongst these organs and cellular methylomes. Furthermore, additional methylomes from specific regions within the heart, such as the atria, valves, and major vessels may also help to elucidate more definitively ventricle-specific DMRs.

Based on the *in silico* analysis, using the methylomes that were accessible, three candidate DMRs, Chr 9-1, Chr 9-2, and Chr 12 were selected for further analysis. This was based on the fact that these regions had over 3 CpG sites, were less than 100 bp in length (Table 3), and displayed low levels of methylation at these regions in gDNA obtained from ventricular cells (Tables 5-7). Furthermore, we were able to successfully amplify these DMRs, without off-target amplification, within both gDNA and cfDNA extracted from the plasma of heart transplant recipients (Figure 14). All of these features made these DMRs very compelling for the ability to function as a non-invasive blood biomarker for the detection of ACR. Interestingly, a mean methylation difference of approximately 60% (Table 3) was expected to be observed between these three regions within genomic DNA derived from ventricular cells in comparison to that of other tissues in the body. We attempted to recapitulate this difference *in vitro* using bisulfite converted gDNA from various tissues within the human body and PCR amplification of these three regions of interest. We found

that the differences in methylation percentages within these regions in gDNA from the ventricles and other tissues in the human body were not as robust *in vitro* in comparison to the estimates determined *in silico* (Figure 15). Ultimately, this raised concerns regarding the specificity of these regions and the degree to which these methylation patterns were truly unique to the ventricles. In addition to testing the differences in methylation at these regions between the ventricles and other tissues within the human body, a more important comparison would have been between these regions in the ventricles and hematopoietic cells. If a large difference in methylation can be observed between these two sets of methylomes *in vitro*, we can be more confident that the fraction of dd-cfDNA has been accurately quantified and distinguished from cfDNA derived from hematopoietic cells, which are the main contributor of total cfDNA within recipients' plasma (*65*).

It should be noted that prior to assessing the quantity of cfDNA derived specifically from the donated heart, it has been suggested that an increase in the total amount of cfDNA within the recipient's plasma may also be an indicator of adverse outcomes (*66*). Overall, we did see an increase in the mean concentration of total cfDNA as the severity of rejection increased (Figures 16 and 17). However, there was a large amount of overlap between the total concentrations of cfDNA within the recipient's plasma at each of the three rejection grades (Figures 16 and 17). Therefore, there was no statistical significance in the differences observed between the three rejection grades. As such, based on our data it would be difficult to ascertain the severity of rejection using the concentration of total cfDNA within a given plasma sample alone. Thus, we tested the utility of three DMRs for the identification and quantification of cfDNA derived from the donated heart within the circulation due to ACR.

In order to assess the efficacy of the DMRs at Chr 9-1, Chr 9-2, and Chr 12 we obtained serial plasma samples from four heart transplant recipients undergoing routine EMBs at the FMC. Very

little total cfDNA was detected in the plasma of patient 1002 during the 11th and 12th biopsies, in which moderate rejection was observed (Figures 18A, 22A, 26A). In contrast to this, very large amounts of total cfDNA were extracted from the plasma samples taken of this recipient during the 14th and 15th biopsy, despite having only experienced mild rejection (Figures 18A, 22A, 26A). As a result, the concentration of all three DMRs within the plasma of patient 1002 were contradictory to the biopsy proven rejection grades, as the concentration of the DMRs were contingent on the total concentration of cfDNA (Figures 18, 22, 26, Appendix V: sample calculation). Upon analysis of medical records, the immunosuppressive therapy for patient 1002 was changed during these routine EMBs, whereby MMF and tacrolimus were replaced by sirolimus, but the patient was restarted on tacrolimus a few weeks later due to an adverse reaction to the change. As such, this may account for the large increase in the total cfDNA, and the concentration of the three DMRs, detected within the plasma of patient 1002, despite having been consistently assigned a biopsy-proven rejection grade of 1R between 802- and 858-days post-HT (Figures 18, 22, 26). This alteration in the immunosuppressive regimen has been regarded as exclusion criteria in other non-invasive assays for the detection of ACR, such as AlloMap, and may be a consideration for future validation of this assay (*19*).

Interestingly, patient 1021 only experienced at most mild rejection over the time period in which samples were collected. Despite this, very large amounts of total cfDNA were detected within the plasma of this heart transplant recipient, which ranged from 58,080 copies/mL to 415,800 copies/mL (Figures 19A, 23A, 27A). This inherently created large discrepancies between the concentration of the three DMRs within the recipient's plasma and the severity of rejection that was determined by the biopsy. Notably, these samples were taken between 22-190 days post-HT when the levels of dd-cfDNA tend to fluctuate considerably and can remain high following

the transplantation should complete quiescence not be achieved (*34*). As such, this may have accounted for the extremely high concentrations of total cfDNA and therefore, the three DMRs, within the plasma of patient 1021. Especially since this recipient wavered between quiescence and mild rejection over the course of this sampling period. Thus, many previously established non-invasive circulating nucleic acid-based assays do emphasize the use of these assays only after the first 6-months have passed post-HT, when the concentration of total cfDNA tends to become more stable (*19*, *34*, *67*).

The data collected for patient 1017 was much more consistent with expected outcomes, especially in terms of total cfDNA extracted from each plasma sample collected from this recipient. An increase in the concentration of the total cfDNA was only observed at days 269 and 374 post-HT when moderate to severe rejection events occurred, with 76,890 copies/mL and 78,870 copies/mL detected, respectively (Figures 20A, 24A, 28A). Interestingly, despite the total concentration of cfDNA remaining consistent with the severity of rejection for this patient, the DMR at Chr 9-1 failed to be detected at a high concentration at day 269 post-HT when patient 1017 experienced moderate to severe rejection (Figure 20B). However, a spike in the concentration of this DMR was observed in the plasma of this recipient at day 374 post-HT when the second moderate rejection event occurred (Figure 20B). This inconsistent result makes it difficult to ascertain the efficacy of this DMR as it may be due to a lack of specificity and sensitivity of this DMR, or it may be a result of an error in the amplification or sequencing of this DMR within the pool of amplicons for the sample taken at day 269.

In contrast to this, the results obtained for the DMRs on Chr 9-2 and Chr 12 for patient 1017 were very promising. More specifically, for the DMR on Chr 9-2, we observed an obvious increase in the concentration of this DMR during both moderate to severe rejection events at days 269 and

375 post-HT (Figure 24B). A steady decline in the concentration of this DMR was also observed following the 2R-3R rejection event at day 269 post-HT (Figure 24B). This suggested that the patient responded well to the anti-rejection therapy and was consistently diagnosed with only mild rejection according to the biopsies. Notably, the concentration of this DMR on days 94 and 178 post-HT were higher than expected as the patient was noted to have no signs of rejection based on the biopsy (Figure 24B). It should be kept in mind that the EMB itself is flawed, as the sampling region is restricted to the right side of the interventricular septum and the myocardium is not equally impacted by ACR (*11*, *12*). Therefore, it is possible that mild ACR may have been occurring in the patient's donated heart but the biopsy did not capture the effected regions. As such, it is difficult to establish whether this DMR lacks sensitivity and specificity or if this result may be a contraindication of the efficacy of the EMB. Similar to the DMR at Chr 9-2, a large concentration of the DMR on Chr 12 was detected in the plasma of the recipient at day 269 post-HT when a 2R-3R rejection event was noted (Figure 28B). The concentration of this DMR was also higher at day 374 days post-HT, however, the increase was not substantial when compared to the concentrations observed during the other biopsies in which mild or no rejection was observed (Figure 28B). Once again, the concentrations of this DMR on days 94 and 178 post-HT when the patient was quiescent were similar to those observed in samples obtained when the recipient experienced mild rejection. As such, this may be a consequence of a lack of specificity and sensitivity of this DMR or it may highlight the drawbacks of the EMB and the subjective assignment of a rejection grade (Figure 28B).

Majority of the samples collected from patient 1025 took place within the first six months post-HT, specifically between days 14-236 post-HT. As a result, the total amount of cfDNA detected within this recipient's plasma was quite high, much like for patient 1021, and ranged between

17,688 copies/mL and 191,400 copies/mL (Figures 19A, 23A, 27A). Upon analyzing the data for the DMR at Chr 9-1, we noted contradictory results for the concentration of this DMR relative to the severity of rejection reported by the EMB (Figure 21B). Since this was consistently noted across all four patients, it suggested poor sensitivity and specificity of this DMR within cfDNA despite the promising results observed at this region within ventricular gDNA (Table 5). In contrast to this, the results obtained for the DMRs at Chr 9-2 and Chr 12 within the plasma of patient 1025 were much more favourable. More specifically, we observed a steady increase in the concentration of both of these DMRs within the recipient's plasma leading up to a moderate rejection event (Figures 23B and 27B). This suggested that these DMRs may have a predictive value and could potentially prompt a physician to make changes to the immunosuppressive therapy to prevent a moderate rejection event from even taking place. Furthermore, we also observed a decline in the concentration of these DMRs following the 2R rejection event at day 145 post-HT, which implied that the patient responded well to the anti-rejection therapy that was implemented (Figures 23B and 27B). Finally, in both cases, a spike in the concentration of these DMRs was observed at day 236 post-HT when the patient was diagnosed with mild (1R) rejection (Figures 23B and 27B). This may have been an indication of an oncoming moderate rejection event, and could be a signal to modify the immunosuppressive therapy to prevent an increase in the severity of rejection. However, further testing and more serial samples would have been necessary to determine if this was true. Thus, these DMRs could have the potential to be more sensitive and accurate for the determination of the severity of ACR in comparison to the EMB.

Overall, we observed a great deal of variation in the concentration of the three DMRs of interest and the corresponding biopsy-proven rejection grade, especially for samples that were assigned a grade of 1R. As such, the average proportion of myocardial cells that underwent apoptosis or

necrosis within tissue samples obtained during routine EMBs was correlated with the concentration of each DMR of interest from matched blood samples. Since the release of cfDNA is directly associated with the process of apoptosis, we expected to see a positive and more robust correlation between the concentration of the DMRs of interest and the degree of tissue apoptosis observed. It should be noted that because we could not determine an accurate value that represented the overall degree of apoptosis at each individual biopsy, due to the lack of statistical power and the complexity of the data sets, we were constrained to the use of the mean degree of apoptosis at each associated biopsy-proved rejection grade. As such, the negative correlation between the mean percentage of cells that had undergone apoptosis or necrosis and the concentration of all three DMRs within the plasma of patient 1002 reiterated the observation that the concentrations of the three DMRs decreased despite the increasing degree of myocardial apoptosis due to ACR and vice versa (Figures 30A, 31A, 32A). The strong positive correlation between the mean percentage of cells that stained positively for both TUNEL and DAPI and the concentration of the DMRs at Chr 9-2 (Figure 31 B and C) and Chr 12 (Figure 32 B and C) within the plasma samples obtained from patients 1021 and 1025 suggested a more promising utility of these two DMRs. More specifically, as the average percentage of myocardial cells that underwent apoptosis or necrosis increased, the concentration of these cfDNA-based biomarkers also increased, as expected. However, due to the small sample sizes and the use of a mean percentage of apoptosis at a given rejection grade, we cannot fully ascertain the correlation between the amount of apoptosis and the concentration of the DMR of interest at each individual biopsy.

3.6 Conclusion

We have successfully established a pipeline for the identification of organ-specific DMRs for the non-invasive detection of tissue injury. More specifically, we introduced the potential use of ventricle-specific DMRs as a non-invasive, cfDNA-based method, for the identification and quantification of cfDNA derived from the donated heart in the circulation due to ACR following HT. However, much like other previously established non-invasive cfDNA based assays, specific parameters may need to be met in order for this assay to be successfully implemented; including a stable concentration of total cfDNA, which typically occurs when a patient is more than 6-months post-HT, and consistent immunosuppressive therapy. The DMRs at Chr 9-2 and Chr 12 not only more successfully predicted the onset of a moderate rejection event, but also accurately reflected the severity of rejection. In some cases, the concentration of these DMRs may have been more indicative of the severity of rejection in comparison to the results of the flawed EMB. Also, as expected, the correlation between the concentration of the DMRs at Chr 9-2 and Chr 12 and the degree of tissue apoptosis observed in patient 1021 and 1025 was positive, as predicted. Thus, with increased tissue and cellular methylomes, patient numbers, and samples taken during biopsy-proven moderate rejection events, we will be able to more confidently assess the utility of this novel non-invasive cfDNA-based assay for the detection of ACR following HT.

CHAPTER FOUR: SUMMARY

4.1 Conclusions

The current gold standard for the detection of rejection involves the use of an EMB, which is followed by histological analysis for the assignment of a rejection grade, based on the guidelines determined by ISHLT. Using TUNEL staining, we were able to successfully quantify the mean percentage of apoptotic or necrotic cells within samples from 6 adult heart transplant recipients obtained by routine EMBs during quiescence, and mild and moderate ACR. At the individual biopsy level, we elucidated the variation present within the ISHLT rejection grade of 1R in terms of the amount of myocardial cell death that had occurred across these "mild" rejection samples. While the ISHLT guidelines for the assignment of rejection grades provides a straightforward method for classification, our results suggested that this grading system may be oversimplified. Therefore, certain 1R samples may in fact warrant some kind of medical action in order to ensure patient health and allograft survival, as 0R and 1R patients are currently treated the same clinically.

Our lab had previously established a SNP-based cfDNA assay for the detection of ACR, however, this assay lacked sensitivity and specificity. As such, we implemented changes by employing an automated extraction approach, the Illumina MiSeq sequencing platform, and alternative informative SNPs. It should also be noted that the HID-Ion AmpliSeq identity panel and the new custom SNP panel were validated using identical libraries, which included two 2R samples, along with 0R and 1R samples. However, due to the lower sequencing error rate of the MiSeq platform, a novel algorithm must be developed in order to ascertain the efficacy of these improvements.

As an alternative to the SNP-based assay, we introduced the potential use of ventricle-specific DMRs as a non-invasive, cfDNA-based method, for the identification and quantification

of cfDNA derived from the donated heart due to ACR following HT. However, specific parameters may need to be met in order for this assay to be successfully implemented, including a stable concentration of total cfDNA and consistent immunosuppressive therapy. The results for the DMRs at Chr 9-2 and Chr 12 were the most promising as both of these biomarkers displayed the capacity to predict the onset of a moderate rejection event and accurately reflected the severity of rejection. In some cases, these DMRs may have been more demonstrative of the severity of rejection in comparison to the results of the flawed EMB. Also, as expected, the concentration of these DMRs increased as the degree of tissue apoptosis also increased as these processes are directly linked.

In conclusion, a blood test that allows clinicians to closely monitor the donated heart for damage would be an important advance since this would enable increased and non-invasive surveillance of the allograft. In turn, this could open the possibility of individualized immunosuppressant dosing to prevent rejection or over-immunosuppression and toxicity. Furthermore, non-invasive surveillance of the allograft would improve patient comfort and safety, and reduce costs. This is especially pertinent as the current gold standard for monitoring heart transplant rejection requires an EMB, which provides a limited understanding of the overall status of the transplanted heart, is highly invasive, and has the potential for severe complications. Overall, this novel cfDNA-based assay that utilizes organ-specific methylation patterns has the potential to be a superior assay to SNP-based assays as *a priori* knowledge of the donor and recipient's genomes are not required and estimations based on theoretical frequencies of the donor's "genetic fingerprint" are not required. Finally, the pipeline we have established for the identification of ventricle-specific DMRs can be modified to be applicable to any other type of solid organ transplant.

4.2 Future Directions

In order to determine if the changes that were made to the previously established SNP-based assay successfully improved the specificity and sensitivity of this assay, a novel algorithm will need to be developed to analyze the sequencing data that was collected from the Illumina MiSeq platform. The most prominent difference in this algorithm will be in the function that removes the known fraction of miscalled SNPs, which will be a much smaller proportion for this newly collected data, as this platform has a much lower sequencing error rate.

In terms of the identification of ventricle-specific DMRs *in silico*, we used an unbiased approach by interrogating whole bisulfite-sequenced genomes of the tissues and hematopoietic cells. Instead, we could take a more targeted approach by utilizing regions of genes that are known to be unique to the ventricles, and therefore, highly differentially methylated relative to other cells and tissues. One such example would be *IRX4*, which is exclusively expressed in the ventricular myocardium (*68*). Another is *SCN5A*, a gene that is highly expressed in cardiac muscle cells and plays a key role in these cells' ability to generate and transmit electrical signals (*69*). In addition to this, with the potential increase in the number of publicly available methylomes of tissues within the body, hematopoietic cells, and specific regions within the heart, more robust DMRs could be identified. Alternatively, several input files may be created by randomly selecting up to ten tissue and cell methylomes to compare against the ventricular methylomes using Metilene. The DMRs that are consistently identified amongst these several output files could represent an even more robust list of candidate DMRs for this novel assay. Also, other softwares could be implemented to identify DMRs and the regions that are consistently recognized across each software may function as highly ventricle-specific DMRs. In terms of the validation of these DMRs *in vitro*, the methylation patterns at these regions of interest must be compared between the ventricles and

hematopoietic cells in order to confidently ascertain the specificity of these DMRs to the ventricles. This will ultimately improve our ability to identify and quantify the fraction of cfDNA that is truly derived from the ventricles of the donated heart due to rejection following heart transplantation.

Finally, the selected DMRs and SNPs have been retrospectively analyzed, as the rejection grades of the samples were known prior to the evaluation. However, to accurately determine which of these cfDNA-based assays is superior, a prospective analysis will need to be conducted. This will allow us to ascertain which assay has the capacity to more accurately determine the severity of rejection without the use of an EMB. This will be based on how accurately the concentration of dd-cfDNA can be determined, using either the ventricle-specific DMRs or donor-specific SNPs to identify and quantify the dd-cfDNA, which in turn can be used to elucidate the severity of rejection.

References

1. C. N. Barnard, The operation a human cardiac transplant: an interim report of a successful operation performed at Groote Schuur Hospital GROOTE SCHUUR HOSPITAL, CAPE TOWN (available at http://journals.co.za/docserver/fulltext/m_samj/41/48/34907.pdf?expires=1516140518&id=id&accname=guest&checksum=66AA91313DA13ED941B57DC64E92AF18).

2. J. W. Rossano *et al.*, The Registry of the International Society for Heart and Lung Transplantation: Nineteenth Pediatric Heart Transplantation Report—2016; Focus Theme: Primary Diagnostic Indications for Transplant MPH and for the International Society for Heart and Lung Trans (2016), doi:10.1016/j.healun.2016.08.018.

3. L. H. Lund *et al.*, The Registry of the International Society for Heart and Lung Transplantation: Thirty-third Adult Heart Transplantation Report—2016; Focus Theme: Primary Diagnostic Indications for Transplant. *J. Hear. Lung Transplant.* **35**, 1158–1169 (2016).

4. C. Sivathasan, C. P. Lim, K. L. Kerk, D. K. L. Sim, M. R. Mehra, Mechanical circulatory support and heart transplantation in the Asia Pacific region. *J. Hear. Lung Transplant.* **36**, 13–18 (2017).

5. M. H. Goldman *et al.*, Cyclosporine in Cardiac Transplantation. *Surg. Clin. North Am.* **65**, 637–659 (1985).

6. L. D. Cornell, R. N. Smith, R. B. Colvin, Kidney Transplantation: Mechanisms of Rejection and Acceptance. *Annu. Rev. Pathol. Mech. Dis.* **3**, 189–220 (2008).

7. S. Sakakibara, S. Konno, Endomyocardial Biopsy (available at https://www.jstage.jst.go.jp/article/ihj1960/3/6/3_6_537/_pdf/-char/en).

8. P. K. Caves *et al.*, Percutaneous Transvenous Endomyocardial Biopsy. *JAMA J. Am. Med. Assoc.* **225**, 288 (1973).

9. M. H. Yamani, D. O. Taylor, in *Current Clinical Medicine* (Elsevier, 2010;

http://www.crossref.org/deleted_DOI.html), pp. 180–186.

10. S. Stewart *et al.*, Revision of the 1990 Working Formulation for the Standardization of Nomenclature in the Diagnosis of Heart Rejection. *J. Hear. Lung Transplant.* **24**, 1710–1720 (2005).

11. T. Khan *et al.*, The value of endomyocardial biopsy in diagnosis and guiding therapy. *Pathology*. **49**, 750–756 (2017).

12. J. F. McMinn *et al.*, Biomarkers of acute rejection following cardiac transplantation. *Biomark. Med.* **8**, 815–832 (2014).

13. C. Baraldi-Junkins *et al.*, Complications of endomyocardial biopsy in heart transplant patients. *J. Heart Lung Transplant.* **12**, 63–7.

14. J. W. Mason, Techniques for right and left ventricular endomyocardial biopsy. *Am. J. Cardiol.* **41**, 887–892 (1978).

15. S. C. Greenway *et al.*, Magnetic resonance imaging of the transplanted pediatric heart as a potential predictor of rejection. *World J. Transplant.* **6**, 751–758 (2016).

16. C. R. Butler *et al.*, Correlation of cardiovascular magnetic resonance imaging findings and endomyocardial biopsy results in patients undergoing screening for heart transplant rejection. *J. Hear. Lung Transplant.* **34**, 643–650 (2015).

17. M. C. Deng *et al.*, Noninvasive Discrimination of Rejection in Cardiac Allograft Recipients Using Gene Expression Profiling. *Am. J. Transplant.* **6**, 150–160 (2006).

18. L. Prokunina *et al.*, A regulatory polymorphism in PDCD1 is associated with susceptibility to systemic lupus erythematosus in humans. *Nat. Genet.* **32**, 666–669 (2002).

19. M. X. Pham *et al.*, Gene-Expression Profiling for Rejection Surveillance after Cardiac Transplantation. *N. Engl. J. Med.* **362**, 1890–1900 (2010).

20. E. Crowley, F. Di Nicolantonio, F. Loupakis, A. Bardelli, Liquid biopsy: monitoring

cancer-genetics in the blood. *Nat. Rev. Clin. Oncol.* **10**, 472–484 (2013).

21. P. Mandel, P. Metais, Les acides nucléiques du plasma sanguin chez l'homme. *C. R. Seances Soc. Biol. Fil.* **142**, 241–3 (1948).

22. J. Atamaniuk *et al.*, Increased Concentrations of Cell-Free Plasma DNA after Exhaustive Exercise. *Clin. Chem.* **50**, 1668–1670 (2004).

23. R. Lehmann-Werman *et al.*, Identification of tissue-specific cell death using methylation patterns of circulating DNA. *Proc. Natl. Acad. Sci.* **113**, E1826–E1834 (2016).

24. Y. M. Lo *et al.*, Rapid clearance of fetal DNA from maternal plasma. *Am. J. Hum. Genet.* **64**, 218–24 (1999).

25. Y. M. Lo *et al.*, Presence of fetal DNA in maternal plasma and serum. *Lancet (London, England)*. **350**, 485–7 (1997).

26. H. C. Fan *et al.*, Non-invasive prenatal measurement of the fetal genome. *Nature*. **487**, 320–4 (2012).

27. L. A. Diaz, A. Bardelli, A. Bardelli, Liquid biopsies: genotyping circulating tumor DNA. *J. Clin. Oncol.* **32**, 579–86 (2014).

28. H. Schwarzenbach, D. S. B. Hoon, K. Pantel, Cell-free nucleic acids as biomarkers in cancer patients. *Nat. Rev. Cancer*. **11**, 426–437 (2011).

29. X. Han, J. Wang, Y. Sun, Circulating Tumor DNA as Biomarkers for Cancer Detection. *Genomics. Proteomics Bioinformatics*. **15**, 59–72 (2017).

30. S. Salvi *et al.*, Cell-free DNA as a diagnostic marker for cancer: current insights. *Onco. Targets. Ther.* **9**, 6549–6559 (2016).

31. J. C. H. Tsang, Y. M. Dennis Lo, Circulating nucleic acids in plasma/serum. *Pathology*. **39**, 197–207 (2007).

32. Y. Lo, R. W. Chiu, Plasma nucleic acid analysis by massively parallel sequencing: pathological insights and diagnostic implications. *J. Pathol.* **225**, 318–323 (2011).

33. K. Strimbu, J. A. Tavel, What are biomarkers? *Curr. Opin. HIV AIDS*. **5**, 463–466 (2010).

34. I. De Vlaminck *et al.*, Circulating cell-free DNA enables noninvasive diagnosis of heart transplant rejection. *Sci. Transl. Med.* **6**, 241ra77 (2014).

35. E. M. Gielis *et al.*, Plasma donor-derived cell-free DNA kinetics after kidney transplantation using a single tube multiplex PCR assay. *PLoS One*. **13**, e0208207 (2018).

36. I. De Vlaminck *et al.*, Noninvasive monitoring of infection and rejection after lung transplantation. *Proc. Natl. Acad. Sci. U. S. A.* **112**, 13336–41 (2015).

37. O. Bergmann *et al.*, Evidence for cardiomyocyte renewal in humans. *Science*. **324**, 98–102 (2009).

38. P. M. K. Gordon *et al.*, An Algorithm Measuring Donor Cell-Free DNA in Plasma of Cellular and Solid Organ Transplant Recipients That Does Not Require Donor or Recipient Genotyping. *Front. Cardiovasc. Med.* **3**, 33 (2016).

39. K. Kyrylkova, S. Kyryachenko, M. Leid, C. Kioussi, (Humana Press, 2012; http://link.springer.com/10.1007/978-1-61779-860-3_5), pp. 41–47.

40. Y. Gavrieli, Y. Sherman, S. A. Ben-Sasson, Identification of programmed cell death in situ via specific labeling of nuclear DNA fragmentation. *J. Cell Biol.* **119**, 493–501 (1992).

41. B. A. Bell, W. C. Smiley, M. Ene, G. L. Blue, An Intermediate Primer to Estimating Linear Multilevel Models using SAS ® PROC MIXED (2013), (available at https://www.semanticscholar.org/paper/An-Intermediate-Primer-to-Estimating-Linear-Models-Bell-Smiley/c09c49b59d6a2444f5ebeece137c4c627bcd06e8).

42. G. Egger, G. Liang, A. Aparicio, P. A. Jones, Epigenetics in human disease and prospects for epigenetic therapy. *Nature*. **429**, 457–463 (2004).

43. D. Rodenhiser, M. Mann, Epigenetics and human disease: translating basic biology into clinical applications. *CMAJ*. **174**, 341–8 (2006).

44. G. Kelsey, R. Feil, New insights into establishment and maintenance of DNA methylation imprints in mammals. *Philos. Trans. R. Soc. Lond. B. Biol. Sci.* **368**, 20110336 (2013).

45. H. Ji *et al.*, Comprehensive methylome map of lineage commitment from haematopoietic progenitors. *Nature*. **467**, 338–342 (2010).

46. F. Miao, X. Wu, L. Zhang, A. D. Riggs, R. Natarajan, Histone methylation patterns are cell-type specific in human monocytes and lymphocytes and well maintained at core genes. *J. Immunol.* **180**, 2264–9 (2008).

47. A. G. Wilson, Epigenetic Regulation of Gene Expression in the Inflammatory Response and Relevance to Common Diseases. *J. Periodontol.* **79**, 1514–1519 (2008).

48. C. Abi Khalil, The emerging role of epigenetics in cardiovascular disease. *Ther. Adv. Chronic Dis.* **5**, 178–87 (2014).

49. R. Z. Jurkowska, T. P. Jurkowski, A. Jeltsch, Structure and Function of Mammalian DNA Methyltransferases. *ChemBioChem*. **12**, 206–222 (2011).

50. T. H. Bestor, G. L. Verdine, DNA methyltransferases. *Curr. Opin. Cell Biol.* **6**, 380–389 (1994).

51. H. Leonhardt, A. W. Page, H.-U. Weier, T. H. Bestor ', A Targeting Sequence Directs DNA Methyltransferase to Sites of DNA Replication in Mammalian Nuclei. *Cell*. **71**, 865–873 (1992).

52. E. Li, M. Okano, S. Xie, Cloning and characterization of a family of novel mammalian DNA (cytosine-5) methyltransferases. *Nat. Genet.* **19**, 219–220 (1998).

53. A. Bird, DNA methylation patterns and epigenetic memory. *Genes Dev.* **16**, 6–21 (2002).

54. M. M. Suzuki, A. Bird, DNA methylation landscapes: provocative insights from epigenomics. *Nat. Rev. Genet.* **9**, 465–476 (2008).

55. J. Tsuji, Z. Weng, Evaluation of preprocessing, mapping and postprocessing algorithms for analyzing whole genome bisulfite sequencing data. *Brief. Bioinform.*, bbv103 (2015).

56. A. Kundaje *et al.*, Integrative analysis of 111 reference human epigenomes. *Nature*. **518**, 317–330 (2015).

57. J. H. A. Martens, H. G. Stunnenberg, BLUEPRINT: mapping human blood cell epigenomes. *Haematologica*. **98**, 1487–9 (2013).

58. F. Jühling *et al.*, metilene: fast and sensitive calling of differentially methylated regions from bisulfite sequencing data. *Genome Res.* **26**, 256–62 (2016).

59. L.-C. Li, R. Dahiya, MethPrimer: designing primers for methylation PCRs. *Bioinformatics*. **18**, 1427–31 (2002).

60. S. Andrews, Babraham Bioinformatics - FastQC A Quality Control tool for High Throughput Sequence Data, (available at https://www.bioinformatics.babraham.ac.uk/projects/fastqc/).

61. F. Stephenson, *Calculations for Molecular Biology and Biotechnology: A Guide to Mathematics in the Laboratory* (Elsevier Science, 2010; https://www.researchgate.net/publication/286323136_Calculations_for_Molecular_Biology_and_Biotechnology_A_Guide_to_Mathematics_in_the_Laboratory).

62. J. Wan *et al.*, Characterization of tissue-specific differential DNA methylation suggests distinct modes of positive and negative gene expression regulation. *BMC Genomics*. **16**, 49 (2015).

63. K. Lokk *et al.*, DNA methylome profiling of human tissues identifies global and tissue-specific methylation patterns. *Genome Biol.* **15**, r54 (2014).

64. H.-M. Byun *et al.*, Epigenetic profiling of somatic tissues from human autopsy specimens identifies tissue- and individual-specific DNA methylation patterns. *Hum. Mol. Genet.* **18**, 4808–4817 (2009).

65. Y. Y. N. Lui *et al.*, Predominant hematopoietic origin of cell-free DNA in plasma and serum after sex-mismatched bone marrow transplantation. *Clin. Chem.* **48**, 421–7 (2002).

66. S. D. Zangwill *et al.*, Increase in Total Cell-Free DNA Correlates with Death in Adult and

Pediatric Heart Transplant Recipients: DNA Based Transplant Rejection Test (DTRT)-A Prospective Blinded Multicenter NIH/NHLBI Funded Clinical Study. *J. Hear. Lung Transplant.* **38**, S50–S51 (2019).

67. T. M. Snyder *et al.*, Universal noninvasive detection of solid organ transplant rejection. *Source Proc. Natl. Acad. Sci. United States Am.* **108**, 6229–6234 (2011).

68. B. G. Bruneau *et al.*, Cardiac Expression of the Ventricle-Specific Homeobox Gene Irx4 Is Modulated by Nkx2-5 and dHand. *Dev. Biol.* **217**, 266–277 (2000).

69. F. van Hoorn *et al.*, SCN5A mutations in Brugada syndrome are associated with increased cardiac dimensions and reduced contractility. *PLoS One*. **7**, e42037 (2012).

70. M. Naesens, M. M. Sarwal, Molecular diagnostics in transplantation. *Nat. Rev. Nephrol.* **6**, 614–628 (2010).

71. T. K. Sigdel *et al.*, A Rapid Noninvasive Assay for the Detection of Renal Transplant Injury. *Transplant. J.* **96**, 97–101 (2013).

72. E. Sharon *et al.*, Quantification of transplant-derived circulating cell-free DNA in absence of a donor genotype. *PLOS Comput. Biol.* **13**, e1005629 (2017).

73. E. Schütz *et al.*, Graft-derived cell-free DNA, a noninvasive early rejection and graft damage marker in liver transplantation: A prospective, observational, multicenter cohort study. *PLOS Med.* **14**, e1002286 (2017).

74. C. Phillips *et al.*, Evaluation of the Genplex SNP typing system and a 49plex forensic marker panel. *Forensic Sci. Int. Genet.* **1**, 180–5 (2007).

75. A. J. Pakstis *et al.*, SNPs for a universal individual identification panel. *Hum. Genet.* **127**, 315–324 (2010).

76. T. M. Karafet *et al.*, New binary polymorphisms reshape and increase resolution of the human Y chromosomal haplogroup tree. *Genome Res.* **18**, 830–8 (2008).

Appendices

I. Laboratory Protocols

TUNEL Assay Protocol

Promega (DeadEnd TM Fluorometric TUNEL System) Protocol. Alterations are denoted in *italics.* Section 4B was followed (Pretreatment of paraffin-embedded tissues). Adapted from https://www.promega.ca/-/media/files/resources/protocols/technical- bulletins/0/deadend-fluorometric-tunel-system-protocol.pdf.

Before beginning:

- *Set water-bath to 37*°C.
- *Keep methanol-free formaldehyde in PBS out of fridge*
- *Prepare 100%, 95%, 85%, 70%, 50% Ethanol, 0.85% NaCl, 20µg/ml Proteinase K solution, and 2x SSC solution*

1. Deparaffinize tissue sections (attached to microscope slides) by immersing slides in fresh xylene in a Coplin jar for 5 minutes at room temperature. Repeat one time for a total of two xylene washes.
2. Wash the samples by immersing the slides in 100% ethanol for 5 minutes at room temperature in a Coplin jar.
3. Rehydrate the samples by sequentially immersing the slides through graded ethanol washes (100%, 95%, 85%, 70%, 50%) for 3 minutes each at room temperature
4. Wash the samples by immersing the slides in 0.85% NaCl for 5 minutes at room temperature
5. Wash the samples by immersing the slides in PBS for 5 minutes at room temperature.
6. Fix the tissue sections by immersing the slides in 4% methanol-free formaldehyde solution in PBS for 20 minutes at room temperature. *Paraformaldehyde was substituted for methanol-free formaldehyde.*
7. Wash the samples by immersing the slides in PBS for 5 minutes at room temperature. Repeat once for a total of two PBS washes.
8. Remove the liquid from the tissue and place the slides on a flat surface. Prepare a 20 µg/ml Proteinase K solution from the reconstituted Proteinase K (10mg/ml; see Section 2) by diluting 1:500 in PBS. Add 100 µl of the 20 µg/ml Proteinase K to each slide to cover the tissue section. Incubate slides for 8–10 minutes at room temperature.
9. Wash the samples by immersing the slides in PBS for 5 minutes at room temperature in a Coplin jar.
10. Fix the tissue sections after washing by immersing the slides in 4% methanol-free formaldehyde solution in PBS for 20 minutes at room temperature.
11. Wash the samples by immersing the slides in PBS for 5 minutes at room temperature.

Move onto protocol 4A (beginning with Step 5):

5. Remove excess liquid by tapping the slides. Cover the cells with 100µl of Equilibration Buffer. Equilibrate at room temperature for 5–10 minutes.

6. While the cells are equilibrating, thaw the Nucleotide Mix on ice and prepare sufficient rTdT incubation buffer for all experimental and optional positive control reactions according to the below table:

Buffer Component	Component Volume per Standard 50µl Reaction		Number of Reactions (Experimental Reactions + Optional Positive Controls)		Component Volume
Equilibration Buffer	45µl	x	_____	=	_____µl
Nucleotide Mix	5µl	x	_____	=	_____µl
rTdT Enzyme	1µl	x	_____	=	_____µl
Total rTdT Incubation Buffer Volume				=	**_____µl**

• Keep the Nucleotide Mix and rTdT incubation buffer solution on ice, protected from light.

7. Blot around the equilibrated areas with tissue paper to remove most of the 100 µl of Equilibration Buffer and add 50 µl of rTdT incubation buffer to the cells on a 5 cm^2 area. Do not allow the cells to dry out.
    a. *Avoid exposing the slides to light after completion of Step 7.*
8. Cover the cells with Plastic Coverslips to ensure even distribution of the reagent. Place paper towels soaked with water at the bottom of a humidified chamber. Incubate the slides at 37°C for 60 minutes inside the humidified chamber to allow the tailing reaction to occur. Cover the chamber with aluminum foil to protect from direct light.
9. Dilute the 20X SSC 1:10 with deionized water and add enough of the resulting 2X SSC to fill a standard Coplin jar (40 ml). Remove the Plastic Coverslips and terminate the reactions by immersing the slides in 2X SSC in a Coplin jar for 15 minutes at room temperature. Ensure that all salts of the 20X SSC are in solution before diluting (Step 9).
10. Wash the samples by immersing the slides in fresh PBS for 5 minutes at room temperature. Repeat two times for a total of three washes to remove unincorporated fluorescein-12-dUTP.

The protocol was altered following Step 10 (4A) as follows:

11. Dilute NucBlue Fixed Cell Stain DAPI (Invitrogen) into PBS (2 drops/mL)
12. Cover each section of tissue with 50 µL of the diluted DAPI
13. Wash slides with PBS twice (5 mins each)
14. Place a drop of Calbiochem's Fluorsave glue on each section and place plastic coverslip on top ensuring that no bubbles form.
15. Allow coverslip to set overnight.
16. View slide using spinning disk confocal super resolution microscope

Semi-Automated Cell Free DNA Isolation from Patient Plasma

Based on the protocol outlined in the MagNA Pure 24 Total NA Isolation Kit (Roche) for the isolation of double-stranded cell free nucleic acids from 2000 µL of plasma. Adapted from https://lifescience.roche.com/en_ca/products/magna-pure-24-instrument.html#application

Before purifying cell-free nucleic acids:

- Centrifuge the samples for 5 to 10 min at 1000 to 1900 x *g.* Avoid transferring any of the pellet.
- Avoid introducing foam/bubbles during all pipetting steps.

Protocol	**cfNA ds 2000**
Proteinase K [µL]	200
CELB [µL]	1750
IPA [µL]	300
cfNA buffer mix (CELB + IPA) [µL]	2050

- In a fresh tube compatible with the MagNA Pure 24 Sample Rack, place the appropriate volume of Proteinase K. Add the sample into the tube containing Proteinase K, mix gently, and incubate at 37°C for 20 min.
- According to the number of samples to be processed, prepare the cfNA buffer mix in bulk by mixing Cell-Free Nucleic Acid Enhancement Buffer (CELB) and isopropanol (IPA) in that order, in an appropriately sized container. The volumes listed in the table are the required amounts for one sample.
- Cap and mix gently by inversion. The solution is stable for a maximum of 2 hours.
- Add the appropriate amount of cfNA buffer mix to each sample (ie: 2000 µL of cfNA buffer mix to 2000 µL of the plasma sample).
- Mix thoroughly by dispensing and aspirating the liquid approximately 8 times to produce a homogeneous mixture.
    - Do not store the lysate.
    - If bubbles form, they may be removed by aspiration into a pipette tip held near the side of the tube just above the surface of the liquid.
    - Alternatively, bubbles may be removed by capping tubes and centrifuging at 2000 x *g* for 1 min.
- Load the tubes onto the sample rack.
- Load the sample rack into the instrument.
- Follow the prompts on the instrument to name each sample and ensure the tubes that will contain the output cfDNA are labelled and placed in the appropriate and corresponding slots.
- Load reagent cartridges and consumables in the appropriate chambers
    - All items loaded to the instrument must be decapped: tubes holding the samples, MGP tubes, internal control tubes, and output consumables.
    - Allow the instrument to scan each area to ensure each item is the in appropriate place prior to starting the automated reaction.

Polymerase Chain Reaction (PCR)

A master mix with the appropriate volumes of each of the reagents listed below was created to divide the contents equally into each tube and to reduce pipetting errors due to the small volumes required to carry out this reaction.

Contents of each tube:

- 5 μL 5X EpiMark Hot Start Taq Reaction Buffer
- 0.5 μL 10 mM dNTPs
- 0.5 μL 10 μM forward primer
- 0.5 μL 10 μM reverse primer
- 2.0-5.0 μL bisulfite converted cfDNA from HT recipient's plasma
- 0.125 μL EpiMark Hot Start Taq DNA Polymerase
- Required volume of RNAse-free water to reach a total of 25 μL

The following protocol was used for PCR reaction thermocycling:

1) 94^0 C – 3 minutes
2) 94^0 C – 45 seconds
3) Variable Tm (55^0 C - 65^0 C) – 45 seconds
4) 68^0 C – 1.5 minutes
5) Repeat steps 2-4 40X
6) 68^0 C – 10 minutes
7) 4^0 C – infinite hold

II. Preliminary Improvements To SNP-Based Assay

i. Introduction

Since the presence of cfDNA in the plasma is due to the natural process of apoptosis, all individuals have some detectable levels of cfDNA in their blood (*9*). For healthy individuals, the majority of the cfDNA detected in the plasma is derived from hematopoietic cells (*9*). The use of circulating nucleic acids, such as cfDNA, as a biomarker for rejection has several advantages, as it is derived directly from the cells of the donated organ that have been injured by the cytotoxic immune response. In addition to this, cfDNA can be easily obtained through a simple and minimally-invasive blood draw or urine sample. Furthermore, cfDNA maintains all of the genetic features of genomic DNA, thereby allowing for differentiation between genetic material released from the donated organ and cfDNA derived from the recipient's cells undergoing routine apoptosis (*70*). In cases where the organ donor is male and the recipient is female, this sex-mismatch can be leveraged in order to identify and quantify donor-derived cfDNA (dd-cfDNA) (*71*). As such, injury to the donated organ as a result of rejection is expected to lead to an increase in the copy number of cfDNA derived from the donor's Y chromosome (*71*). This principle was demonstrated in urine samples taken from sex-mismatched female renal transplant recipients, whereby patients who had experienced rejection had elevated levels of dd-cfDNA in their urine, specifically containing regions found within the Y chromosome, as compared to patients without rejection (*71*). Although this approach allows for confident assessment of rejection in the allograft, sex-mismatch between the donor and recipient is a relatively uncommon event and therefore not broadly applicable in transplantation. Methodology that relies upon identifying differences between the donor and recipient cfDNA based on single nucleotide polymorphisms (SNPs) in cfDNA would be more universally applicable.

Given that an organ transplant is also a genome transplant, the concept of genome transplant dynamics (GTD) relies on informative genetic differences between the donor and recipient whereby, at a particular locus, the recipient ideally is homozygous for a single base (e.g. AA) and the donor is homozygous for a different base (e.g. GG) (*34*, *67*). Due to the genetic heterogeneity between individuals, this "two-genomes" model potentially amounts to tens of thousands of possibly useful loci across the genome that could be used to discriminate dd-cfDNA from recipient cfDNA. Thus, high-throughput sequencing of cfDNA allows for the identification of a unique donor "genetic fingerprint". This donor-specific signature can be used to calculate the quantity of dd-cfDNA present within the recipient circulation (*34*, *67*). This concept was first illustrated using previously-collected blood samples and banked splenocytes from the donor to determine the genotype for each donor-recipient pairing (*67*). After sequencing the purified cfDNA, the percentage of donor-specific molecules was determined based on the total number of informative bases. In samples taken at the time of a biopsy-proven rejection event, the percentage of donor-specific SNPs was increased while the rate of errors due to sequencing and incorrect genotyping information remained unchanged (*67*). In addition to this, it was also noted that the percentage of dd-cfDNA within the recipient's circulation in the absence of rejection was relatively negligible (<1%) (*67*). However, this percentage increased to >3–4% during, or even immediately preceding, biopsy-proven rejection, which represented a significant increase in the amount of dd-cfDNA within the recipient's blood (*67*).

Since the establishment of the GTD assay, prospective studies have been conducted to validate this approach. Both pediatric and adult heart and lung transplant patients were recruited and the genotypes of the donors and recipients were determined using whole-genome sequencing (WGS) (*34*). Over the course of the study, serial plasma samples were collected and upon sequencing the

isolated cfDNA, based on the previously-determined SNP differences between the donor-recipient pairs, an average of 53,423 informative SNP markers were available per pairing (*34*). Overall, the predictive capacity of this assay was superior to that of the AlloMap test, and often showed early detection of acute rejection (*34*). However, despite the accuracy of the GTD assay, important limitations are the requirement for *a priori* knowledge of the donor and recipient's genotypes and the requirement for WGS. While the recipient's genetic information can be easily obtained, this is not always true for the donor and WGS for each donor-recipient pair is costly, labour intensive and time-consuming. Thus, alternative strategies that have been developed to address these weaknesses.

An alternative "single-genome" method utilizes all genotyped SNPs as opposed to relying only on those homozygous SNPs that differ between the recipient and donor (*72*). Therefore, *a priori* knowledge of the donor's specific genotype is not required in order to determine the proportion of dd-cfDNA within the circulation of the recipient (*72*). Due to the fact that heart and lung transplants do not typically occur between closely related individuals (unlike kidney and liver), the developed algorithm for heart and lung transplants assumes that the donor genotype is randomly selected from a human population (*72*). Based on this, the probability of a specific donor allele is assumed to be its frequency in the population, as determined from databases such as the 1000 Genomes Project (*72*). The performance of this model was assessed by directly comparing the estimated levels of dd-cfDNA to levels determined using both the donor and recipient's genotypes and it was found that the two algorithms were highly comparable for lung transplantation (*72*). However, for heart transplant recipients, the estimated levels of dd-cfDNA were highly correlated, but not as strongly as was seen in the lung cohort (*72*). This may be due to lower levels of dd-cfDNA in the heart cohort, which made the estimation more difficult. It should

be noted that the predictive value of this assay was greatly reduced when the abundance of dd-cfDNA fell below 0.2% or exceeded 25%, which prevented the application of this assay for the detection of rejection in liver and bone marrow transplants (*36*, *72*). Thus, further improvements to these algorithms are likely required to increase the sensitivity and specificity for the detection of dd-cfDNA within the circulation of transplant recipients, especially for patients who have recently received a transplant when the levels of circulating cfDNA are known to be elevated (*73*).

The requirement of WGS for both the donor and recipient can not only be an unrealistic requirement for time-critical organ transplants from deceased donors but it can quickly become excessively costly to perform such analysis for every donor-recipient pair. As such, an alternative approach that is rapid, does not require WGS or *a priori* knowledge of the donor and recipient's genotypes and only requires plasma collected from the transplant recipient has been developed (*38*). This method was used to determine the level of dd-cfDNA within the plasma of both pediatric and adult heart transplant recipients as well as a case of a pediatric human liver cell transplant (*38*). Instead of WGS, a commercially-available panel of 124 highly polymorphic SNPs was utilized rather than interrogating the entire genome. This significantly reduced the total amount of sequencing required and therefore substantially reduced the sequencing and analysis time. Furthermore, in order to model the mixture of dd-cfDNA and recipient cfDNA, a novel algorithm based on the assumption that the donor and recipient would display biallelic loci was designed (*38*). Using this assay, dd-cfDNA was detectable after the infusion of donor hepatocytes up to 24 weeks post-transplantation and levels of dd-cfDNA were detectable in plasma obtained from adult and pediatric heart transplant recipients (*38*). Notably, due to the algorithm employed, this assay is limited to circumstances where the dd-cfDNA fraction is <14% (*38*). Therefore, this assay would likely be best suited for the detection of rejection in stable heart transplant recipients who are >1

month post-transplant or those patients who are not lung or liver transplant recipients where the proportion of dd-cfDNA can be substantially higher (*36*). Also, since this assay relied upon differences in minor allele frequency between individuals, it would likely not be robustly accurate in the situation of closely related donor–recipient pairs such as occurs in living-related kidney donation (*38*). Thus, the utility of SNP-based assays for the detection of ACR following transplantation may be limited to specific circumstances in which the fraction of dd-cfDNA within the recipient's plasma does not exceeds a given threshold. Furthermore, these assays are limited to an estimation of the fraction of dd-cfDNA based on assumptions within the associated algorithm for the frequency of donor-specific SNPs within a given population. Thus, under specific conditions these assays may be very useful for the non-invasive detection of ACR following solid organ transplantation, such as HT.

ii. Hypothesis and Specific Aims for Chapter Three

The strategy of utilizing informative and highly polymorphic SNPs to estimate the proportion of cfDNA that is derived from the donated heat has been previously developed in the Greenway lab. More specifically, a commercially available panel (HID-Ion AmpliSeq, Thermo Fisher Scientific) was used along with the PGM Ion Torrent (Thermo Fisher Scientific) sequencing platform and an associated algorithm for the analysis of the sequencing data. In addition to this, the previously developed protocol involved manual extraction of the cfDNA from patient plasma. A major concern with this protocol was the high sequencing error rate of the Ion Torrent platform. This had the potential to drastically impact the accuracy of donor-specific SNP identification, and therefore, the quantification of the proportion of dd-cfDNA. Furthermore, manual extraction methods tend to lack uniformity and therefore, the initial absolute amount of cfDNA extracted

impacted the accuracy of the fraction of cfDNA within the recipient's plasma that was derived from the donated heart. Taken together, these factors hindered the utility of this assay for the non-invasive detection of rejection, as the proportion of dd-cfDNA within the recipient's plasma, based on the assay, and the degree of ACR did not correlate well. Since then, Dr. Paul Gordon has identified 154 highly polymorphic SNPs; as well, sequencing platforms with lower sequencing error rates and semi-automated methods for the extraction of cfDNA have become readily available. As such, we **hypothesize** that the use of the Illumina MiSeq platform, which has a much lower sequencing error rate, a semi-automated approach for the extraction of cfDNA from patient plasma, and a new set of informative SNPs, would dramatically improve the utility of this SNP-based assay for the non-invasive detection of ACR following HT.

Specific Aims:

1) To improve the accuracy of quantification of dd-cfDNA by using a more automated and therefore, uniform method for the extraction of cfDNA from 2 mL of patient plasma.
2) To reduce the sequencing error rate so as to improve the accuracy of identifying donor-specific SNPs.
3) To test the utility of alternative informative SNPs for the non-invasive quantification of the fraction of dd-cfDNA within the recipient's plasma during quiescence and ACR.

iii. Materials and Methods

a. Extraction of Cell-Free DNA from Whole Blood

Prior to each routine EMB, consented heart transplant recipients provided 8-10 mL of whole blood, which was extracted from the right jugular vein, the same point of entry for the biopsy, and

transferred to Streck BCT tubes. These tubes contained a preservative that limited cell lysis, thereby minimizing contamination of the plasma from genomic DNA of hematopoietic cells. From there, the whole blood was centrifuged at 1900 x g at room temperature for 10 minutes to fractionate the blood. Then, the entire plasma layer was transferred into 2-3 2.0 mL Eppendorf tubes, which were then centrifuged at maximum speed (13,000 RPM) for 16 minutes at 4^{o}C. The resulting supernatant was then transferred into new 2.0 mL Eppendorf tubes and stored at -80^{o}C until the cfDNA was ready for isolation. Isolation was performed using the semi-automated MagNA Pure 24 System (Roche), which allowed 24 samples to be processed in a single run (Appendix I). In this case, 12 plasma samples (Table 20) were utilized for cfDNA extraction, which then served as samples for testing the utility of both the previously developed, and new custom SNP-based assays for the detection of rejection.

Table 20. The concentration of cfDNA within a given volume of solution and the resulting absolute amount of DNA within each sample taken from patients 1002 and 1021, along with the associated biopsy-proven rejection grade, in order to test the efficacy of the HID-Ion AmpliSeq Identity Panel and custom SNP panel on the Illumina MiSeq platform.

Patient #	Biopsy #	Biopsy-Proven Rejection Grade	Concentration (ng/μL)	Volume (μL)	Absolute Amount (ng)
1002	10	1R	0.281	40	11.24
	11	2R	0.133	75	9.975
	12	2R	0.169	60	10.14
	13	1R	0.0617	100	6.17
	14	1R	0.898	20	17.96
1021	1	0R	0.368	30	11.04
	3	1R	1.26	20	25.2
	4	1R	1.97	15	29.55
	5	1R	3.91	10	39.1
	6	0R	1.81	15	27.15
	8	0R	1.05	20	21
	9	1R	1.14	20	22.8

b. SNP Panel Design

The previously established SNP-based assay utilized the forensic HID-Ion AmpliSeq Identity Panel (Thermo Fischer Scientific), which included 90 autosomal SNPs (*74*, *75*) and 34 upper Y-clade SNPs (*76*) (Table 21). In collaboration with Illumina, a panel was recreated with this same list of SNPs, which allowed us to test the utility of these SNPs on the superior MiSeq sequencing platform, as the original panel was compatible with the PGM Ion Torrent sequencing platform. In addition to this panel, 154 supplementary highly polymorphic SNPs were identified, which was used to develop a custom panel for the MiSeq sequencing platform, again in collaboration with Illumina (Appendix II, Table 22). This provided insight on whether other SNPs may also be useful for the non-invasive detection of acute rejection following heart transplantation.

c. Library Preparation and Sequencing – Illumina MiSeq

As a result of the collaboration with Illumina, all of the necessary reagents were also provided to allow for the preparation of the library and sequencing of the two panels with the cfDNA extracted from the various patient samples (Table 2). As such, the samples and reagents were given to the University of Calgary Core Laboratory whereby the same sequencing libraries were prepared for each panel using the Illumina MiSeq library preparation kit. Libraries for each panel were then sequenced using v3 MiSeq reagent kit v3 (150 cycles) to produce 2x75bp paired-end reads. The results of the run were then accessed through the BaseSpace Sequencing Hub. The quality of each sequencing run, provided in .fastq format, was then assessed through the generation of a FastQC (*60*) report for each file, whereby a Q score ≥30 was used as a threshold.

iv. Results

a. FastQC Reports – HID-Ion AmpliSeq Identity Panel

Upon receiving the sequencing runs from the HID-Ion AmpliSeq Identity Panel (Table 21), which were provided as .fastq files, a FastQC (*60*) report was generated in order to determine the quality and accuracy at which each base was able to be identified within each run. Due to the small size of the amplicons (<150 bp), each amplicon could be fully sequenced in both directions, which created two runs per sample. As such, the FastQC reports (Figure 33) for each run generally indicated that approximately the first 125 bases had a Q score of at least 30, while all remaining bases had to be trimmed prior to being mapped to the hg19 reference genome to allow for accurate alignment. The quality score indicates the probability of an incorrect base call, whereby $Q = -10\log_{10}(e)$. Therefore, a Q score of 30 denotes a rate of one base in every 1000 having been miscalled, which equates to an inferred base call accuracy of 99.9%.

Table 21. The location and identifier of the autosomal and Y chromosome SNPs within the HID-Ion AmpliSeq Panel (Thermo Fisher Scientific)

Chromosome	Start (hg19)	rsID	A1	A2
chr1	4367323	rs1490413	G	A
chr1	105717631	rs4847034	A	G
chr1	160786670	rs560681	A	G
chr1	238439308	rs10495407	G	A
chr1	239881926	rs891700	A	G
chr1	242806797	rs1413212	T	C
chr2	114974	rs876724	C	T
chr2	10085722	rs1109037	G	A
chr2	124109213	rs993934	A	G
chr2	182413259	rs12997453	A	G
chr2	239563579	rs907100	G	C
chr3	961782	rs1357617	A	T
chr3	32417644	rs4364205	T	G
chr3	113804979	rs1872575	G	A
chr3	190806108	rs1355366	T	C
chr3	193207380	rs6444724	T	C
chr4	10969059	rs2046361	T	A
chr4	169663615	rs6811238	T	G
chr4	190318080	rs1979255	C	G
chr5	2879395	rs717302	G	A
chr5	17374898	rs159606	A	G
chr5	159487953	rs7704770	G	A
chr5	174778678	rs251934	A	G
chr5	178690725	rs338882	G	A
chr6	12059954	rs13218440	G	A
chr6	152697706	rs214955	C	T
chr6	165045334	rs727811	G	T
chr7	4310365	rs6955448	C	T
chr7	4457003	rs917118	C	T
chr7	137029838	rs321198	T	C
chr7	155990813	rs737681	T	C
chr8	19811967	rs256	C	T
chr8	19816860	rs298	G	A
chr8	28411072	rs10092491	T	C
chr8	136839229	rs4288409	A	C
chr8	139399116	rs2056277	C	T
chr9	1823774	rs1015250	G	C
chr9	27985938	rs7041158	C	T
chr9	126881448	rs1463729	C	T
chr9	128968063	rs1360288	C	T
chr9	137417308	rs10776839	G	T
chr10	3374178	rs735155	C	T
chr10	17193346	rs3780962	A	G
chr10	118506899	rs740598	G	A
chr10	132698419	rs964681	T	C
chr11	5709028	rs1498553	C	T

chr11	11096221	rs901398	C	T
chr11	115207176	rs10488710	C	G
chr11	134667546	rs2076848	A	T
chr12	6945914	rs2269355	C	G
chr12	106328254	rs2111980	T	C
chr12	130761696	rs10773760	A	G
chr13	20901724	rs1335873	T	A
chr13	22374700	rs1886510	G	A
chr13	100038233	rs1058083	A	G
chr13	106938411	rs354439	A	T
chr14	25850832	rs1454361	T	A
chr14	53216723	rs722290	G	C
chr14	98845531	rs873196	C	T
chr14	104769149	rs4530059	G	A
chr15	24571796	rs2016276	T	C
chr15	39313402	rs1821380	C	G
chr15	55210705	rs1528460	C	T
chr16	5606197	rs729172	G	T
chr16	5868700	rs2342747	A	G
chr16	78017051	rs430046	C	T
chr16	80106361	rs1382387	C	A
chr17	2919393	rs9905977	A	G
chr17	5706623	rs740910	A	G
chr17	80765788	rs2292972	T	C
chr18	1127986	rs1493232	C	A
chr18	9749879	rs9951171	G	A
chr18	55225777	rs1736442	T	C
chr18	75432386	rs1024116	C	T
chr19	28463337	rs719366	G	A
chr19	39559807	rs576261	A	C
chr20	4447483	rs1031825	A	C
chr20	15124933	rs445251	G	C
chr20	39487110	rs1005533	G	A
chr20	51296162	rs1523537	T	C
chr21	28608163	rs2830795	A	G
chr21	29679687	rs2831700	A	G
chr21	42415929	rs914165	G	A
chr21	43606997	rs221956	T	C
chr22	27816784	rs733164	G	A
chr22	33559508	rs987640	T	A
chr22	47836412	rs2040411	G	A
chr22	48362290	rs1028528	A	G

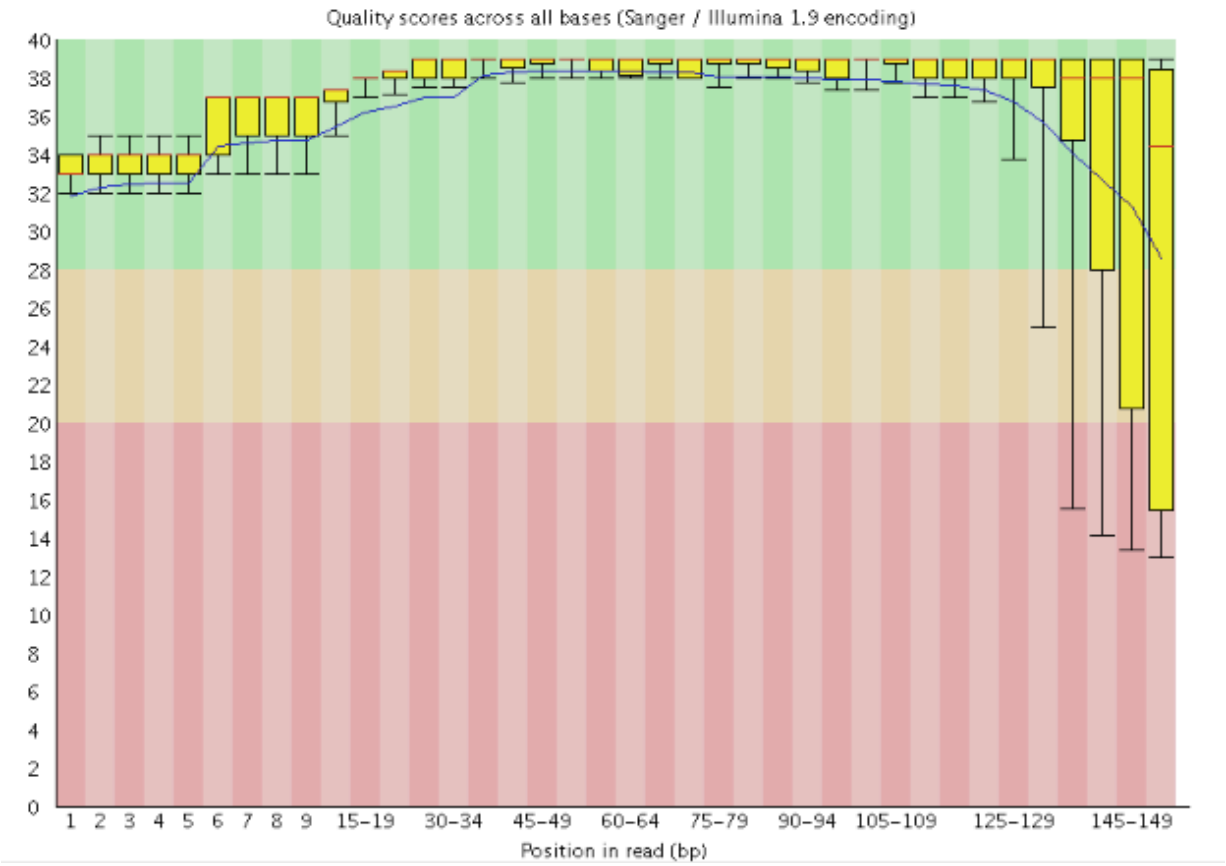

Figure 33. The FastQC report for one sequencing run of the HID-Ion AmpliSeq panel. The quality score, generated from the FastQC report, of each base sequenced in one direction using the previously implemented HID-Ion AmpliSeq (Thermo Fisher Scientific) on the Illumina MiSeq sequencing platform. Sequenced cfDNA was obtained from a blood sample taken at the tenth routine EMB for patient 1002.

b. FastQC Reports – New Custom Panel

Much like the results from the recreated HID-Ion AmpliSeq Identity Panel, the sequencing runs were provided as .fastq files for the new custom panel (Table 22). As such, a FastQC (*60*) report was generated in order to determine the quality and accuracy at which each base was able to be identified. Due to the small size of the amplicons (<150 bp), each amplicon could be fully sequenced in both directions, which created two runs per sample. As such, the FastQC reports (Figure 34) for each run generally indicated that approximately the first 125 bases had a Q score of at least 30, while all remaining bases had to be trimmed prior to being mapped to the hg19 reference genome to allow for accurate alignment.

Table 22. The location and identifier of autosomal SNPs that comprise the custom SNP panel.

Chromosome	Start (hg19)	rsID
1	4,367,323	rs1490413
1	14,155,402	rs7520386
1	45,973,928	rs2275276
1	67,861,520	rs2229546
1	105,717,631	rs4847034
1	158,582,646	rs2251969
1	160,786,670	rs560681
1	179,520,506	rs1410592
1	209,968,684	rs2013162
1	228,431,095	rs1771455
1	238,439,308	rs10495407
1	239,881,926	rs891700
1	242,806,797	rs1413212
2	114,974	rs876724
2	10,085,722	rs1109037
2	49,381,585	rs1394205
2	75,115,108	rs10194657
2	124,109,213	rs993934
2	169,789,016	rs497692
2	182,413,259	rs12997453
2	215,820,013	rs10498027
2	227,896,976	rs10203363
2	239,563,579	rs907100
3	961,782	rs1357617
3	4,403,767	rs2819561
3	32,417,644	rs4364205
3	45,989,044	rs2234358
3	113,804,979	rs1872575
3	148,727,133	rs4938
3	190,806,108	rs1355366
3	193,207,380	rs6444724
4	5,749,904	rs4688963
4	10,969,059	rs2046361
4	86,915,848	rs10003909
4	169,663,615	rs6811238
4	190,318,080	rs1979255
5	2,879,395	rs717302
5	13,719,022	rs30169
5	17,374,898	rs159606
5	40,981,689	rs1061429
5	55,155,402	rs1009639

5	82,834,630	rs309557
5	138,456,815	rs3088052
5	159,487,953	rs7704770
5	171,849,471	rs17074773
5	174,778,678	rs251934
5	178,690,725	rs338882
6	12,059,954	rs13218440
6	56,471,402	rs9382658
6	146,755,140	rs2942
6	152,697,706	rs214955
6	165,045,334	rs727811
7	4,310,365	rs6955448
7	4,457,003	rs917118
7	34,009,946	rs10265207
7	48,450,157	rs17548783
7	100,804,140	rs1048303
7	125,955,821	rs479
7	137,029,838	rs321198
7	151,254,175	rs8961
7	155,990,813	rs737681
8	19,811,967	rs256
8	19,816,860	rs298
8	28,411,072	rs10092491
8	94,935,937	rs4735258
8	136,839,229	rs4288409
8	139,399,116	rs2056277
9	1,823,774	rs1015250
9	27,202,870	rs639225
9	27,985,938	rs7041158
9	77,415,284	rs7859201
9	100,190,780	rs1381532
9	126,881,448	rs1463729
9	128,968,063	rs1360288
9	137,417,308	rs10776839
10	2,406,631	rs826472
10	3,374,178	rs735155
10	17,193,346	rs3780962
10	69,926,097	rs2673794
10	100,219,314	rs10883099
10	118,506,899	rs740598
10	132,698,419	rs964681
11	5,709,028	rs1498553
11	6,629,665	rs1043388
11	11,096,221	rs901398
11	16,133,413	rs4617548

11	30,255,185	rs6169
11	115,207,176	rs10488710
11	134,667,546	rs2076848
12	993,930	rs7300444
12	6,945,914	rs2269355
12	52,200,742	rs60637
12	106,328,254	rs2111980
12	130,761,696	rs10773760
13	20,901,724	rs1335873
13	22,374,700	rs1886510
13	25,466,955	rs3742165
13	39,433,606	rs9532292
13	100,038,233	rs1058083
13	106,938,411	rs354439
14	25,850,832	rs1454361
14	50,769,717	rs2297995
14	53,216,723	rs722290
14	76,045,858	rs2287016
14	98,845,531	rs873196
14	104,769,149	rs4530059
15	24,571,796	rs2016276
15	39,313,402	rs1821380
15	55,210,705	rs1528460
16	5,606,197	rs729172
16	5,868,700	rs2342747
16	70,303,580	rs2070203
16	78,017,051	rs430046
16	80,106,361	rs1382387
17	2,919,393	rs9905977
17	5,706,623	rs740910
17	7,192,091	rs222842
17	42,449,789	rs5910
17	71,197,748	rs1037256
17	77,468,498	rs938283
17	80,765,788	rs2292972
18	1,127,986	rs1493232
18	9,749,879	rs9951171
18	21,413,869	rs9962023
18	55,225,777	rs1736442
18	75,432,386	rs1024116
19	10,267,077	rs2228611
19	28,463,337	rs719366
19	33,353,464	rs11084673
19	39,559,807	rs576261
19	55,441,902	rs269950

20	4,447,483	rs1031825
20	6,100,088	rs10373
20	15,124,933	rs445251
20	19,970,705	rs2076584
20	35,865,054	rs4608
20	39,487,110	rs1005533
20	51,296,162	rs1523537
20	52,786,219	rs2296241
21	16,685,598	rs722098
21	28,608,163	rs2830795
21	29,679,687	rs2831700
21	42,415,929	rs914165
21	43,606,997	rs221956
21	44,323,590	rs4148973
22	21,141,300	rs4675
22	27,816,784	rs733164
22	33,559,508	rs987640
22	37,469,591	rs4820268
22	47,836,412	rs2040411
22	48,362,290	rs1028528

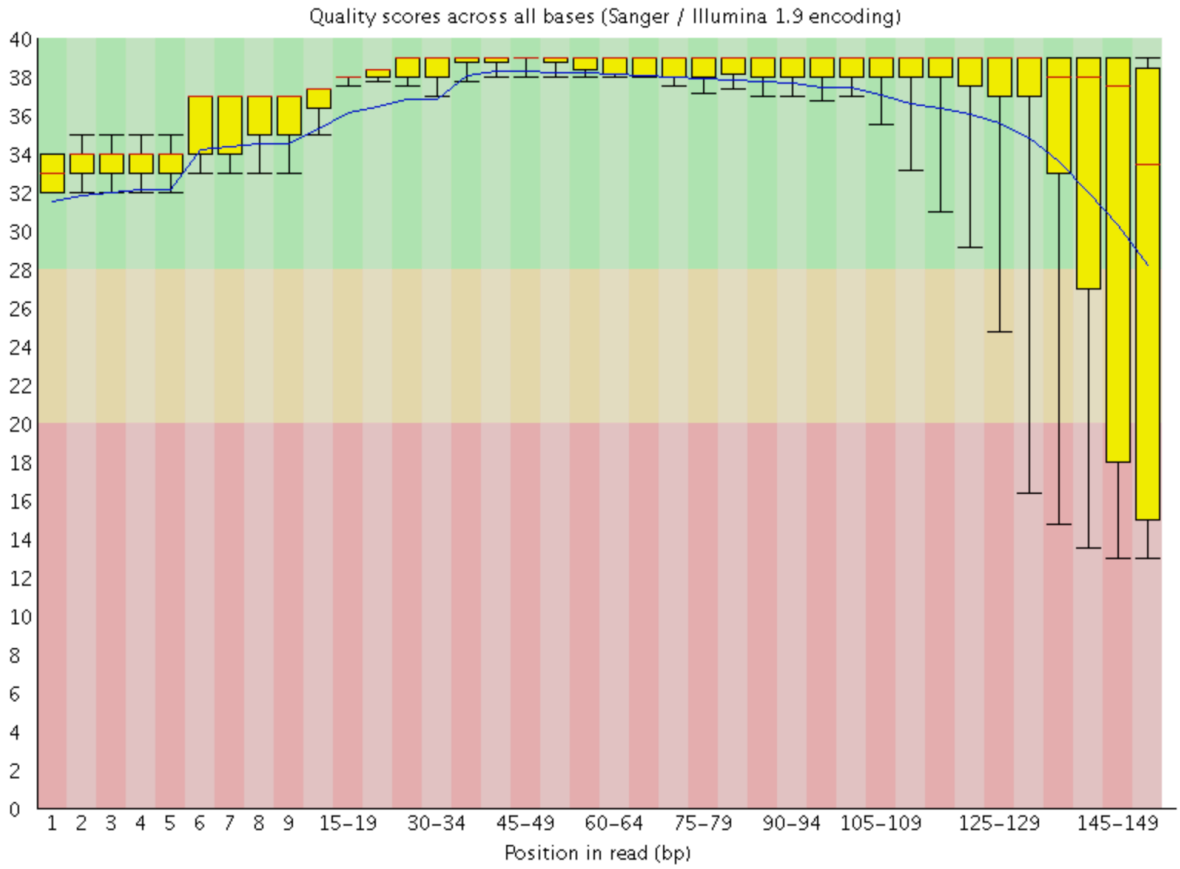

Figure 34. The FastQC report for one sequencing run of the custom SNP panel. The quality score, generated from the FastQC report, of each base sequenced in one direction using the new custom panel of highly polymorphic SNPs on the Illumina MiSeq sequencing platform. Sequenced cfDNA was obtained from a blood sample taken at the tenth routine EMB for patient 1002.

v. Discussion

The previously established SNP-based assay developed by the Greenway lab has the capacity to detect donor-derived cfDNA levels in recipient plasma and does not require donor genotyping or whole-genome sequencing (*38*). However, the clinical applicability of this assay in regards to the accurate assessment of the severity of ACR remained problematic, as initial testing indicated insufficient sensitivity and specificity. Therefore, by modifying both the method by which cfDNA was isolated from patient plasma and the sequencing platform used, the lack of correlation previously observed between the SNP-based assay and EMB results may be resolved through improved the sensitivity and specificity of this assay.

More specifically, the previous manual method for isolating cfDNA often resulted in significant variations in the amount of cfDNA extracted from each plasma sample (*38*). This ultimately reduced the accuracy of the quantification of the total concentration of donor-derived cfDNA in the patients' plasma, which was an integral aspect of this assay. Thus, by using an automated approach, such as the QIAamp MinElute ccfDNA Mini Kit for the QIAcube (Qiagen), we were able to minimize the sample-to-sample variation for the yield of cfDNA. Notably, the previously established SNP-based assay underwent preliminary validation using cfDNA extracted from patients with no (0R) or mild (1R) rejection. Therefore, in order to further validate the improvements to this assay we also tested the 90 autosomal SNPs (*74*, *75*) and 34 upper Y-clade SNPs (*76*) from the HID-Ion AmpliSeq identity panel (Thermo Fischer Scientific) and the 154 SNPs from the new custom panel on the MiSeq sequencing platform using cfDNA from the 11th and 12th biopsy of patient 1002 when moderate (2R) rejection was experienced, according to the biopsy results.

In addition to this improved uniformity, the previously implemented Ion Torrent PGM sequencing platform was replaced by the Illumina MiSeq platform. Using the Ion Torrent PGM platform for the previously established assay tended to result in discrepancies between the estimated concentration of dd-cfDNA and the severity of rejection (*38*). More specifically, the difference in the fraction of dd-cfDNA extracted from the plasma of HT recipients that were assigned a rejection grade of 0R and 1R was not found to be statistically significant (*38*). It has been previously determined that healthy patients typically have a dd-cfDNA level of 0.75±1% (*38*), while patients with significant ACR have a level of 2±1% (*67*). As such, serial data from a single adult HT patient who experienced both no and mild rejection indicated that the fraction of dd-cfDNA remained below 1.5% but the fraction observed in 0R samples was occasionally higher than samples assigned a rejection grade of 1R (*38*). Thus, the use of the improved Illumina MiSeq platform, which had a much lower sequencing error rate, was imperative for improving the utility of this assay as donor-specific SNPs must be accurately called in order to ascertain a precise estimate of the concentration of dd-cfDNA within the recipients' plasma.

It should be noted that the previously established algorithm that was used to estimate the concentration of dd-cfDNA based of donor-specific SNP frequencies was no longer applicable for the analysis of this newly collected sequencing data from the MiSeq platform. This was due to the fact that this algorithm accounted for the high error rate of the Ion Torrent PGM platform by removing the known proportion of inaccurately identified bases to parse out the fraction of cfDNA fragments that actually contained donor-specific SNPs. Therefore, a new algorithm that addresses the lower sequencing error rate of the MiSeq sequencing platform will have to be developed in order to analyze the new sets of data for both the previously utilized HID-Ion AmpliSeq identity panel (Thermo Fischer Scientific) and the new custom SNP panel. This will allow us to determine

the efficacy of a SNP-based assay for the non-invasive detection of ACR and the varying severities of rejection, using either the HID-Ion AmpliSeq identity panel or the new custom SNP panel.

vi. Conclusion

We have implemented changes to the previously established protocol by adopting a more uniform and automated cfDNA extraction approach, a sequencing platform with a lower error rate, and alternative informative SNPs. Also, the previously established SNP-based assay had only been validated with non-rejection (0R) and mild (1R) rejection samples. As such, the sequencing of both panels was completed using identical libraries derived from the 12 cfDNA samples from patients 1002 and 1021, which included two 2R samples. This allowed for further potential validation of both the previously utilized HID-Ion AmpliSeq identity panel (Thermo Fischer Scientific) and the new custom SNP panel. However, until a novel algorithm has been developed to better analyze the less noisy sequencing results obtained from the MiSeq platform, the efficacy of these improvements cannot be fully evaluated.

III. Publicly Available Methylomes

Table 23. Publicly accessible datasets of epigenomes of both ventricle and non-ventricle tissues, as well as hematopoietic cells, used for *in silico* DMR identification.

Tissue/Cell Type	Project	Accession
Left Ventricle	Roadmap	GSM1010978
Left Ventricle	Roadmap	GSM983650
Right Ventricle	Roadmap	GSM1010988
Adipose Tissue	Roadmap	GSM1010983
Adrenal Gland	Roadmap	GSM1010981
Aorta	Roadmap	GSM983648
Breast Myoepithelial Cells	Roadmap	GSM1127054
Esophagus	Roadmap	GSM983649
Gastic Tissue	Roadmap	GSM1010984
Hippocampus	Roadmap	GSM916050
Hippocampus	Roadmap	GSM1112838
Liver	Roadmap	GSM916049
Lung	Roadmap	GSM983647
Ovary	Roadmap	GSM1010980
Pancreas	Roadmap	GSM983651
Psoas Muscle	Roadmap	GSM1010986
Right Atrium	Roadmap	GSM1010987
Sigmoid Colon	Roadmap	GSM983645
Sigmoid Colon	Roadmap	GSM1010989
Small Intestine	Roadmap	GSM983646
Spleen	Roadmap	GSM983652
Thymus	Roadmap	GSM1010979
CD34	Roadmap	GSM916052
Plasma Cell (Bone Marrow)	Blueprint	EGAX00001128259
Erythroblast (Cord)	Blueprint	EGAX00001208464
Inflammatory Macrophage (Cord)	Blueprint	EGAX00001236255
Neutrophil (Cord)	Blueprint	EGAX00001097771
Eosinophil (Venous)	Blueprint	EGAX00001236260
Macrophage (Venous)	Blueprint	EGAX00001147725
Memory B Cell (Venous)	Blueprint	EGAX00001195936
Neutrophil (Venous)	Blueprint	EGAX00001086969
Neutrophil (Venous)	Blueprint	EGAX00001086971
Neutrophil (Venous)	Blueprint	EGAX00001086972
Neutrophil (Venous)	Blueprint	EGAX00001097776
Regulatory T Cell (Venous)	Blueprint	EGAX00001236257
CD4+ Alpha Beta Cell (Venous)	Blueprint	EGAX00001208466

IV. Bioinformatics

Converting File Formats (BigWig to Sorted Bedgraph Files)

BigWig to Wig: $ bigWigToWig <file_name.bw> <file_name.wig>

Wig to Bed: $ convert2bed -i wig <file_name.wig> <file_name.bed>

Bed to Bedgraph: $ awk '{ print $1"\t"$2"\t"$3"\t"$5 }' file_name.bed > file_name.bedgraph

Sorted Bedgraph: $ sortBed -i file_name.bedgraph > file_name_sorted.bedgraph

Creating Input Files for Analysis via Metilene

Comparing Ventricular Methylomes to Non-Ventirclular Tissue Methylomes

$ metilene_input.pl -in1 GSM1010978_Left_Ventricle.sorted,GSM1010988_Right_Ventricle.sorted,GSM983650_Left_Ventricle2.sorted -in2 GSM1010979_Thymus.sorted,GSM1010980_Ovary.sorted,GSM1010981_Adrenal_Gland.sorted,GSM1010983_Adipose_Tissue.sorted,GSM1010984_Gastric.sorted,GSM1010986_Psoas_Muscle.sorted,GSM1010987_Right_Atrium.sorted,GSM1010989_Sigmoid_Colon.sorted,GSM1112838_Brain_Hippocampus_Middle.sorted,GSM1127054_Breast_Myoepithelial_Cells.sorted,GSM916049_Adult_Liver.sorted,GSM916050_Brain_Hippocampus_Middle2.sorted,GSM983645_Sigmoid_Colon2.sorted,GSM983646_Small_Intestine.sorted,GSM983647_Lung.sorted,GSM983648_Aorta.sorted,GSM983649_Esophagus.sorted,GSM983651_Pancreas.sorted,GSM983652_Spleen.sorted -h1 Ventricles -h2 Tissues -out Metilene_Ventricles_Tissues.input & > Metilene_Ventricles_Tissues.input

General Script: $ metilene_input.pl -in1 <comma separated sorted bedgraph files of epigenomes from left and right ventricle tissues> -in2 <comma separated sorted bedgraph files of epigenomes from non-ventricular tissues> -h1 Ventricles -h2 Tissues/Cells -out Metilene_Filename.input

Comparing Ventricular Methylomes to Hematopoietic Cell Methylomes

$ metilene_input.pl -in1 GSM1010978_Left_Ventricle.sorted,GSM1010988_Right_Ventricle.sorted,GSM983650_Left_Ventricle2.sorted -in2 EGAX00001086969_Neutrophil_venous.sorted,EGAX00001086971_Neutrophil_venous.sorted,EGAX00001086972_Neutrophil_venous.sorted,EGAX00001097771_neutrophil_cord.sorted,EGAX00001097776_Neutrophil_venous.sorted,EGAX00001128259_plasma_cell_bone.sorted,EGAX00001147725_macrophage_venous.sorted,EGAX00001195936_memory_B_venous.sorted,EGAX00001208464_erythroblast_cord.sorted,EGAX00001208466_CD4_alpha_beta_T_cell_venous.sorted,EGAX00001236255_inflammatory_macrophage_cord.sorted,EGAX00001236257_regulatory_T_cell_venous.sorted,EGAX00001236260_eosinophil_venous.sorted,GSM916052_CD34_Primary_Cells.sorted -h1 Ventricles -h2 Cells -out Metilene_Ventricles_Cells.input & > Metilene_Ventricles_Cells.input

General Script: $ metilene_input.pl -in1 <comma separated sorted bedgraph files of epigenomes from left and right ventricle tissues> -in2 <comma separated sorted bedgraph files of epigenomes from hematopoietic cells> -h1 Ventricles -h2 Tissues/Cells -out Metilene_Filename.input

Filtering and Sorting DMRs by 10% to Obtain an Output File

Filtering and Sorting DMRs Between Ventricles and Non-Ventircular Tissues

$ metilene -M 25 -m 4 -d 0.1 -t 4 -f 1 -a Ventricles -b Tissues -X 1 -Y 1 -v 0.7 Metilene_Ventricles_Tissues.input > Metilene_Ventricles_Tissues.output | sort -V -k1,1 -k2,2n

Filtering and Sorting DMRs Between Ventricles and Hematopoietic Cells

$ metilene -M 25 -m 4 -d 0.1 -t 4 -f 1 -a Ventricles -b Tissues -X 1 -Y 1 -v 0.7 Metilene_Ventricles_Cells.input > Metilene_Ventricles_Cells.output | sort -V -k1,1 -k2,2n

Filtering the Output File to Obtain DMRs with a Methylation Difference of 50-80%

Filtering DMRs Between Ventricles and Non-Ventircular Tissues with a Difference of 50%

$ metilene_output.pl –q Metilene_Ventricles_Tissues.output –o Metilene_Ventricles_Tissues_Filtered –p 0.05 –d 0.5 –c 4 –l 0 -a Ventricles –b Tissues

This will produce a .bedgraph file

Filtering DMRs Between Ventricles and Hematopoietic Cells with a Difference of 80%

$ metilene_output.pl –q Metilene_Ventricles_Cells.output –o Metilene_Ventricles_Cells_Filtered –p 0.05 –d 0.8 –c 4 –l 0 -a Ventricles –b Cells

This will produce a .bedgraph file

Finding common DMRs between the Non-Ventricle Tissues and Hematopoietic Cells

$ bedtools intersect –a < Metilene_Ventricles_Tissues_Filtered.bedgraph> -b < Metilene_Ventricles_Cells_Filtered.bedgraph>

It should be noted that only the common DMRs within autosomal chromosomes were considered to avoid variability in dosage depending on the sex of the patient.

V. Characteristics of Input Materials from Each Patient for the *In Vitro* Validation of Ventricle-Specific Differentially Methylated Regions

Table 24. The days post-HT at which a routine EMB took place for patient 1002, the total concentration of cfDNA obtained from a blood sample taken immediately before the EMB, the concentration of the amplified DMR at Chr 9-1, and peak molarity of the amplified DMR, which dictated the volume of the amplicon added to the pooled sample for sequencing.

Biopsy #	Days Post-Transplant	Biopsy-Proven Rejection Grade	Total [cfDNA] (ng/μL)	[Amplified DMR] (ng/μL)	Peak Molarity of DMR (nM)	Volume of Amplicon in Pool (μL)
11	760	2R	0.0754	1.74	19.7	4.67
12	781	2R	0.163	1.66	18.8	4.88
13	802	1R	0.0617	0.35	4.05	21
14	816	1R	0.302	0.396	4.67	21
15	858	1R	0.482	0.595	6.76	13.79

Table 25. The days post-HT at which a routine EMB took place for patient 1002, the total concentration of cfDNA obtained from a blood sample taken immediately before the EMB, the concentration of the amplified DMR at Chr 9-2, and peak molarity of the amplified DMR, which dictated the volume of the amplicon added to the pooled sample for sequencing.

Biopsy #	Days Post-Transplant	Biopsy-Proven Rejection Grade	Total [cfDNA] (ng/μL)	[Amplified DMR] (ng/μL)	Peak Molarity of DMR (nM)	Volume of Amplicon in Pool (μL)
11	760	2R	0.0754	0.275	4.38	21
12	781	2R	0.163	0.366	5.75	15.96
13	802	1R	0.0617	0.333	5.22	16.29
14	816	1R	0.302	0.657	10.6	9.25
15	858	1R	0.482	0.281	4.44	21

Table 26. The days post-HT at which a routine EMB took place for patient 1002, the total concentration of cfDNA obtained from a blood sample taken immediately before the EMB, the concentration of the amplified DMR at Chr 12, and peak molarity of the amplified DMR, which dictated the volume of the amplicon added to the pooled sample for sequencing.

Biopsy #	Days Post-Transplant	Biopsy-Proven Rejection Grade	Total [cfDNA] (ng/μL)	[Amplified DMR] (ng/μL)	Peak Molarity of DMR (nM)	Volume of Amplicon in Pool (μL)
11	760	2R	0.0754	0.627	6.37	14.44
12	781	2R	0.163	0.433	4.37	21
13	802	1R	0.0617	0.448	4.6	18.49
14	816	1R	0.302	0.63	6.11	16.05
15	858	1R	0.482	1.1	11.3	8.25

Table 27. The days post-HT at which a routine EMB took place for patient 1021, the total concentration of cfDNA obtained from a blood sample taken immediately before the EMB, the concentration of the amplified DMR at Chr 9-1, and peak molarity of the amplified DMR, which dictated the volume of the amplicon added to the pooled sample for sequencing.

Biopsy #	Days Post-Transplant	Biopsy-Proven Rejection Grade	Total [cfDNA] (ng/μL)	[Amplified DMR] (ng/μL)	Peak Molarity of DMR (nM)	Volume of Amplicon in Pool (μL)
1	22	0R	0.304	0.479	5.90	17.76
3	57	1R	1.26	0.344	3.90	21
6	120	0R	0.176	1.90	22.0	10.31
7	141	1R	0.191	1.08	12.9	21
8	190	0R	1.02	0.557	6.96	21

Table 28. The days post-HT at which a routine EMB took place for patient 1021, the total concentration of cfDNA obtained from a blood sample taken immediately before the EMB, the concentration of the amplified DMR at Chr 9-2, and peak molarity of the amplified DMR, which dictated the volume of the amplicon added to the pooled sample for sequencing.

Biopsy #	Days Post-Transplant	Biopsy-Proven Rejection Grade	Total [cfDNA] (ng/μL)	[Amplified DMR] (ng/μL)	Peak Molarity of DMR (nM)	Volume of Amplicon in Pool (μL)
1	22	0R	0.304	0.763	12.3	8.52
3	57	1R	1.26	0.332	5.19	15.78
6	120	0R	0.176	0.725	11.6	19.55
7	141	1R	0.191	0.868	13.8	19.63
8	190	0R	1.02	0.743	11.9	12.28

Table 29. The days post-HT at which a routine EMB took place for patient 1021, the total concentration of cfDNA obtained from a blood sample taken immediately before the EMB, the concentration of the amplified DMR at Chr 12, and peak molarity of the amplified DMR, which dictated the volume of the amplicon added to the pooled sample for sequencing.

Biopsy #	Days Post-Transplant	Biopsy-Proven Rejection Grade	Total [cfDNA] (ng/μL)	[Amplified DMR] (ng/μL)	Peak Molarity of DMR (nM)	Volume of Amplicon in Pool (μL)
1	22	0R	0.304	0.501	4.99	21
3	57	1R	1.26	0.978	9.79	8.37
6	120	0R	0.176	1.05	10.8	21
7	141	1R	0.191	1.46	15.2	17.82
8	190	0R	1.02	1.42	14.3	10.22

Table 30. The days post-HT at which a routine EMB took place for patient 1017, the total concentration of cfDNA obtained from a blood sample taken immediately before the EMB, the concentration of the amplified DMR at Chr 9-1, and peak molarity of the amplified DMR, which dictated the volume of the amplicon added to the pooled sample for sequencing.

Biopsy #	Days Post-Transplant	Biopsy-Proven Rejection Grade	Total [cfDNA] (ng/μL)	[Amplified DMR] (ng/μL)	Peak Molarity of DMR (nM)	Volume of Amplicon in Pool (μL)
6	94	0R	0.0563	1.74	20.1	2.84
7	150	1R	0.0415	0.286	3.52	21
8	178	0R	0.0767	0.133	1.78	21
9	206	1R	0.0714	0.339	4.05	21
10	269	2-3R	0.233	1.61	18.6	7.24
11	290	1R	0.104	1.35	16.4	11.32
13	318	1R	0.0617	0.412	5.05	17.84
15	374	2R	0.239	1.01	12.3	15.91

Table 31. The days post-HT at which a routine EMB took place for patient 1017, the total concentration of cfDNA obtained from a blood sample taken immediately before the EMB, the concentration of the amplified DMR at Chr 9-2, and peak molarity of the amplified DMR, which dictated the volume of the amplicon added to the pooled sample for sequencing.

Biopsy #	Days Post-Transplant	Biopsy-Proven Rejection Grade	Total [cfDNA] (ng/μL)	[Amplified DMR] (ng/μL)	Peak Molarity of DMR (nM)	Volume of Amplicon in Pool (μL)
6	94	0R	0.0563	0.403	6.26	9.12
7	150	1R	0.0415	0.275	4.41	16.76
8	178	0R	0.0767	0.341	5.39	6.94
9	206	1R	0.0714	0.498	7.98	10.66
10	269	2-3R	0.233	0.418	6.53	20.61
11	290	1R	0.104	0.789	12.6	14.73
13	318	1R	0.0617	0.36	5.65	15.95
15	374	2R	0.239	0.745	11.9	16.45

Table 32. The days post-HT at which a routine EMB took place for patient 1017, the total concentration of cfDNA obtained from a blood sample taken immediately before the EMB, the concentration of the amplified DMR at Chr 12, and peak molarity of the amplified DMR, which dictated the volume of the amplicon added to the pooled sample for sequencing.

Biopsy #	Days Post-Transplant	Biopsy-Proven Rejection Grade	Total [cfDNA] (ng/μL)	[Amplified DMR] (ng/μL)	Peak Molarity of DMR (nM)	Volume of Amplicon in Pool (μL)
6	94	0R	0.0563	0.266	2.72	21
7	150	1R	0.0415	1.03	10.6	6.97
8	178	0R	0.0767	0.501	5.18	7.22
9	206	1R	0.0714	0.731	7.68	11.07
10	269	2-3R	0.233	0.614	6.41	21
11	290	1R	0.104	0.834	8.84	21
13	318	1R	0.0617	0.429	4.29	21
15	374	2R	0.239	0.933	9.32	21

Table 33. The days post-HT at which a routine EMB took place for patient 1025, the total concentration of cfDNA obtained from a blood sample taken immediately before the EMB, the concentration of the amplified DMR at Chr 9-1, and peak molarity of the amplified DMR, which dictated the volume of the amplicon added to the pooled sample for sequencing.

Biopsy #	Days Post-Transplant	Biopsy-Proven Rejection Grade	Total [cfDNA] (ng/μL)	[Amplified DMR] (ng/μL)	Peak Molarity of DMR (nM)	Volume of Amplicon in Pool (μL)
1	40	0R	0.0536	0.797	9.01	8.9
4	117	1R	0.442	1.84	21.6	4.38
5	131	1R	0.318	0.616	7.61	14.02
6	145	2R	0.721	0.915	11.2	12.58
7	166	1R	0.131	Tested in First Round of Sequencing		
8	236	1R	0.580	1.36	16.8	7.73

Table 34. The days post-HT at which a routine EMB took place for patient 1025, the total concentration of cfDNA obtained from a blood sample taken immediately before the EMB, the concentration of the amplified DMR at Chr 9-2, and peak molarity of the amplified DMR, which dictated the volume of the amplicon added to the pooled sample for sequencing.

Biopsy #	Days Post-Transplant	Biopsy-Proven Rejection Grade	Total [cfDNA] (ng/μL)	[Amplified DMR] (ng/μL)	Peak Molarity of DMR (nM)	Volume of Amplicon in Pool (μL)
1	40	0R	0.0536	0.271	4.26	18.83
4	117	1R	0.442	0.53	8.35	11.34
5	131	1R	0.318	0.459	7.26	14.69
6	145	2R	0.721	0.533	8.4	16.78
7	166	1R	0.131	Tested in First Round of Sequencing		
8	236	1R	0.580	0.666	10.4	12.48

Table 35. The days post-HT at which a routine EMB took place for patient 1025, the total concentration of cfDNA obtained from a blood sample taken immediately before the EMB, the concentration of the amplified DMR at Chr 12, and peak molarity of the amplified DMR, which dictated the volume of the amplicon added to the pooled sample for sequencing.

Biopsy #	Days Post-Transplant	Biopsy-Proven Rejection Grade	Total [cfDNA] (ng/μL)	[Amplified DMR] (ng/μL)	Peak Molarity of DMR (nM)	Volume of Amplicon in Pool (μL)
1	40	0R	0.0536	0.366	3.82	21
4	117	1R	0.442	0.446	4.51	21
5	131	1R	0.318	0.509	5.08	21
6	145	2R	0.721	0.674	6.71	21
7	166	1R	0.131	Tested in First Round of Sequencing		
8	236	1R	0.580	0.605	6.18	21

Sample Calculations:

The Determination of the Concentration of Total cfDNA (copies/mL)

Example: Biopsy 11 from patient 1002 (Tables 24-26).

$$\left(\frac{0.0754\ ng}{\mu L}\right)\left(\frac{1000\ \mu L}{mL}\right)\left(\frac{1\ genome\ copy}{0.00303\ ng}\right) = 24{,}884\ copies/mL$$

The Determination of the Concentration of DMRs within Recipients' Plasma (copies/mL)

Example: Biopsy 11 from patient 1002 and the DMR at Chr 9-1 (Tables 8 and 24).

$$\left(\frac{9}{100}\right)\left(\frac{0.0754\ ng}{\mu L}\right)\left(\frac{1000\ \mu L}{mL}\right)\left(\frac{1\ genome\ copy}{0.00303\ ng}\right) = \ 2{,}240\ copies/mL$$